12-2014

Metal Assisted Nanowire Growth for Silicon Nanowire/ Amorphous Silicon Composite Solar Cell

Asmaa Ali Sadoon
University of Arkansas, Fayetteville

Metal Assisted Nanowire Growth for Silicon Nanowire/Amorphous Silicon Composite Solar Cell

Metal Assisted Nanowire Growth for Silicon Nanowire/Amorphous Silicon Composite Solar Cell

A thesis submitted in partial fulfillment
of the requirements for the degree of
Master of Science in Microelectronics-Photonics

By

Asmaa Sadoon
University of Thi-Qar
Bachelor of Science in Physics, 2005

December 2014
University of Arkansas

This thesis is approved for recommendation to the Graduate Council.

Dr. Hameed Naseem Thesis Director	Dr. Surendra Singh Committee Member
Dr. Rick Wise Committee Member	Prof. Ken Vickers Ex-Officio Member

The following signatories attest that all software used in this thesis was legally licensed for use by Asmaa Sadoon for research purposes and publication.

Mrs. Asmaa Sadoon, Student	Professor, Hameed Naseem Director

This thesis was submitted to http://www.turnitin.com for plagiarism review by the TurnItIn company's software. The signatories have examined the report on this thesis returned by TurnItIn and attest that, in their opinion, the items highlighted by the software are incidental to common usage and are not plagiarized material.

Dr. Rick Wise, Program Director	Dr. Hameed Naseem, Thesis Director

Abstract

Solar cells are photovoltaic devices that convert the energy of light to electricity by the photovoltaic effect. Crystalline silicon-based solar cells are the most dominant solar cells in the market today due to the high efficiency and relatively low cost. However, the cost of such solar cell is still high due to the large amount of material that is consumed in fabricating such a device. Polycrystalline/amorphous thin films and nanomaterial technologies have emerged to reduce the high cost of c-Si based solar cells and increase the efficiency. In this research, we combined these two technologies to propose and fabricate silicon nanowires (SiNWs)/amorphous Silicon (a-Si) composite solar cell structure at low temperatures using heavily doped polycrystalline silicon/glass as a substrate.

Silicon Nanowire (SiNW) is one of the promising 1D semiconductor nanomaterial which has recently attracted significant attention due to its potential applications in many fields, including photovoltaic (PV) solar cells. SiNW is a term that is used widely to describe a rod with a diameter of between 1 to 100 nm and length of several microns. The vertical array geometry of such a device has great advantages in increasing the efficiency of solar cells due to its high light absorption and efficient light scattering. Replacing the silicon with polycrystalline silicon that was fabricated on glass substrate by means of aluminum induced crystallization method of amorphous silicon is considered a significant step in reducing the cost since glass is a cheaper material. In this research, heavily doped polycrystalline (p+ polySi/ITO/glass) silicon film was fabricated successfully by the means of aluminum induced crystallization of a-Si on ITO/glass substrate. Raman spectroscope, optical microscope, Hall Effect measurement, and SEM were used for the characterizing the (p+ polySi/ITO/glass). p-type SiNWs were grown successfully in the PECVD system on silicon, a-Si/ITO/glass, and p+ polySi/ITO/glass substrates using Au

nanoparticles as a catalyst at temperatures between (310 ˚C and 346 ˚C). It is to be noted that this temperature range is still lower than the eutectic temperature of Au-Si (363 ˚C). SEM and TEM systems were used to characterize the SiNWs on c-Si and p+ polySi/ITO/glass substrates.

Acknowledgements

First of all, I would like to thank God for giving me the power and patience to achieve my goal that I have pursued during the last three years. Second, I would like to thank my husband, Mr. Muhenned, for his support, encouragement, and motivation during my studying. Also, I would like to thank my parents, brothers, and sisters in Iraq for their support and encouragement, and for their prayers to me for success in my life.

I would like to give a special thanks to my thesis director, Professor Hameed Naseem, for his guidance and pushing me to the right path during my research. I would also like to thank Dr. Husam Abu Safe for his time to train me on how to use the equipment and do experiments in the first year of my research. Also, I would like to thank the post-doctorate, Dr. Murtadha Alher, for his assistance during my research. I would like to acknowledge that without his assistance, I would not have been able to achieve such results in my research. I would like to thank Professor Vickers for his advice to students in either during the operation seminars or advising meetings to push students to go forward in their research or courses. Also, I would like to thank the new director of the μEP program, Dr. Rick Wise, for completing what Professor Ken Vickers started in helping students and pushing them to achieve more progress in their research.

Research was possible through the use of the High Density Electronics Center at the University of Arkansas, Fayetteville campus. I would like to thank specifically, Mr. Errol Porter, for his quick response whenever I asked him for assistance for doing some things in HIDEC. Also, I would like to thank Dr.Mourad Benamara for his help in taking good SEM and TEM images for my samples.

Moreover, I would like to thank others who helped me in my research. I would like to thank Hafeez Khaja for his assistance in training me and answer my questions. Also, I would like

to thank Larry Cousar who helped me in doing the Hall Effect measurement for some of my samples. Also, I would like to thank Sattar Al-kabi for his assistance in analyzing my samples with Raman spectroscopy. Also I would like to thank my classmate Manal Aldawsari for her support and help during my research. I would like to thank everybody who cares about me and wishes all the best for me. Finally, I would like to thank my sponsor, the Higher Committee for Education Development in Iraq, for giving me the chance to study in the United States and supporting me financially during my studying and research.

Dedication

I would like to dedicate this effort to my daughters, Zeinib and Rukayyah, my husband, Mr.Muhenned Abdul Sahib, parents, brothers, sisters, friends and my country, Iraq.

Table of Contents

List of Figures

List of Tables

Chapter 1: Introduction

Chapter one of this thesis consists of three sections. The first section includes some background information about renewable energy systems, including photovoltaic (PV) solar cells. The second section discusses the motivation behind this research. The third section is about thesis organization.

1.1 Renewable energy sources

During the last two decades, the reality and danger of environmental deterioration has become more obvious. Factors that lead to environmental problems are increasing energy consumption and industrial activity. The combination of these two factors increases the impact on the environment. Long-term potential actions are required to implement sustainable development in order to solve these environmental problems. The most effective solution for environmental deterioration is the use of renewable energy sources [1]. Renewable energy technologies are based on converting natural resources into beneficial forms. The most potential forms of renewable energy sources are: wind, hydroelectric, solar, and biomass [2]. Sun and its effects on the earth such as, solar radiation, wind, gravitational forces, and the heat of the earth's core (geothermal) are resources that can be harnessed to produce energy. Renewable energy resources are potentially more cost effective than conventional fossil fuel based energy production systems [1].

Renewable energy systems carry multiple benefits. First of all, renewable energy systems save energy by avoiding the use of expensive resources like fossil fuels. Second, due to the demands of installation and operation of the renewable energy equipment, job opportunities are created. Job creation is considered nowadays as an important issue in many countries. Third, decreasing environmental pollution is one of the most important advantages of renewable energy

systems. This advantage is due to the substitution of conventional fuels with renewable energy sources, which leads to reduction in air emissions [1].

The photoelectric effect was discovered in the selenium by Becquerel in 1839 [3]. He found out that an electric current could be generated by a certain amount of materials during their exposing to the light. In 1905 [3], Albert Einstein described the photoelectric effect and nature of light as photovoltaic technology. In 1959 [3], the first photovoltaic model was built by Bell laboratories. In 1960 [3], solar cell was used seriously by space industry in the spacecraft to provide the power. Silicon was used in the solar cell with efficiency of 11%, but the cost was very high around $1000 per Watt. Later, gallium arsenide (GaAs) was discovered as another photovoltaic materials which can operate at high temperature compared to silicon. In addition to silicon and GaAs, the two other photovoltaic materials that have been used most commonly in the fabrication of solar cells are cadmium sulphide (CdS), cuprous sulphide (Cu_2S), cadmium telluride (CdTe), and copper indium selenide ($CuInSe_2$) due to their good conductivities to electricity. Silicon still is the most dominant semiconductor material that has been used in the fabrication of solar cells due to its superior properties such as non-toxicity and availability (Si forms about 25% of the Earth's crust) [3] [1].

Photovoltaic (PV) solar cells are one of the renewable energy resources that transform sunlight to electricity by the photovoltaic effect. Solar cells are one of the most attractive devices to industry nowadays due to their minimal impact on the environment, cost effectiveness, and increasable efficiency. About 30 years ago, when the PV solar cells were used for large-scale commercial application, the efficiency was below 10%. Nowadays, it has increased to nearly 20% and it is expected to be about 30% in the future [1].

Solar cells can be classified into three generations. The first generation is based on crystalline silicon. Crystalline silicon divides into three types: monocrystalline (single crystal silicon), multicrystalline (polycrystalline), and ribbon silicon. The monocrystalline silicon means that atoms arranged in continuous ordered or regular structure [4]. Polycrystalline silicon consists of small regions of crystalline silicon that are separated by boundaries, and these small regions are called grains. In spite of the high efficiency that have been provided by monocrystalline solar cells, multicrystalline solar is the most attractive to be used in the fabrication of crystalline solar cell due to its cheapness [5].

In general, the practical application of the crystalline silicon solar cells is limited due to the high consumption of raw materials and required purity in the used silicon wafers. The high purity of single crystalline silicon is required in order to get high or optimal collection efficiency, minimize carrier recombination and increase the diffusion length of minority carriers. Moreover, in order to absorb about 90% of the incident light at wavelength from 700-1100 nm, the thickness of silicon cells should be several micrometers to millimeters. As a result, researchers try to reduce the high cost that associated in the fabricating of crystalline solar cells by replacing it by thin film technology [6].

Thin film- based solar cells is the second generation of solar cells. In this type of solar cells, an extremely thin layer of photosensitive material was deposited on a low cost substrate such as glass, steel, and stainless. Amorphous silicon (a-Si) is the first production of thin film solar cells. Amorphous silicon consists of atoms that arranged randomly, and this unordered structure of atoms leads to have dangling bonds in their structure. The absorption of light by a-Si is better than that with crystalline silicon although the absorbed band-width reduces. Due to the high absorption of a-Si, the amounts of materials that are required in the fabrication of a-Si solar

cells are little compared to crystalline silicon solar cells. However, the efficiency of amorphous silicon is less than that with crystalline silicon. Thin films such as cadmium telluride (CdTe) and copper-indium-gallium-diselenide (CIGS) can be produced by compounds between II-VI groups [7].

The third and most recent generation of solar cells is based on silicon nanowires (SiNWs). SiNWs are 1-D semiconductor materials that have received a great deal of attention recently. SiNW is a term that is used commonly to describe a rod with large aspect ratio (width/length) [6]. The diameters of these SiNWs range from a few nanometers to a few hundreds of nanometers and lengths range from several hundreds of nanometer to a few micrometers. SiNWs have some good properties that give them special advantage when applied in various fields such as chemistry, biology, mechanic, and physics. One of these properties is the size of SiNWs. The size of SiNW in the nanometers scale is equivalent to the wavelength of visible light that ranges from 400-650 nm, and that means the light on the nanometer scale can be handled by SiNWs [8]. Second, the vertical array geometry of SiNWs has great advantages in increasing the efficiency of solar cells due to their high light absorption and efficient scattering, especially at short wavelengths [6].

The emission and absorption properties of SiNWs are affected by the length, diameter and alignment of SiNWs. There are several factors that affect the absorption and emission of SiNWs, and these factors are: composition, impurity, doping level, defect concentration, crystal structure, growth direction, and nature of the facets [8]. The potential advantages that are available in SiNWs-based solar cells exceed those in the Si wafer or thin film solar cells, and these benefits related to electrical, optical, and relaxation effects, new charge separation mechanism, and cost [9].

1.3 Motivation

The motivation behind this research is to push forward the technology to fabricate SiNW/a-Si composite solar cell device with low cost, high efficiency and simple fabrication methods. The solar cell device that was fabricated in this study is based on three important technologies: thin film, polycrystalline silicon and nanoscale technologies. Figure 1.1 shows the schematic diagram of the SiNWs/a-Si composite solar cell using glass as a substrate.

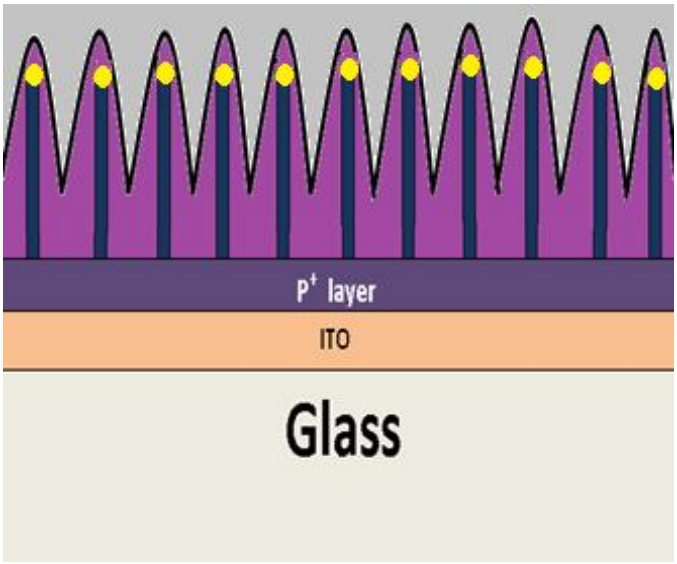

Figure 1.1. Schematic diagram of SiNWs/a-Si composite solar cell.

Combining these three technologies gives the advantage for the solar device to be a cost effective and efficient device compared to solar cells based on crystalline Si wafers. In spite of the high efficiencies that have been provided by crystalline Si- based solar cells, the high costs required in fabricating this type of solar cells remain the most challenging thing. Large amounts of raw material are usually used in fabricating the crystalline silicon in order to get high efficiency. Also, preparing highly pure single crystalline silicon wafers cost a lot and demand

long manufacturing process times. Therefore, thin film technology helps in reducing the amount of consumed materials and high costs.

Amorphous silicon thin film was the first production of this technology. The light absorption of a-Si is very high reaching around 90% of the incident light, but the efficiency is low [1]. Researchers found that the efficiency of a-Si can be increased by converting it to a polycrystalline silicon thin film using different techniques such as solid phase, laser induced crystallization, aluminum induced crystallization methods, etc. In order to increase the efficiencies of the solar cells, nanomaterials such as, nanodots and silicon nanowires have the attracted attention for use in the fabrication of solar cells.

SiNW is a 1-D semiconductor material that has diameter range from 1-100 nm and length up to micrometers. The vertical geometry of SiNWs give them the advantage of trapping the light, so photons will have the chance to stay longer without reflecting outside the surface. Also, the absorption of these SiNWs is high and can handle the light of short wavelength which leads to increasing the efficiency.

Figure 1.2 shows a comparison between the standard p+-i-n+ solar cell and the SiNW-based solar cell.

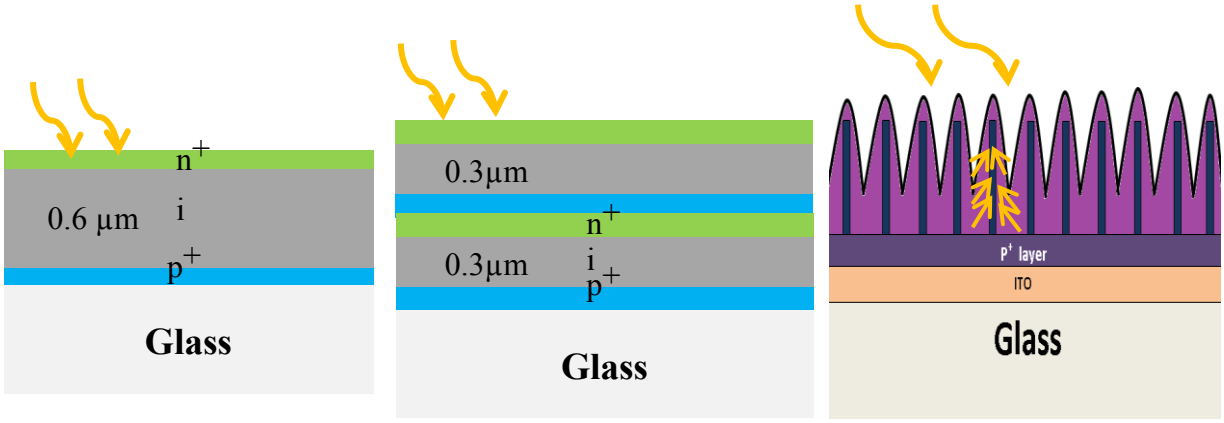

Figure 1.2. Comparison between standard p+-i-n+ solar cell and SiNW-based solar cell.

In spite of the high efficiency that has been provided by p+-i-n+ solar cell on glass substrate, it has a degradation problem that brings the efficiency of the solar cell down after exposing it to light. This problem was due to the thickness of the intrinsic layer (0.6 μm). This problem has been solved by using two p+-i-n+ solar cells on glass substrate with intrinsic layer of 0.3 μm thickness for each solar cell. However, the cost was doubled. If these solar cells are compared to SiNW/a-Si composite solar cell, the advantages of SiNW/a-Si composite solar cell will be more. The vertical geometry of SiNWs gives the advantage of trapping, reflecting, and scattering the light which enhances the light absorption and then increases the efficiency [10].

In this research, heavily doped p-type polycrystalline silicon thin film was fabricated on non-silicon, glass substrate by means of aluminum induced crystallization of a-Si. P-type SiNWs were grown on the heavily doped p-type polySi thin film using Au as a catalyst at low temperature of 310 ˚C in the plasma enhanced chemical vapor deposition. The idea of fabrication SiNWs on heavily doped p-type polycrystalline silicon thin film has not been done before except by one group who did this on a fused quartz wafer in the hot wall horizontal chemical vapor deposition system at 1050 ˚C [11].

1.3 Thesis organization

This thesis consists of six chapters. This chapter provides an introduction and motivation for this research. The second chapter includes a literature review about methods and techniques that have been used in fabricating the silicon nanowire (SiNW) in addition to the most important applications of SiNW in different fields including solar cells. The third chapter includes the equipment that has been used in fabrication and characterization and the experimental procedures that have been used in fabricating the SiNWs. The fourth chapter of this thesis discusses the

results obtained in this research. The last chapter includes the summary of this research and future work.

Chapter 2: Literature Review

In this study, the fabrication of solar cell device is based on two important steps. The first step is the fabrication of p+ polySi thin film on the ITO/glass substrate by means of aluminum induced crystallization of a-Si (AlIC) method. The second step is the fabrication of SiNWs using Au and Al as catalysts. Therefore, this chapter is divided into two sections. The first section will include background information about the fabrication of poly-Si thin film by means of AlIC of a-Si. The second section will be devoted for background information about SiNWs fabrication methods, techniques, and types of catalysts that have been used in the growth of SiNWs .

2.1 The fabrication of polySi (poly-Si) by AlIC

Amorphous silicon solar cell technology is a well-established technology for the large scale manufacturing of solar panels due to its successful implementation of in-line deposition tools as compared to batch processing of its more conventional crystalline counterpart. Using thin film polycrystalline silicon in the fabrication of solar cells combines the cost benefit of thin film technology and high efficiency of crystalline silicon technology [12]. The two most common techniques that have attracted the attention in the preparing of large-grained polycrystalline silicon film on non-silicon substrates, like glass, are solid phase crystallization (SPC) and laser induced crystallization (LIC). However, there are problems associated with the fabrication of polycrystalline silicon thin film by the SPC and LIC techniques. On the one hand, SPC technique requires high temperature around 600˚C to fabricate poly-Si film and long processing time. On the other hand, LIC is an expensive and complex technique and causes contamination due to the melting in the silicon during the fabrication by laser [13] .

As an alternative technique for the SPC and LIC techniques, aluminum induced crystallization method (AlIC) has been proposed. AlIC has attracted attention for use in the

fabrication of polycrystalline thin film of a-Si due to its low temperature processing, simplicity and short processing times. AlIC method can be done by different mechanisms, including the aluminum-induced layer exchange (ALILE) and reverse aluminum induced layer exchange (R-ALILE). In the ALILE mechanism, a layer of Al is deposited on a substrate and then the Al layer is exposed to the air to oxidize it. After that, a layer of a-Si is deposited on top of the Al oxide layer. After annealing the sample in temperature range from 350-500 ˚C, the outcome is substrate/poly-Si/oxide/Al+Si+hillock (see Figure 2.1) [12].

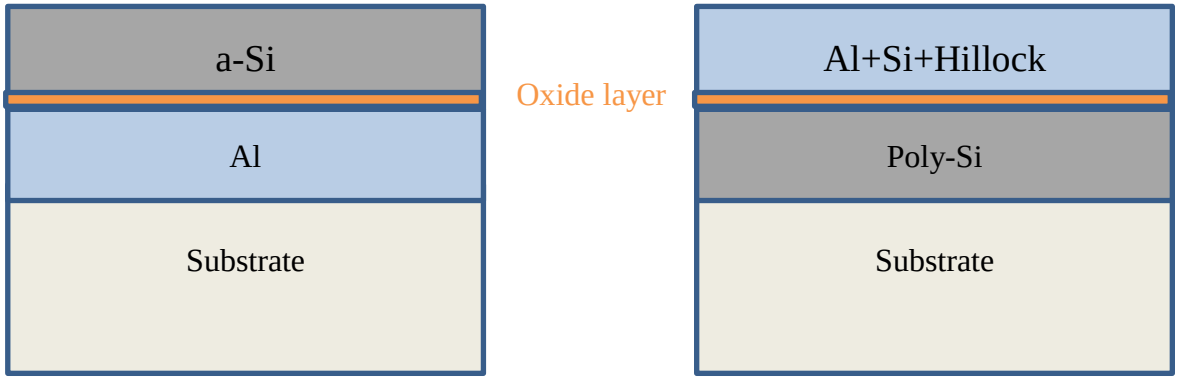

Figure 2.1. Schematic diagrams for the AlILE mechanism: a. before annealing; b. after annealing.

Nast et.al, Schneider et.al and Widenborg et.al developed a model to explain the behavior of the AlILE growth in seven phases including: dissociation, Si diffusion, nucleation, Si grain growth, Al diffusion, formation of secondary crystallite with extra Si dissociation, and crystallization of the remaining silicon. In the first phase of the AIILE mechanism, Si starts to dissociate at the Al/Si interface aided by Al. Upon annealing, Si diffuses through aluminum oxide layer into the Al layer due to the non-equilibrium situation. According to the binary phase

diagram, the amount of Si that can be thawed in the Al layer is around 0.8% at 500 ˚C and up to 1.5% at temperature lower than the eutectic point of Al-Si [12].

In general, when an Al layer becomes in contact with a c-Si layer, the saturation concentration of Si in the Al at the eutectic point is 12% according to the binary phase diagram. Moreover, if two layers become in contact at an interface, the chemical potential of these two phases should be equal in the equilibrium situation. For a-Si, the situation is different due to its high chemical potential which depends on the concentration of Si in Al. To explain, when Al is in contact with a-Si layer, the Si concentration in the Al layer will exceed the given saturation concentration of Si in Al and exceed the critical concentration of Si nucleation in Al due to a difference in Gibbs free energy. As the Si concentration continues to exceed the critical concentration, the Si nucleation will initiate at grain boundaries of Al and lead to the grain growth. When the Si reaches the maximum concentration in Al, the nucleation ratio also will be in its maximum. As a result, the Si concentration will drop below the critical Si concentration, and nucleation will stop due to the Si consumption during the nucleation and grain growth. After that, a depletion region will exist around the already growing grains preventing any more nuclei around these grains. At this point, the existence of grains with large size is established by the AlIC process [12].

Initially, the direction of the growth will be in isotropic. However, when the growing crystal reaches the substrate, it will grow only laterally. During the grain growth, Al starts to leave the growth interface towards the top layer. The migration of Al to the top layer brings some benefits. First of all, it helps in separating the Si into large islands, and the doping of these growing Si layer will be around ($3x10^{18}$ /cm^3) due to the low solubility of Al in Si. Moreover, there is a chance of having another AIC in the top layer due to the availability of Al and some of

the remaining a-Si. The presence of Al in the top layer will also help accelerate the grain growth in the bottom layer, and finally the remaining Si that did not participate in the formation of poly-Si film will crystallize [12].

The other mechanism of AlIC is called reverse aluminum induced layer exchange (R-ALILE). This mechanism was suggested by Jeager et al who claimed that reversing the structure to substrate/a-Si/Al would reduce the formation of hillocks that exist after annealing the Al layer at a temperature lower than the eutectic temperature of Al-Si alloy. Hillocks is the formation of crystalline silicon islands on the top of the poly-Si film. After annealing the substrate/a-Si/Al substrate, the result will be substrate/Al+Si/oxide+hillock/poly-Si (see Figure 2.2). An advantage of using R-ALILE mechanism is getting a smooth surface with Si- islands underneath it so there is no need for more steps to remove these islands. Moreover, this reverse configuration leads to a highly conductive layer on the top of glass, which can be considered as a back contact for the solar cell. That reduces the series resistance and increases the efficiency [14].

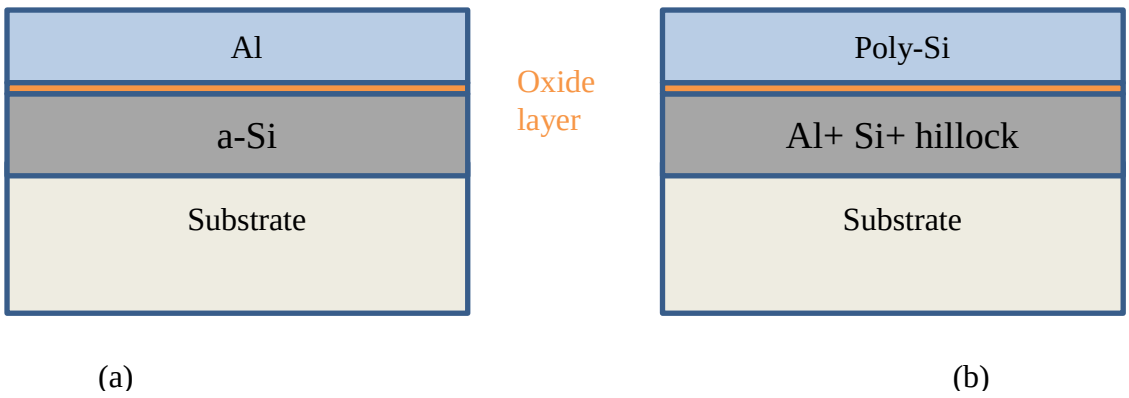

Figure 2.2. Schematic diagram for reverse aluminum-induced layer exchange (R-ALILE): a. before annealing; b. after annealing.

2.2 The fabrication of nanowires (NWS)

Generally, the fabrication of nanomaterial such as, nanoparticles and nanowires, etc., can be divided into two methods: top-down and bottom-up. In the top-down method, the fabrication process starts from a bulk substrate and ends with the desired nanomaterial after a long process of removing or etching the material out of the bulk, whereas in the bottom-up methods, the fabrication process is the opposite. Atoms or molecules start to accumulate from gaseous precursor until the desired nanostructure materials is formed [15]. In the next two sections, more details about these two methods will be discussed.

2.2.1 Top-down approach

Top-down methods include many fabrication technologies that are based on the lithography methods that have been used in the semiconductor industry to fabricate different components of integrated circuits. All of the lithography methods share the same principle of converting images from a mask into a desired substrate. The main three steps of any lithography process are coating a substrate, such as silicon wafer or glass substrate, with a resist, exposing the resist to light, electrons, or ions beams, and finally developing the resist images. There are multiple top-down methods, but the most common are: conventional lithography, photolithography, scanning lithography, electron-beam lithography, nanosphere lithography, soft lithography, nano-imprint lithography, and colloidal lithography [15].

Top-down methods have been used widely in the fabrication of crystalline silicon nanowires. In these methods, distinguishing between the fabrication of vertical and horizontal SiNWs is important to be considered due to the differences in fabrication processes of vertical and horizontal SiNWs. Horizontal nanowires lie on a substrate plane, while the orientation of vertical nanowires is perpendicularly to the substrate. Moreover, horizontal nanowires can be

fabricated on silicon-on-insulator (SOI) or bulk silicon wafers with diameters below 10 nm by using different types of top-down techniques, including electron-beam lithography and reactive ion etching. Whereas, vertical SiNWs can usually be fabricated by a reactive-ion etching method. [16].

The fabrication method that was used in this research is the bottom-up method due to its low cost and simplicity. In the next sections more details will be discussed about this bottom-up method.

2.2.2 Bottom-up approach

Bottom-up approach can be classified into four mechanisms: vapor-liquid-solid, vapor-solid, electrochemical deposition, and solution deposition.

2.2.2.1 Vapor-Liquid-Solid (VLS)

VLS mechanism is still considered to be the most common approach for SiNW synthesis. VLS mechanism was suggested in the mid-1960s by Wagner and Ellis [17]. The name of VLS originated from the changing in the silicon's behavior during the deposition, which transfers from vapor phase into the diffusion in a liquid droplet, and finally stabilized as solid silicon wires [17]. The fabrication of nanowires (NWs) by the VLS mechanism can be described in two steps. The first step includes the formation of small liquid droplets, alloying, and nucleation, while the second step includes the growth of nanowires (NWs).

In the first step, after substrates are cleaned, small metal clusters less than 100 nm in diameter are deposited on the surface of the substrate by using different techniques to initiate the growth of NWs. After that, the substrate is placed inside a reaction chamber and heated to an appropriate temperature ranging from 300-1100 ˚C. These temperatures are set according to the

eutectic points between metals and silicon in the binary phase diagram. After the clusters are heated up to the desired temperature, they will melt and form the liquid droplets due to the reduction in the melting temperature of these clusters. In the second step, a gas that has the desired growth material is introduced into the reaction chamber. The precursors atoms of the gas will deposit on the liquid's surface and form an alloy since the sticking coefficient of the liquid droplet's surface are higher than that on the solid substrate. Due to the continued integration of precursor atoms into the liquid droplets, the semiconductor component will reach supersaturation, and that leads to the initiation of the growth of NWs [17]. Figure 2.3 shows the schematic diagram of VLS mechanism.

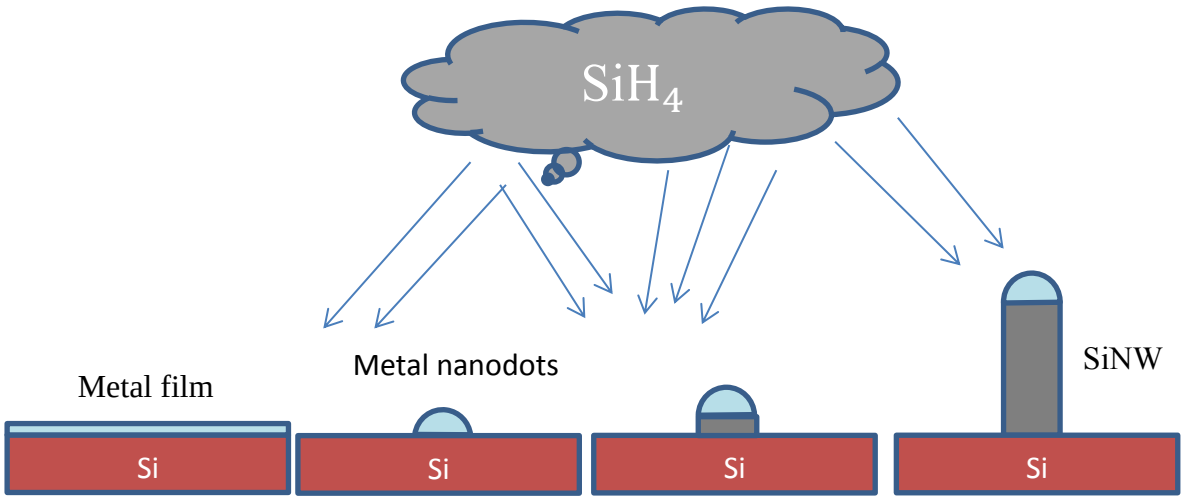

Figure 2.3. Schematic diagram for SiNW growth by VLS mechanism.

In the VLS mechanism, the droplet's size determines the diameter of NWs, while the growth ratio can be determined by the supersaturation of the target material and metal,

concentration of precursor vapor and the substrate temperature. In the VLS mechanism, the relationship between the radius of the catalyst droplet (R) and that of nanowire (r) is given by:

$$R=r\sqrt{1/(1-(\sigma_{1s}/\sigma_1)^2)} \quad \text{(Equation 2.1)}$$

where σ_1 and σ_{1s} are the surface tension and interface tension of the liquid droplet, respectively [16].

Vapor-solid-solid (VSS) is a mechanism that is similar to the vaper-liquid-solid (VLS) mechanism principle except that solid particles catalyze the wire growth instead of the liquid catalyst droplet.VLS and VSS mechanisms can be determined depending on growth temperature and catalyst material [16].

2.2.2.2 Vapor solid process (VS)

In the VS process, NWs grow without the need to use metal catalysts by thermal evaporation for a source material to the melting point and depositing at lower temperature. The name of the VS mechanism is due to the change in the source behavior from vapor phase into solid phase without passing through liquid state. In this process, the diameter of NWs can be controlled by changing in the evaporation, collection temperature and vapor pressure [17].

2.2.2.3 Electrochemical deposition

NWs can be grown by using electrochemical deposition method with various templates, such as porous anodic aluminum oxide (AAO), nano-channel glass, and porous polymer films self-organized from diblock co-polymers [17]. AAO is the most commonly template that have been used in the NWs growth in the electrochemical deposition. In this process, the template is attached to the cathode, which is later contacted to the deposition solution. The anode and cathode are placed in parallel. Once an electric field is applied, cations diffuse from anode to the

cathode, which leads to the growth of NWs inside the templates' pores. After the pores are filled with NWs, the template membrane is etched away, which leads to free- standing NWs.

2.2.2.4 Solution growth

The solution method is a common method for nanowire growth for the II-VI materials. This method was used by Korgel et al. to fabricate SiNWs in a liquid media [17]. In this technique, the liquid is the medium where the nanowires growth takes place instead of the gaseous medium. Korgel et al used supercritical organic fluids that were improved with a liquid Si precursor, like diphenylisilane, and Au or Ni as a catalyst for SiNWs growth at temperatures above the eutectic temperature of the Au or Ni-Si. After the silicon precursor is etched away, metal alloy forms once the reactor reaches a temperature that is above the eutectic point for the metal-silicon. The nanowires that are prepared by using this method are crystalline with diameters of 5 nm and lengths of several micrometers. There are drawbacks associated with the solution growth method. The aspect ratio of NWs that are grown by this method is smaller than those grown by vapor-phase methods. Moreover, the vertical alignment of NWs is poor. The main advantage of this method is the possibility of fabricating nanowires on different substrates at large scales, low cost, and low temperature [17].

2.2.3 Bottom-up fabrication techniques

There are various techniques that have been used in the fabrication of NWs. In this section, the most common NWs fabrication techniques will be discussed.

2.2.3.1 Chemical vapor deposition (CVD)

CVD is one of the most popular techniques that has been used widely to synthesize SiNWs. In the CVD process, an unstable gaseous silicon precursor, such as silane (SiH_4) or

silicon tetrachloride ($SiCl_4$) works as the silicon source and metals that have low eutectic temperature with silicon work as the catalyst. After the gaseous silicon precursor is introduced to the CVD chamber, it cracks into its main components and deposits on the surface of the heated substrate. In order to produce epitaxial uniform SiNWs and to reduce the effect of contamination on the SiNWs growth, the pressure of CVD chamber should be pumped down to high or ultrahigh vacuum to rid the chamber of residual oxygen or water vapor. There are advantages of the CVD technique. The deposition rate of a CVD system is high and can produce films micrometers thick. Moreover, by decreasing or increasing the deposition time, the diameters and lengths of nanowires can be controlled from below 10 nm to several hundred micrometers. The other advantage is the CVD process can not only modify the size of nanowires but also the nanowire properties [16]. However, there is a limitation of CVD system, which is the deposition requires high temperatures of around 600 ˚C and above, and that means the substrates that are used in this system should be able to withstand such of high temperatures. This problem was solved by using plasma enhanced chemical vapor deposition (PECVD) systems which can work at lower temperatures.

PECVD is the most recent CVD fabrication method that has been used for deposition thin films like SiO_2, Si_3N_4 (SixNy), $Si_xO_yN_z$, and amorphous Si films on large area surfaces. Plasma is a gas that has charged particles, positive ions, and negative electrons. Electrons comprise around 50% of the plasma. The PECVD system has two electrodes in parallel configuration and the substrate is placed on the top of the grounded electrode. After the reactive gas is introduced to the chamber, rf energy is applied in order to form plasma between the two electrodes. When the plasma is excited, the reactive gas dissociates to various deposition precursor radicals on the

surface of the substrate to form the desired film. The advantages of the PECVD system are low processing temperature, high film density, and the system easy is to be cleaned [18].

2.2.3.2 Annealing in reactive atmosphere

This technique was used in the 1960s to produce silicon whiskers due to its technical simplicity. In this technique, crystalline silicon first was covered with certain metal impurities, and then it was exposed to reactive gases such as hydrogen, iodine, or bromine. After that, the reactor was heated up to 900 ˚C. When the reactor reaches this temperature, the gases introduced into the chamber decompose into its main components and deposit on the crystalline silicon. The catalyst in this method is the metal- droplet impurity, and the growth process of NWs is similar to the conventional CVD process [16].

2.2.3.3 Evaporation of SiO

Evaporation of SiO is a cost-effective technique that has been used to produce SiNWs on a large scale by the evaporation of solid silicon monoxide SiO. The basic requirement in this method is connecting a two zone tube furnace to an inactive gas supply and small amounts of SiO granulate. The temperature in this technique slopes from 900-1350 ˚C along the tube furnace. At the hot end of the tube furnace, SiO evaporates and flows to the cool side of the tube. At the cooler side of the tube, SiO undergoes of a disproportionation reaction into Si and SiO_2, and that leads to the forming of the nanowires. The synthesis of Si nanowires in this technique is done either with or without a metal catalyst. The growth with the metal catalyst is similar to that of the growth in the VLS mechanism. SiNWs that are grown without the metal catalyst in this technique have various diameters that range from 5 to 100 nm, and they are covered with several tens of nanometers of an amorphous silicon shell [16].

2.2.3.4 Molecular beam epitaxy (MBE)

In the MBE technique, a gaseous beam of silicon atoms is directed onto the substrate where they will be adsorbed and crystalized. To avoid contamination associated with the MBE system, the base pressure of the MBE system should always be pumped down to ultrahigh vacuum. MBE is designed for epitaxial layer-by-layer deposition. Epitaxial Si (111) substrates are usually used for nanowire growth in the MBE technique. There are two disadvantages of the MBE technique. The first one is that the diameters of SiNWs obtained are limited to those that are greater than 40 nm because of Gibbs-Thomson effect. The second disadvantage of this method is the velocity of nanowires growth is low at a few nanometers per minute [16].

2.2.3.5 Laser ablation

Laser ablation is an early method that was used to synthesize SiNWs at high temperature [19]. Laser ablation produces silicon nanowires that are different from those produced by MBE. The nanowires produced by using this technique are ultrathin nanowires with high aspect ratios [16]. In this technique, a mixture of Si and catalyst target is placed in a tube furnace, and then a high-power pulsed laser is used to heat to it to high temperatures around 1200˚C. After, the ablated material cools down through colliding with inert-gas molecules, liquid nanodroplets will be generated due to accumulation of the atoms. The structure of these liquid nanodroplets should be in the same structure as the target, so the final nanoparticles will include both silicon and catalyst material. The growth of SiNWs starts as soon as the catalyst reaches the supersaturation with the Si according to the VLS mechanism, and this process continues as long as the catalyst nanoparticles are still in its liquid state. There are two advantages of laser ablation technique. First, a substrate is not required in this technique. Second, by changing in the structure of the laser target, the structure of the resulting nanowires can be modified [19].

2.2.4 Types of catalysts that have been used for SiNWs growth

Different types of metals have been widely used as catalysts for the SiNW growth. The most common metals are Au, Ag, Al, Cu, Ga, In, Pt, Ti, and Zn. The qualities and conditions of the wires produced by using these catalysts are extremely different; however, they share some common behaviors. These catalysts can be classified into three groups, according to the binary phase diagram. The first group is group A which includes, Au, Al and Ag. The phase diagram of group A has a single eutectic point, and the concentration of Si atoms in the droplets reaches more than 10%. Also, there are no metal-silicide phases in this group. The second group is group B, which includes, In, Ga, and Zn. The phase diagram of this group has a single eutectic point, but the Si concentration in the droplet is less than 1% with no silicide phases. The third group is group C, which includes, Cu, Pt, and Ti. In the phase diagram of group C, the silicide metals were found with a eutectic temperature that exceeds the 800˚C [20].

In this study, the growth of SiNWs was done by using Au and Al as catalysts. In the next sections, more details will be discussed about these two metals.

2.2.4.1 Gold

Gold (Au) is the first, and most common, metal that has been used widely for SiNW growth. There are reasons behind this wide use of Au for the growth of Si nanowires. One of these reasons is the availability of Au. Moreover, equipment that is used for Au deposition can be found in the semiconductor industry. Another reason is that Au has high chemical stability which means that it does not oxidize when exposed to the air. This leads to reduction in the high vacuum requirements on the growth system. Moreover, Au is a nontoxic metal which gives it advantage in safety. Furthermore, the eutectic temperature for Au-Si is low with high solubility

of Si in Au about 19% (see Figure 2.4). Also, the surface tension of Au-Si alloy is high enough tension required to have a stable droplet-nanowire. All of these properties give the Au the advantages to be a preferable catalyst [16].

2.2.4.2 The growth of SiNWs using Au as a catalyst

The first use of gold as a catalyst for the SiNW growth by using VLS mechanism was by Wagner and Ellis in 1964 [21]. Gold impurities were placed on a <111> Si substrate, and annealed the substrate at 950 ˚C. After the annealing, an alloy of small droplets of Au-Si would be formed. After a mixture of H_2 and $SiCl_4$ were introduced to the chamber, the silicon atoms diffused into the liquid alloy of Au-Si forming whiskers with 1000 Å length in the <111> direction. After the success in using gold as a catalyst for the fabrication of whiskers or nanowires, different types of metals such as, Pt, Ag, Pd, Cu, and Ni were used to synthesize nanowires using VLS mechanism [21].

Au can be used as a catalyst in the fabrication of SiNWs using the solid-liquid-solid mechanism (SLS) which is different from the VLS mechanism described above. The growth of SiNWs in the SLS mechanism was done without the need to use silane gas. The growth just depends on the silicon in the substrate. In the SLS mechanism, gold was deposited on the silicon substrate using a sputter coater and then the coated silicon was annealed at temperature of 1000˚C for 2 hours in a quartz furnace with a flow of nitrogen gas to reduce the effect of oxygen in the chamber. During annealing, the Au particles diffused into the substrate gradually, and SiNWs start to grow until the Au reaches saturation in Si [22].

SiNWs have been synthesized by using various types of bottom-up techniques. PECVD is one of the chemical vapor deposition techniques that has been used lately for SiNWs growth due to its low processing temperature.

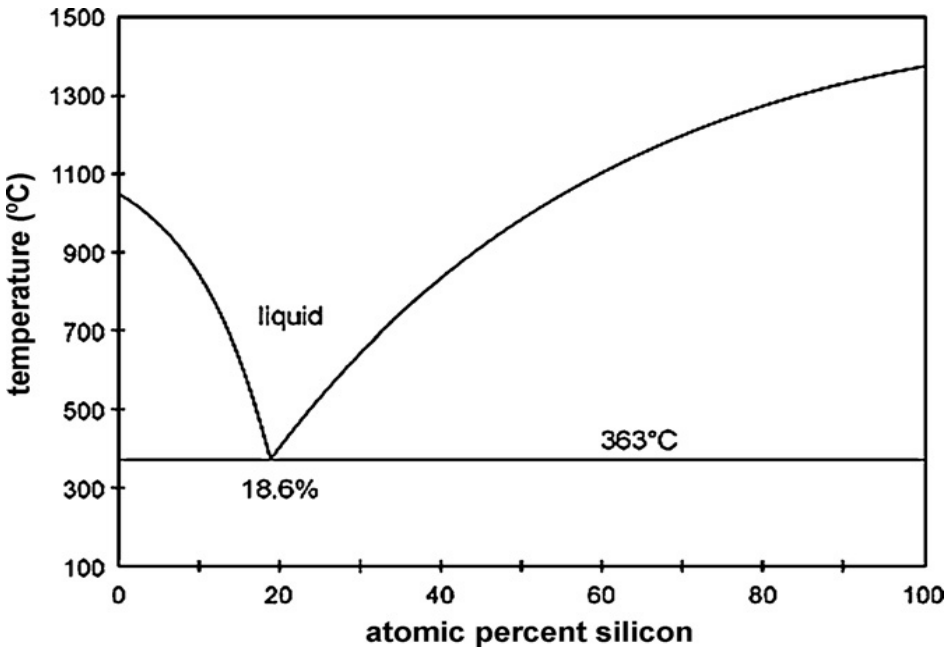

Figure 2.4. Binary phase diagram of Au-Si alloy [21].

Hofman and colleagues used the plasma enhanced CVD to synthesize SiNWs using gold as a catalyst [23]. They used Si <100> substrates that were coated with Au film. The Au film was heated up to 380˚C under vacuum, and then silane gas was introduced to the chamber for growth purpose. They used 13.6 MHz rf plasma in order to increase the growth rate. The deposition time and pressures were maintained between 15-90 min and 0.4 - 2.4 mbar, respectively, with 10 watts rf power. They studied the effect of different thickness of gold on the SiNW structures. They found that as the thickness of the gold film decreases, the diameters of the obtained SiNWs decreases [23].

Another group did the synthesis of SiNW at temperature below Au-Si eutectic temperature by using very high frequency plasma enhanced CVD (VHF-PECVD). The growth temperatures ranged from 230 ˚C to 363 ˚C. They reported that the growth of resultant SiNWs was not homogenous as the temperature decreased, and at 230 ˚C they observed no growth of SiNWs [24].

2.2.4.3 Aluminum

In spite of the advantages that gold has, there is a one serious drawback associated with Au; Au causes a potential detrimental contamination in the nanowires. Au is a deep-level defect in Si which affects the carrier lifetime and enhances the charge-carrier recombination [25]. Aluminum has attracted the attention as an alternative catalyst in place of Au due to some good properties that Al has. One advantage of aluminum is that it is not a deep-level defect in Si. Rather, aluminum is a p-type dopant. So, the nanowires that are expected to grow by using aluminum as a catalyst are heavily doped p-type. Furthermore, Al is cheap, nontoxic, and a readily available metal – the third most abundant element in the earth crust [26]. However, there is a drawback of using Al, as a catalyst, which is its high sensitivity to oxygen. Therefore, the prevention of Al oxidation during the whole growth process is required, and that limits the usability of Al. The binary phase diagram of Al is close to the Au phase diagram. According to the Al-Si binary phase diagram, the eutectic point of Al-Si is 577 ˚C which is higher than that of Au with a lower Si concentration of about 12%. Figure 2.5 shows the binary phase diagram of Al-Si alloy [20]. Since Al readily forms a self-limiting but very sturdy surface large of Al_2O_3 even in the presence of trace amount of O_2 or H_2O, the deposition chamber must be pumped down to a very high vacuum. A UHV-CVD with a background of 10^{-10} mbar has been used during the growth of SiNWs using Al nanoparticle as catalyst [20].

2.2.4.4 The growth of SiNWs using Al as a catalyst

Vapor-liquid-solid mechanism has been used by some groups to synthesize the SiNWs. Kohen et al. [26] did the growth of SiNWs at 600 ˚C which is above the eutectic temperature of Al-Si (577˚C) by using the CVD reactor.

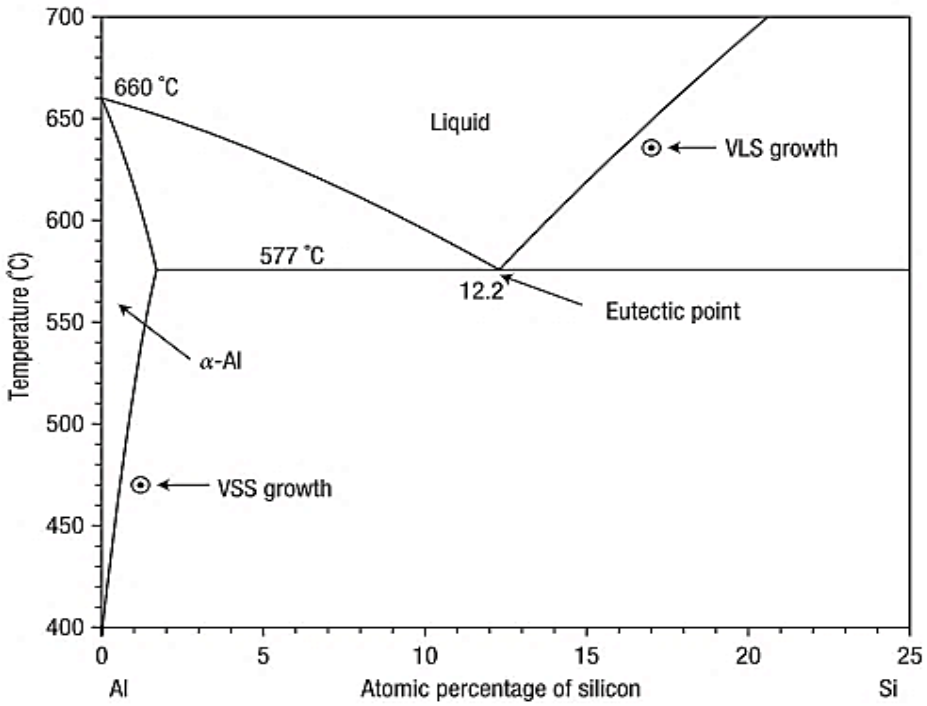

Figure 2.5. Binary phase diagram of Al-Si alloy [19].

They found that the growth temperature of 600 ˚C leads to vertical SiNWs, while the growth at 550 ˚C, which is less than the eutectic temperature of Al-Si, results in curled SiNWs that orient randomly. Also, they studied the effect of the silane partial pressure on the morphology and crystallinity of the resulting SiNWs [26].

Wang et al. [27] grew SiNWs using Al as catalyst on Si (111) substrate under vapor-solid-solid mechanism at a temperature range between 430-490 ˚C. But, before the SiNW growth, they annealed the Al film for 20 min at 580 ˚C so that the Al film breaks down into a distribution of Al-Si nanodots. They studied the effect of temperature on the growing nanowires. They found that as the growth temperature is increased, the tapering of the nanowires is increased [27]. Moutanabbir et al. [28] followed the same procedure that Wang et al. used in the growth of SiNWs except that the growth temperature was lower at around 410 ˚C.

Chapter 3: Equipment and Experimental Procedures

This chapter includes the equipment and the experimental procedures that were used during the fabrication of the solar cell device in this research.

3.1 Equipment

Equipment that was used in this is divided into two sections. The first section is the deposition equipment and the second section is the characterization equipment.

3.1.1 Deposition equipment

The fabrication of p+ polySi substrate and SiNWs using Al and Au as catalysts were accomplished in lab 350A at the University Arkansas Engineering Research Center (ENRC). The two deposition systems that are available in this lab are MVSystems, Inc (MVS) and GSI, Inc system (GSI). GSI system is also called hot wire chemical vapor deposition system (HWCVD)

3.1.1.1 MVSystem (MVS) Tool

The MVSystem or multi-chamber system consists of five chambers or MPZs. MPZ1 and MPZ2 are plasma enhanced chemical vapor deposition systems that are devoted to deposit a thin film of intrinsic a-Si and doped a-Si, respectively, by using plasma ambient for the reactions inside the chamber. MPZ3 and MPZ4 are devoted for sputtering Si and AZO thin film, respectively. MPZ5 is the electron beam evaporator system that is used to deposit thin films of different metals, such as, Al, Au, Si, Ni and Ag. In the center of the MVS, the intermediate transfer zone (ITZ) connects to all of these MPZs. The ITZ is pumped down to 4 mTorr using a mechanical pump. The samples were transferred from the loading zone (MPZ6) to the other MPZs using a robotic arm that can be set by using a controller. Figure 3.1 is a photograph of a

front view of the MVS. For this study, MPZ2, MPZ4, and MPZ6 were used for deposition. In the next sections, more details will be provided to describe these three MPZs.

Figure 3.1. A photograph for multi-chamber system (MVS).

Figure 3.2 shows the schematic diagram of the MVS in the lab had been configured to deposit thin films using either plasma enhanced or hot wire chemical vapor deposition (PECVD or HWCVD). GSI system or hot wire chemical vapor deposition system (HWCVD) is used for depositing a polycrystalline or crystalline silicon film due to its capability to reach high temperature of just above 750 ˚C. More details about the HWCVD system will be mentioned later in this chapter

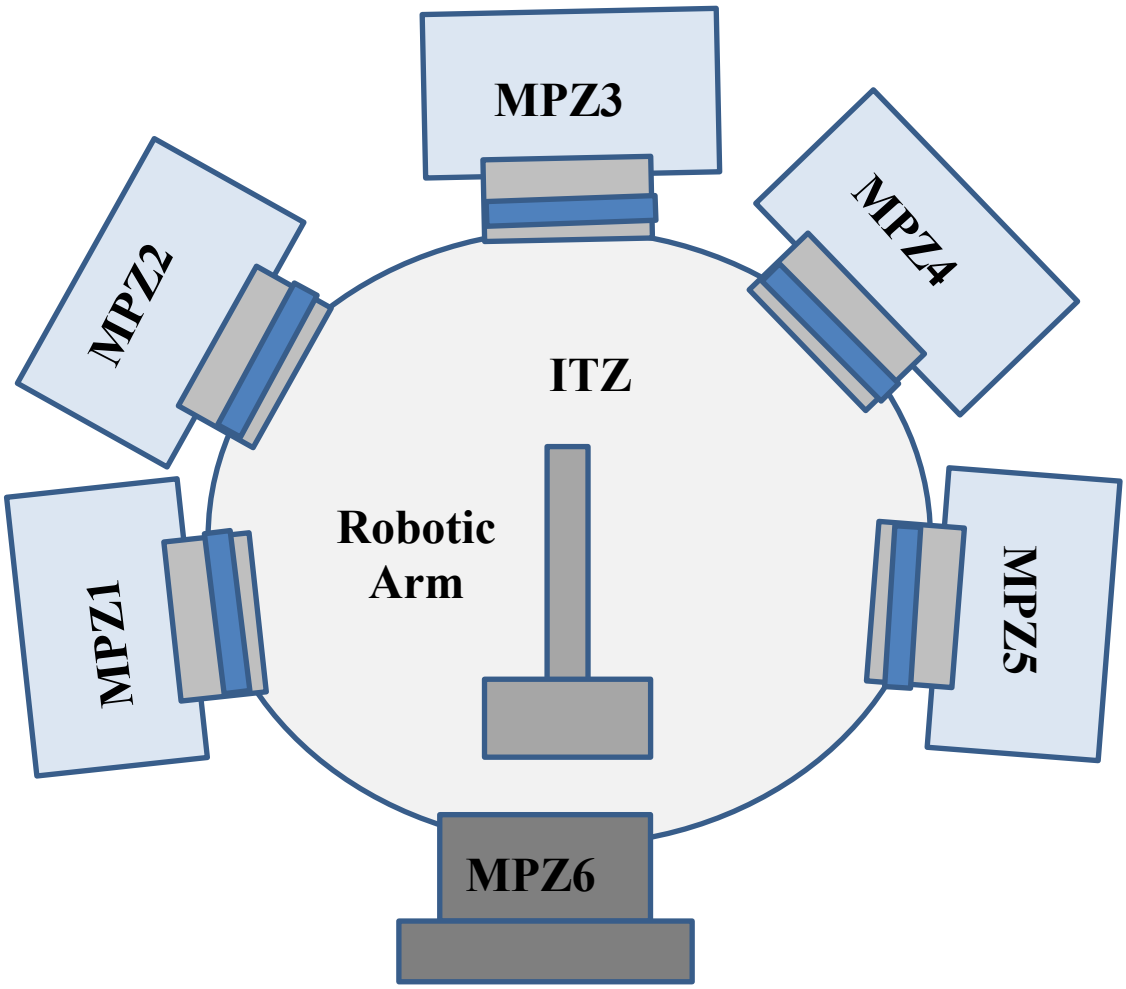

Figure 3.2. Schematic diagram of multi-chamber system MVS.

3.1.1.1.1 Plasma enhanced chemical vapor deposition (PECVD)

MPZ2 is the PECVD system used for chemical vapor deposition by using plasma. Figure 3.3 shows a schematic diagram of the PECVD system used in this research. MPZ2 system was used to deposit amorphous silicon (a-Si) on the ITO/glass and glass substrates and to grow SiNWs by using Au and Al as catalysts. MPZ2 has a heater located underneath the upper cover of the MPZ2 called the well. A thermocouple attached to the well through a controller measures the temperature at that point. Samples are placed on the substrate holder which sits just below the heater well inside the PECVD. The distance between the heater and substrate holder is around 5

cm. Therefore, the temperature that is read by the controller is not the actual substrate temperature.

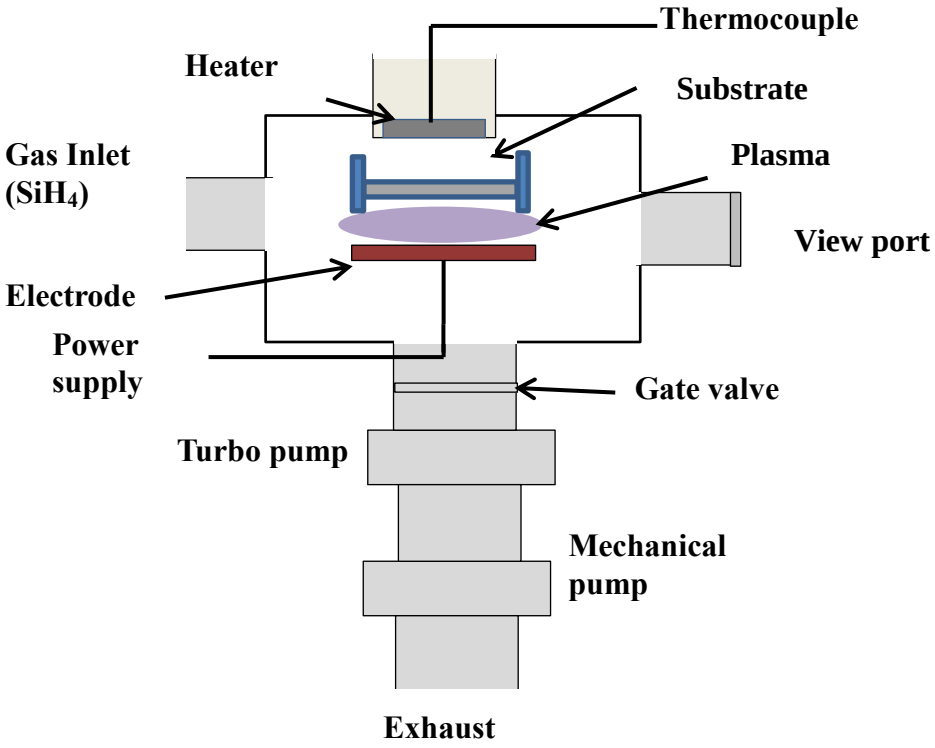

Figure 3.3. Schematic diagram of the PECVD system.

A calibration chart that was obtained by Dr. Husam [29] about two years ago that showed the actual substrate temperatures that were measured by using a thermocouple attached to the substrate holder versus the well temperatures that were read by the controller. Figure 3.4 shows the calibration between the actual substrate temperature and the well temperature.

The rf electrode sits just below the substrate holder, and it is connected to the power supply. Turbo molecular and mechanical pumps are connected to the bottom of the MPZ2 chamber to evacuate the system down to the 10^{-8} Torr. Plasma is created after the silane (SiH_4)

gas is introduced to the chamber by applying rf power. Figure 3.5 shows photographs for different parts of the PECVD system that were described above.

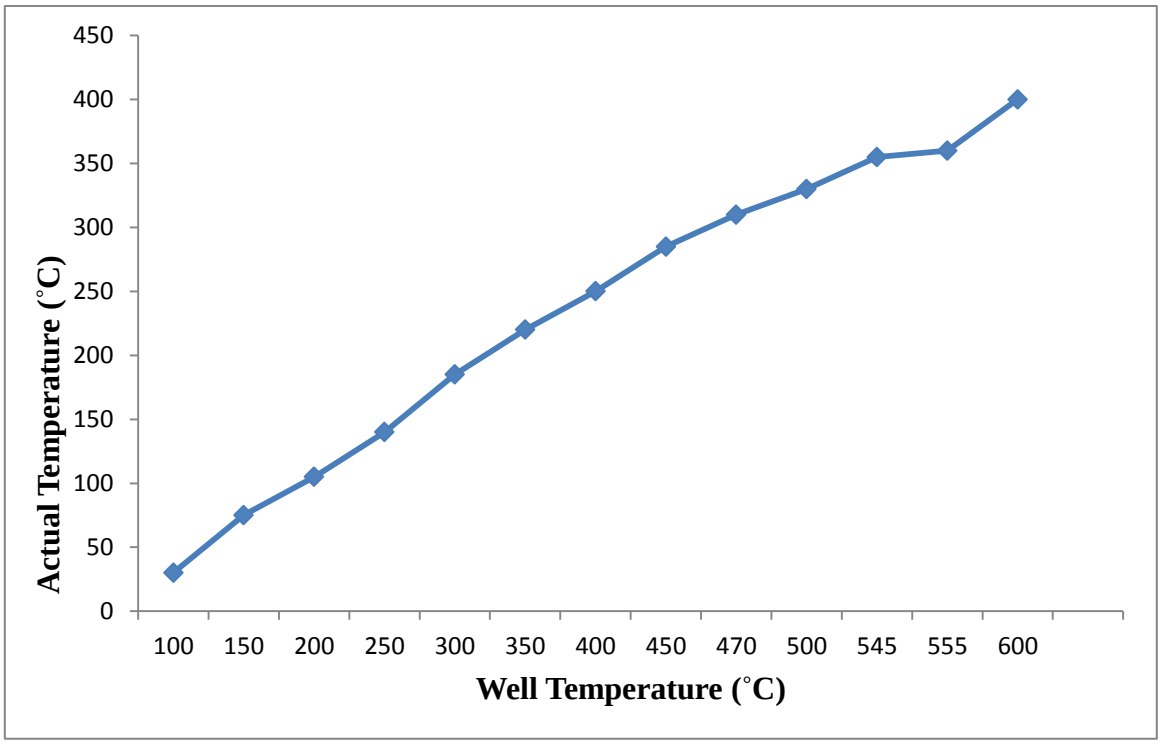

Figure 3.4. Relationship between the well temperature and actual substrate temperature of PECVD system.

3.1.1.1.2 Electron-beam evaporator system

Electron-beam evaporator (EBE) or MPZ5 is a system which is used for physical vapor deposition. In this study, EBE was used for depositing Au and Al film on c-Si, glass, and ITO glass substrates. EBE system can be divided into two parts, a deposition part and controller part. The deposition part located within the MVS system which is called MPZ5. MPZ5 is a big cylindrical chamber pumped by a turbo molecular / scroll pump stack, which contains the quartz crystal, temperature and pressure sensors, substrate stage, halogen lamps, four crucibles, electron gun and shutter. The substrate holder is placed under the halogen lamp in the upper part of the

chamber. The thermocouple touches the substrate holder to measure its temperature. The highest temperature the halogen lamp can reach is around 650 ˚C

.

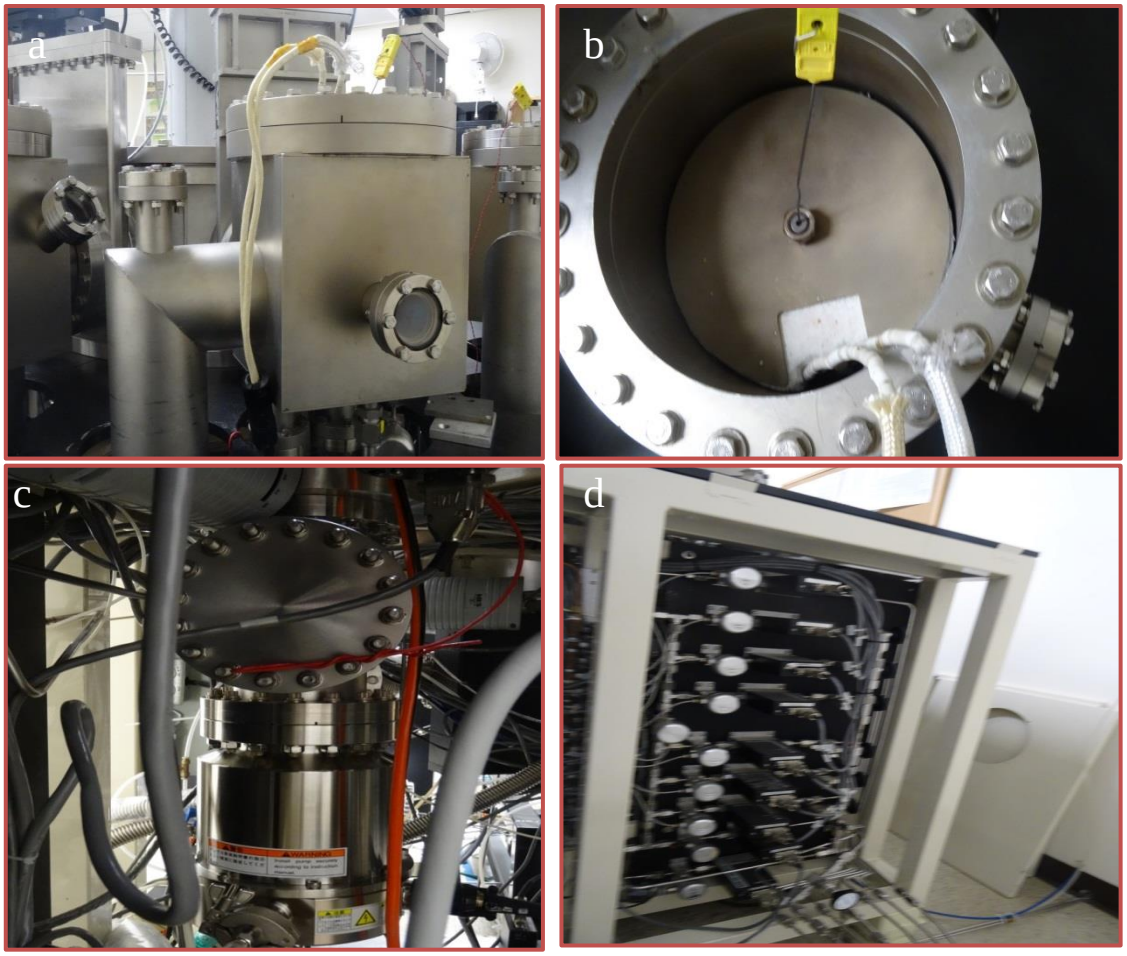

Figure 3.5. Photographs for different parts of PECVD system: a. side view of PECVD showing a viewing port and the pumping port; b. top view of the heater well (notice the TIC connect to the well; c. turbo-molecular pump shown here delivers a base pressure of 10-8 before gases are introduced for deposition of PECVD; d. the gas manifold that is used to control the supply of SiH4 and other gases (N2, H2, Ar).

The quartz crystal sensor was placed between the substrate and the crucible to measure the thickness and the deposition rate during the deposition process. The electron gun is placed near the bottom of the chamber.

When the power supply is turned on and set up to 7.8 kV, electrons are emitted out of the filament as an electron beam and go directly to hit the source material inside the crucible by the effect of magnetic field and melt the sources to make them evaporate. The source materials that are placed in the crucible are Al, Ag, Si, and Au. Turbo molecular and mechanical pumps are connected to the bottom of the chamber to evacuate the EBE system to a high vacuum of about $1x10^{-8}$ Torr (2.3 mbar).

The other part of the EBE system is the controller. This part includes SQC- 310 deposition controller, source controller, XY programmable sweep controller, electron beam power supply, heater controller, crucible controller, and throttle valve controller. Each controller has its own function. The setting of the parameters for any deposition process can be done by the SQC- 310 deposition controller. It has a main menu in which the desired processes and film conditions for each process, such as thickness, deposition rate, maximum power, ramps and soak times can be programmed. Shutter is connected to the deposition controller, so that when the deposition process is started or finished, the shutter automatically moves away or toward the crucible, respectively. The crucible controller is a switch having four positions numbered 1 to 4. Each number refers to a source inside the crucible; for Al is numbered one, 2 for Ag, and 3 and 4 for Si and Au, respectively. Figure 3.6 shows the schematic diagram of the EBE system.

3.1.1.1.3 Sputtering system

The sputtering system, or MPZ4, is also located within the MVS. The configuration of MPZ4 is similar to MPZ2 except that a target works as a negative electrode to attract the positive ions of Ar gas (see Figure 3.7).

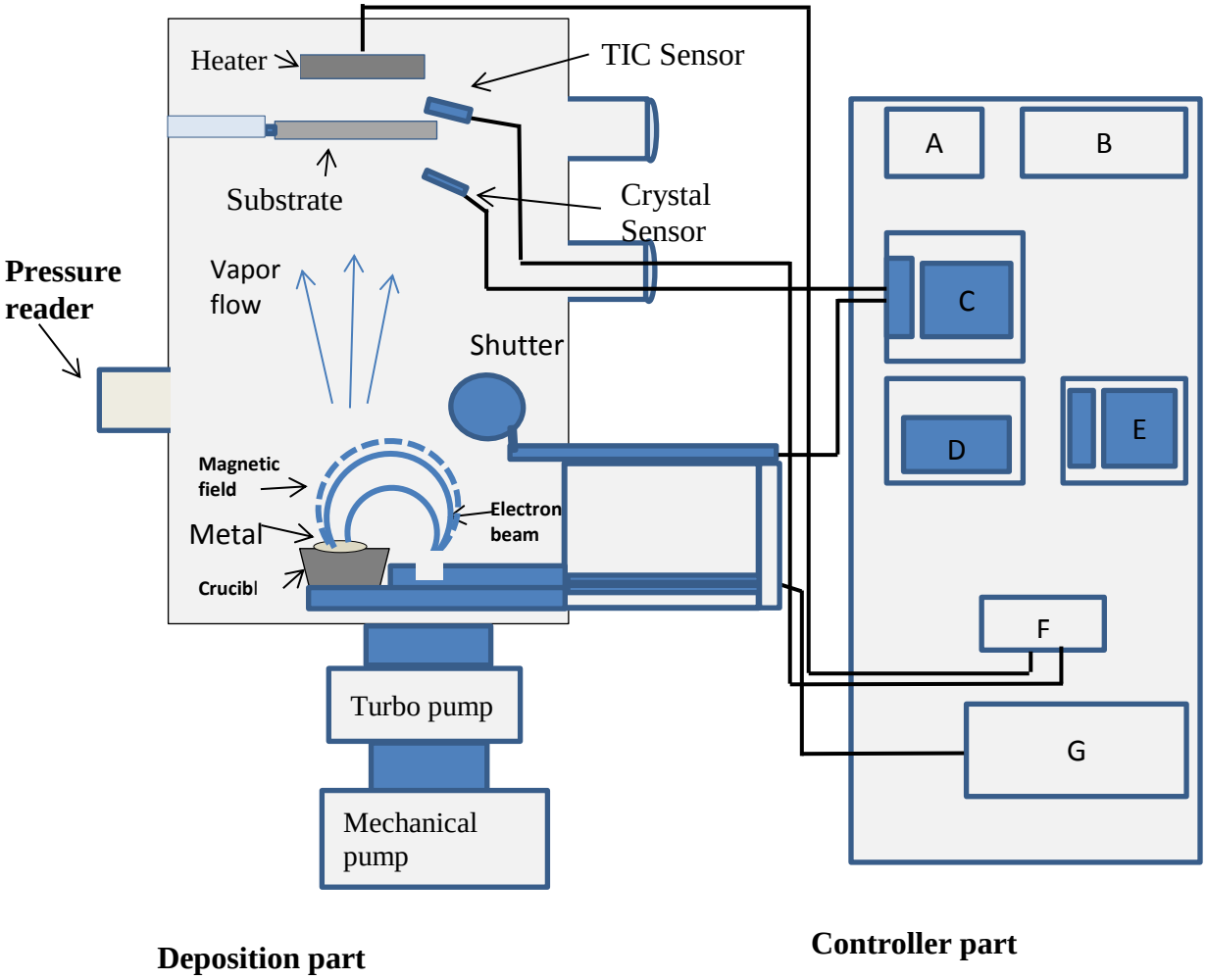

Figure 3.6. Schematic diagram of E-beam evaporator system. The letters in the controller part refer to: A. throttle valve, B. crucible switches, C. deposition controller, D. XY sweep controller, E. source controller, F. heater controller, and G. power supply.

The substrate holder is placed on the upper part of MPZ4. The heater is placed above the substrate holder within a distance of 5 cm from the substrate holder. The target was positioned under the substrate holder so that the target atoms deposit on it during the deposition process. The target consists of aluminum doped zinc oxide (AZO) which contains 98% of ZnO and 2% of Al_2O_3. Turbomolecular and mechanical pumps are connected to the MPZ4 chamber to pump the down to $4x10^{-8}$ Torr.

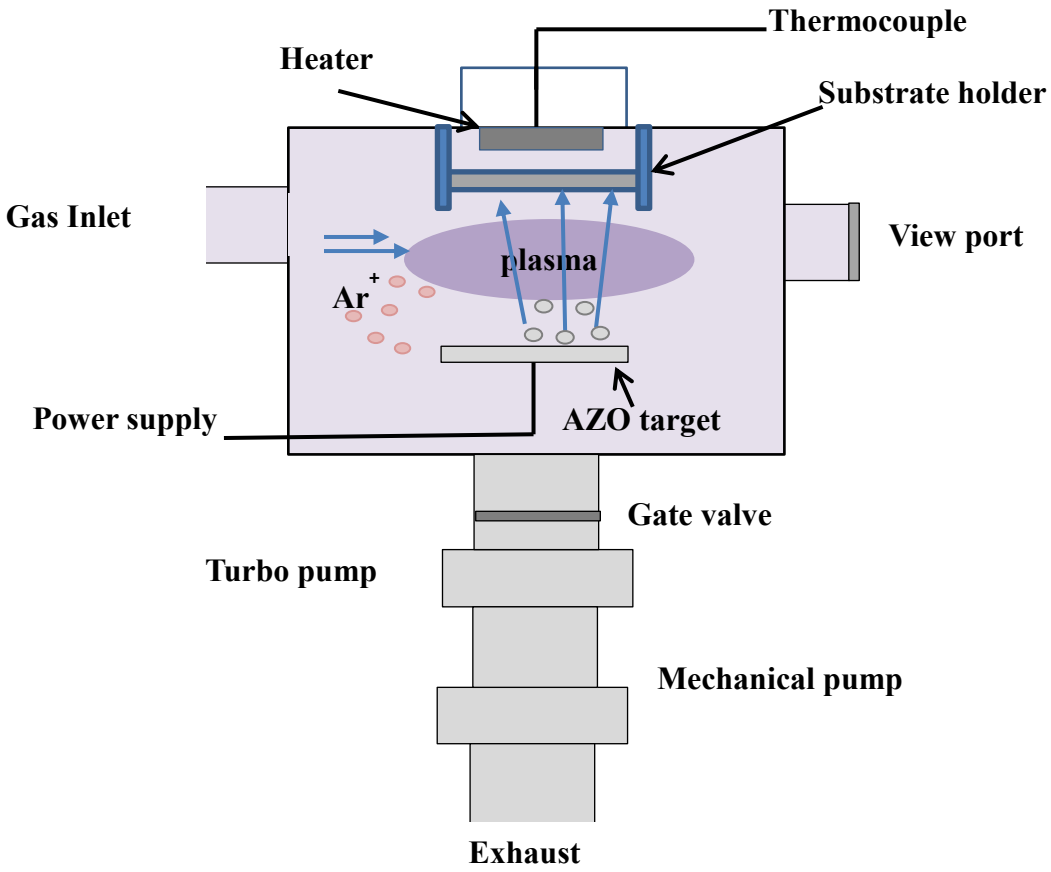

Figure 3.7. Schematic diagram of sputtering system (MPZ2).

The sputtering process is a physical vapor deposition process. The process in brief is after the MPZ4 chamber pumps down to high vacuum, 15-20 sccm of Ar gas is introduced to the chamber. When 100-150 watt of power is applied to the target by the power supply, the Ar molecules become ionized and plasma is formed along the magnetic field. The free electrons in the plasma hit the Ar atoms and convert them to positive ions and secondary electrons. Continuously, these positive ions are accelerated toward the negatively charged target. After the argon ions hit the target surface, the energy of these ions transfers to the target atoms. Therefore,

these atoms will be ejected from the target toward the substrate at different angles to form the thin film on the substrate [30].

3.1.1.2 Hot wire chemical vapor deposition system (HWCVD)

HWCVD systems have been used for the fabrication of high quality crystalline silicon and polycrystalline silicon, and a-Si thin films. The HWCVD system has a chamber in which the deposition of the thin films occurs. The substrate holder is directly attached to the chamber's lid which is connected to a thermocouple and a heater. A tungsten filament is placed under the substrate holder to crack the precursor gas into its main components when power is applied to the filament. The chamber of the HWCVD system is connected to turbomolecular and mechanical pumps to evacuate the chamber down to $7x10^{-4}$ mTorr. A gate valve was placed between the turbo pump and the chamber to isolate the chamber from the pumps during the venting and purging of the chamber. Figure 3.8 shows a schematic diagram of HWCVD system.

A throttle valve was connected to the chamber to control the chamber pressure during the deposition. A gas manifold system was next to the chamber, and it includes the mass flow controller to feed the chamber with gases like SiH_4, H_2, N_2, and Ar. These gases can be controlled by switches that were specialized for each gas. A program in a computer was used for setting some parameters like chamber pressure by closing and opening the throttle valve. There are mass flow controllers for each gas in which the amount of the desired gas can be determined except SiH_4 which had its own controller placed separately from the other gas controllers. Substrate temperature can be set by the substrate controller. The highest temperature the substrate can reach is 750 ˚C.

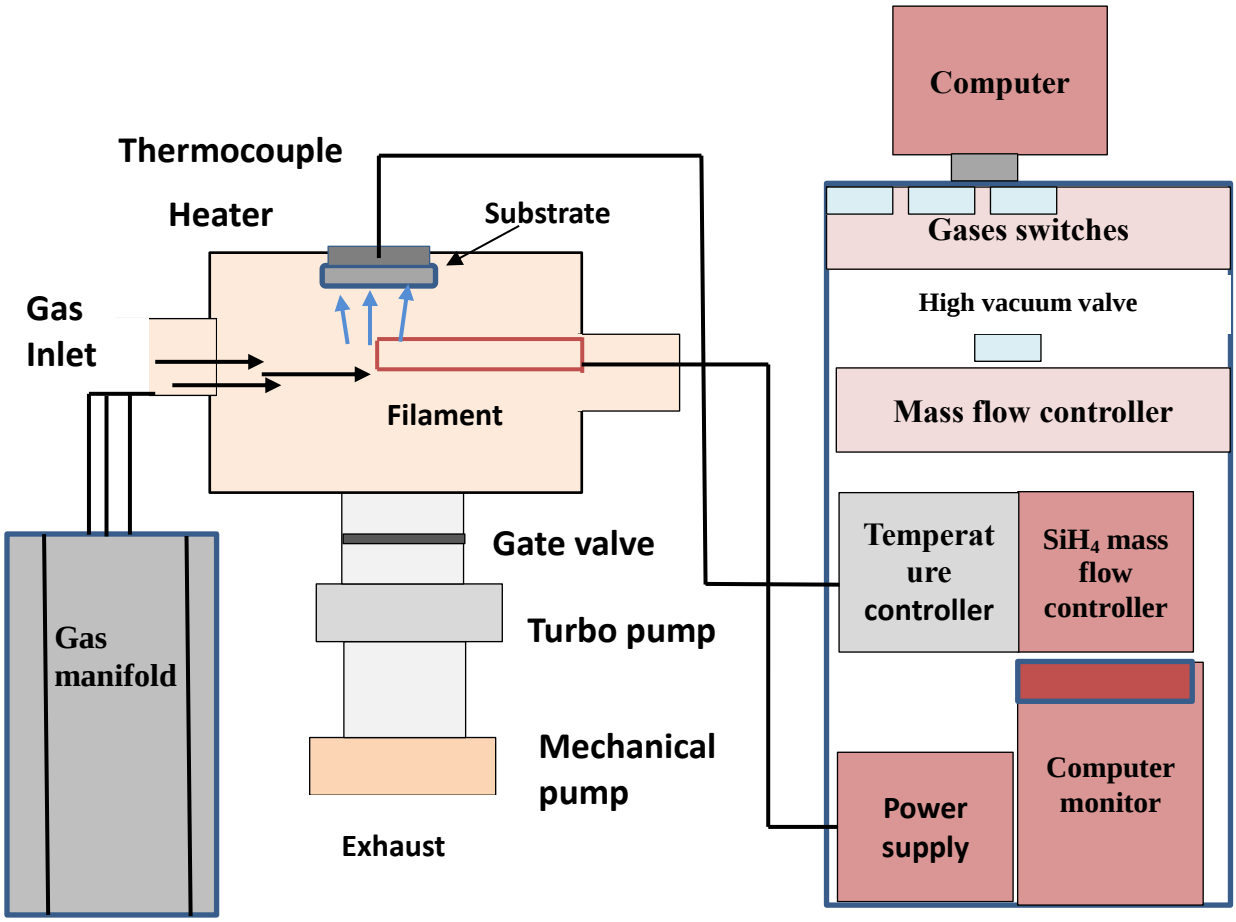

Figure 3.8. Schematic diagram of HWCVD system.

3.1.2 Characterization tools

3.1.2.1 Scanning electron microscope (SEM)

In this study, most of the samples were analyzed in the FEI NOVA NANOLAB DB SEM/FIB. SEM is a tool that is used to examine objects with a very accurate scale by using a beam of highly energetic electrons. The information that can be yielded out of this examination is related to the topography, morphology, composition, and crystallography of the objects. A typical SEM consists of electron column, scanning system, detector, display, vacuum system, and electron controls. The main components of electron column are electron gun and two or more electromagnetic lenses [31].

The purpose of the electron gun is to produce free electrons and speed up these electrons to energies of 1-40 keV in the SEM. In order to form an acceptable image by an SEM, an electron beam with a diameter of less than 10 nm can be generated at the surface of the specimen with sufficient current [32].

After the scanning coils scan the surface of the specimen with electron beam, electron beam is then focused into a fine probe in order to produce the images. An Electromagnetic radiation signal is emitted after each point of the specimen is hit by the accelerated electrons. After the detector collects a portion of the electromagnetic radiation (secondary or backscattered electrons), the output is used to modify the brightness of a cathode ray tube (CRT) in which its x- and y- inputs are related synchronously with the x-y voltage of electron beam. Figure 3.9 shows the schematic diagram of SEM system.

The magnification (M) of the image can be represented by equation below:

$$M=L/I \qquad \text{(Equation 3.1)}$$

where L and I represent the raster length of the CRT monitor and the raster's length on the surface of the sample respectively [31]. The images created usually by the SEM are secondary electron images, backscattered electron images and elemental x-ray map. The secondary and backscattered electrons can be determined according to their energies. When the emitted electrons have energy that is less than the 50 eV, it is called secondary electrons, and when it exceeds the 50 eV, it is called backscattered electrons

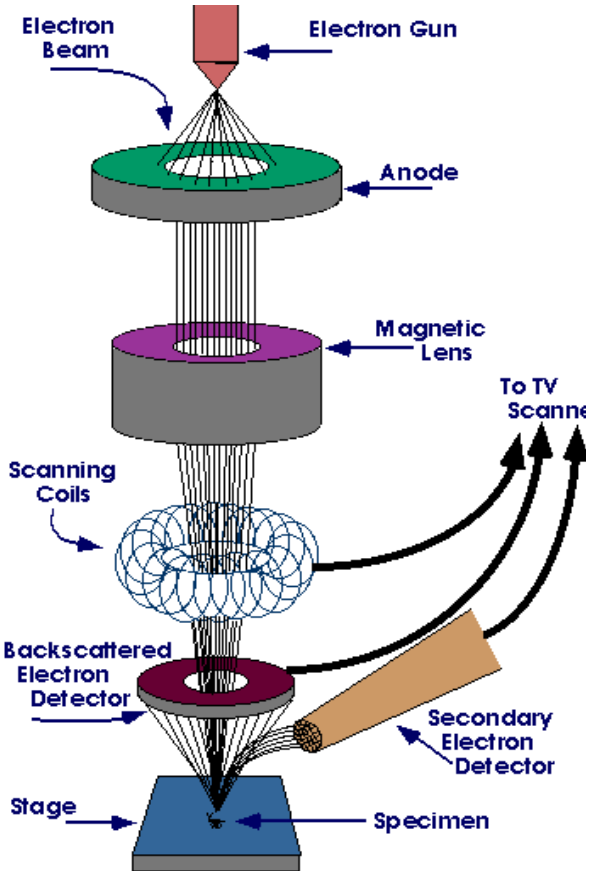

Figure 3.9. Schematic diagram of scanning electron microscope [31].

The approximate depth that the electron beam can interact with the specimen is 1 µm. Wide variety of radiation is created due to complex interaction of the beam electron with the specimen's atoms. To prevent any contamination, the vacuum of the specimen should be compatible with the vacuum of the SEM which is about 10^{-5} torr. The two special types of the SEM are variable-pressure SEM (VP-SEM) and environmental SEM (ESEM) [32].

3.1.2.2 Transmission electron microscope (TEM)

A Titan TEM was used to analysis the morphology of the SiNWs in this study. TEM can be used to see the structure and atomic column of the specimen, and that leads to information

about the composition and crystallography of the specimen. In the TEM, an electron beam interacts with the specimen while passing through it. These electrons are emitted by the source, and then magnified by a system of magnetic lenses. The two condenser lenses confine the electron beam and control its brightness [32].

After the electron beam passes the condenser lens, it passes through the condenser aperture to hit the surface of the sample. The transmitted beams are formed after they are scattered elastically and pass through the objective lens to form the image in the display. The electron beams go to the magnification system that consists of three lenses. The first and second lenses control the magnification of the image, while the objective lens helps to expand the beam onto a fluorescent screen or a computer monitor. The preparation of the sample should be very precise and may need several efforts to get good results. The specimen should be less than 100 nm thick due to the strong effects of the interaction of the electrons and matter. The sample is stuck on a holder using glue. A hole should be made in the center of the sample to enable the TEM to get data from the edge of the hole. This hole is made using ion thinning. The embedded sample can be covered with a metal deposition layer to reduce the damage that might be associated with the focus ion beam milling [31].

3.1.2.3 van der Pauw technique for Hall effect and resistivity measurements

This technique proposed by van der Pauw in 1958, was used for measuring resistivity, mobility, and carrier concentration for the poly-Si thin film.

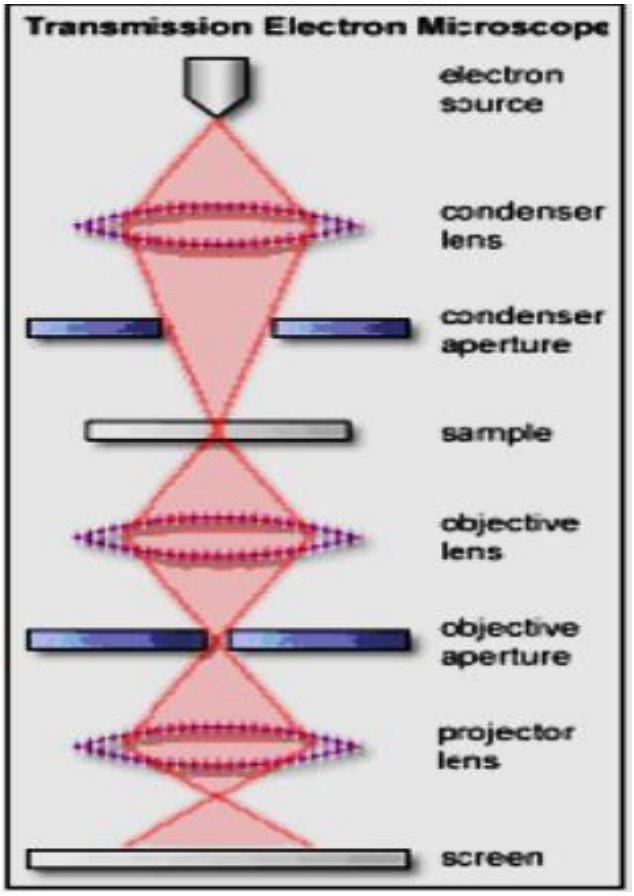

Figure 3.10. Schematic diagram of transmission electron microscope TEM [31].

The sample thickness should be thinner than its width. Four very small Ohmic contacts should be placed on the corners of the sample before starting the measurement (see Figure 3.11.a). In order to calculate the resistivity (ρ), the sheet resistance, R_S, should be obtained from

$$\rho = R_S \, d \qquad \text{(Equation 3.2)}$$

As shown in the van der Pauw equations below, there are two characteristic resistances that are related to the sheet resistance, R_A and R_B:

$$\exp(-\pi R_A / R_S) + \exp(-\pi R_B / R_S) = 1 \qquad \text{(Equation 3.3)}$$

$$R_A = V_{41}/I_{12} \qquad \text{(Equation 3.4)}$$

$$R_B = V_{43}/I_{23} \quad \text{(Equation 3.5)}$$

V_{43} can be determined by applying a dc current I into contact 1 and out of contact 2, and then by measuring the voltage V_{43} from contact 4 to contact 3 as shown in Figure 3.11 (b). By applying current into contact 4 and out of contact 2, V_{14} can be measured from contact 1 to contact 4. By using the numerical solutions for Eq.3.3, R_S can be calculated [33].

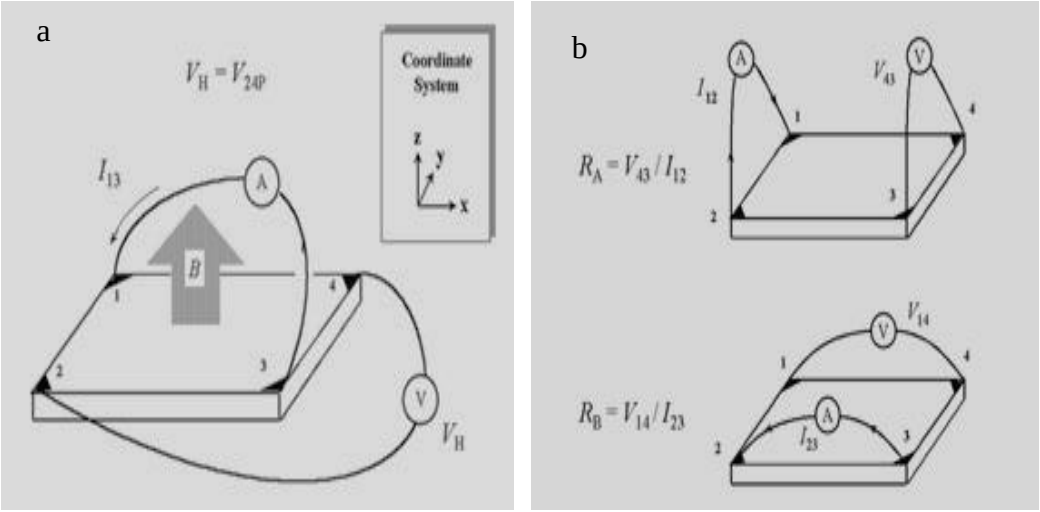

Figure 3.11. Hall effect measurements for a sample [33].

Various parameters such as Hall voltage, carrier mobility, carrier concentration, Hall coefficient, resistivity, magnetoresistance and conductivity type (n or p) can be determined by using Hall effect measurements. In order to find the carrier sheet density, n_s, and mobility, μ, of the sample, Hall voltage (V_H) should be found first according to:

$$n_s = I\,B/q|V_H| \quad \text{(Equation 3.6)}$$

$$\mu = |V_H| / R_s\,IB \quad \text{(Equation 3.7)}$$

I, B and q, the current, magnetic field and the charge of electrons of the sample, respectively, can be calculated from the Hall voltage. Hall voltage is the transverse voltage which is created perpendicularly to the combination of the magnetic field and current along the sample. For n-type semiconductors, Hall voltage is negative and for p-type semiconductors it is positive. By applying current through the opposite pair of contacts, 1 and 3, the Hall voltage, $V_H = (V_{24})$, can be measured from the remaining two pairs of contacts 3 and 4 as in Figure 3.11 (a). The carrier conentration (n) and carrier mobilty (μ_m) were calculated from:

$$R_H = 1/qn \quad \text{(Equation 3.8)}$$

$$\mu_m = R_H / p \quad \text{(Equation 3.9)}$$

Where R_H is the Hall coeffcient, q is the electron charge, and p is the carrier concentartion [33].

3.1.2.4 Raman spectroscope

Raman spectroscope was used to measure the crystallinity of the thin film that was fabricated on ITO/glass or glass substrate. Figure 3.12 shows the schematic diagram for Raman spectroscopy setup [34].

In general, Raman spectroscope is a technique that is based on inelastic scattering of monochromatic light such as a laser source. The meaning of inelastic scattering is that the frequency of photons in the monochromatic light changes during the interaction with the samples. After the laser light photons are absorbed by the sample, they will be re-emitted. The shifting up and down in the frequency of the re-emitted photon is called the Raman effect. Rayleigh, or elastic scattering, means that the majority of the scattered light is at the same frequency of the excitation light. The interaction of incident electromagnetic waves and the vibrational energy levels of the molecules in the sample lead to shift of a very small amount of the scattered light energy from the laser frequency. Some information such as vibrational,

rotational and other low frequency transitions in molecules can be provided by this shifting. Solid, liquid, and gaseous samples can be studied by using Raman spectroscopy [35].

The five major components of Raman spectroscope are the excitation source (laser), sample illumination system and light collection optics, wavelength selector (filter or spectrophotometer), detector (photodiode array, CCD or PMT) and display (computer). After the sample is placed on the sample holder, it is illuminated with a laser beam in the ultraviolet (UV), visible or near infrared range. After the lenses collect the scattered light, the light is sent to the interference filter or spectrophotometer to get the Raman spectrum of the sample [35].

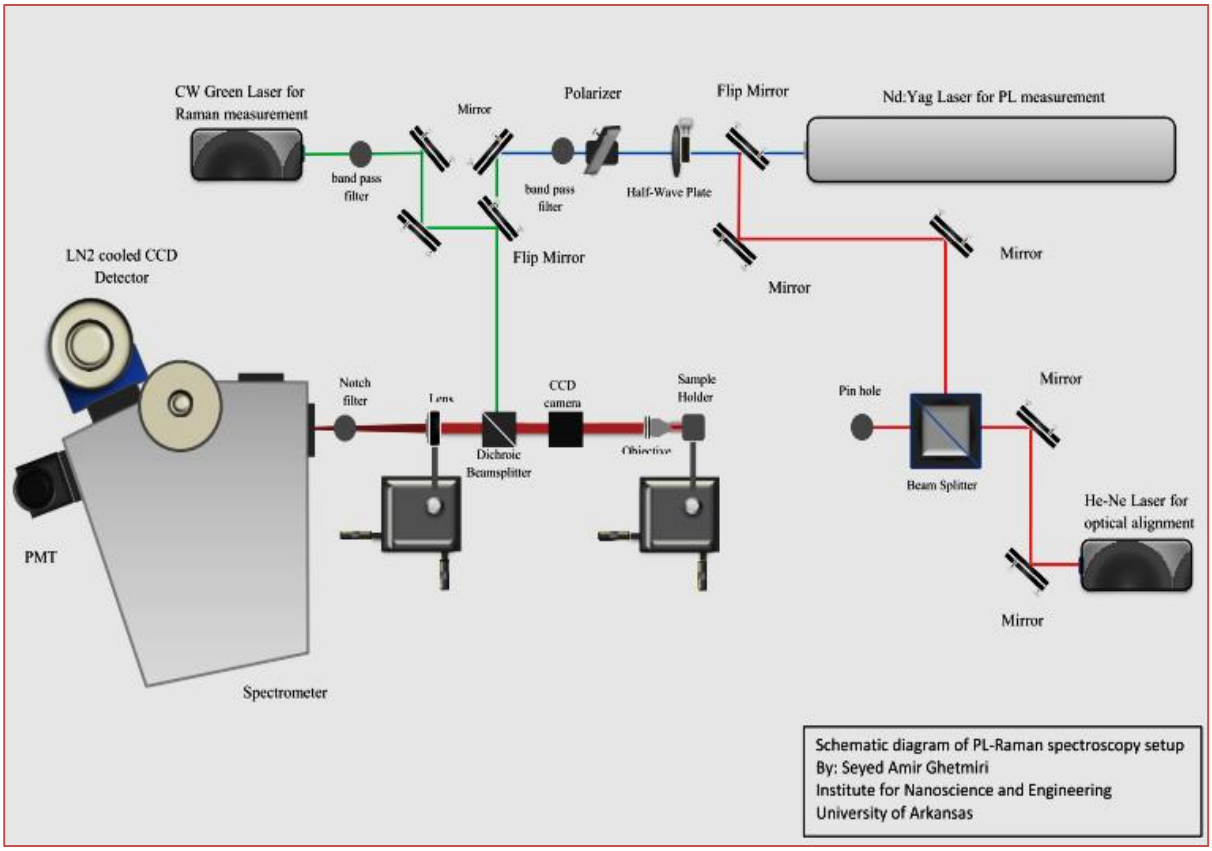

Figure 3.12. Schematic diagram of Raman spectroscope setup [34].

3.1.2.5 Nikon optical microscope

A Nikon optical microscope was also used for characterization purposes. The general use of any optical microscope is to magnify images of small samples by using visible light and a group of lenses. The Nikon microscope is considered as a digital microscope that used a CCD camera in addition to eyepieces for the sample investigation. The images in the Nikon microscope are shown directly in the computer screen so that the images can be shown easily and clearly, and can be saved [35].

The main components of optical microscope are eyepieces, objective lenses, stage and illumination source (see Figure 3.13). The eyepieces are cylinders that have one or more lenses to focus the images to the eyes. The most common magnification values for eyepieces are 5x, 10x and 20x.

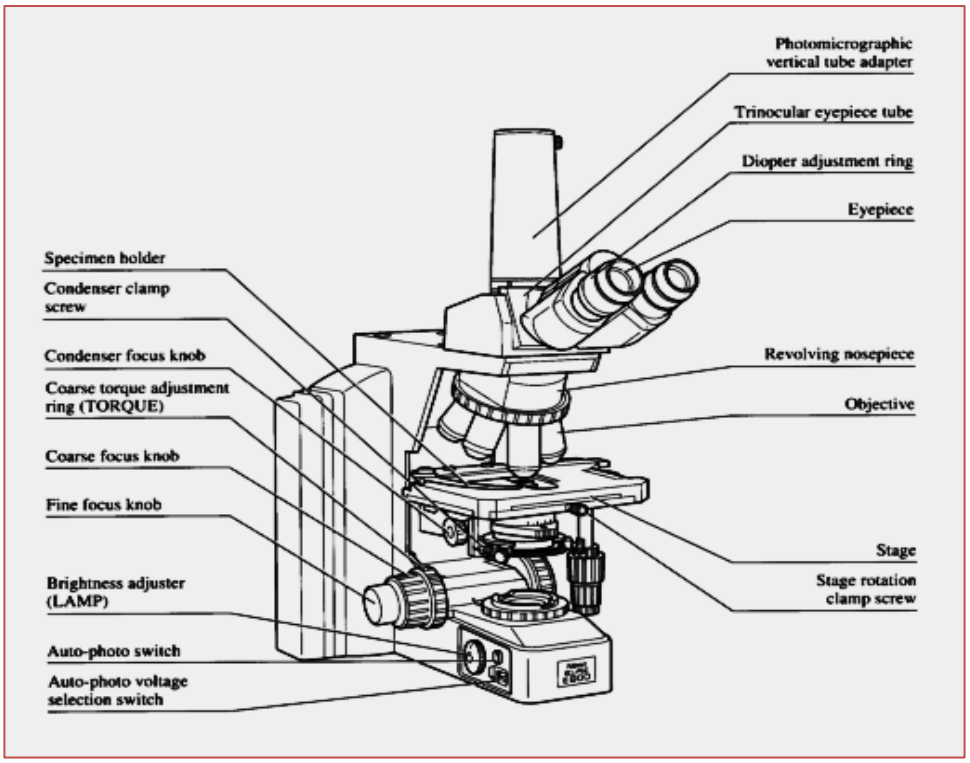

Figure 3.13. Schematic diagram of Nikon optical microscope [36].

The objective lens is also compound lenses that are made of glass in order to gather the light from the sample. The typical magnification values of these objective lenses are 4x, 5x, 10x, 20x, 40x, 50x and 100x . The stage is a platform located under the objective lenses to enhance the specimen that will be viewed. In the center of the stage, there is a hole to allow for light to pass through it to the specimen. The illumination source is located below the stage to provide the light to the specimen, and this illumination can be controlled by different methods either by using mirrors or condensers. The basic principle of any optical microscope is that the objective lens is made of very high magnifying glass with a short focal length which brings the specimen very close to be examined. The light from the specimen comes to focus a few millimeters inside the microscope tube. As a result, enlarged images of the specimen can be seen by the eyepiece or computer screen. Figure 3.14 is a photograph for the optical microscope that was used in this study [35].

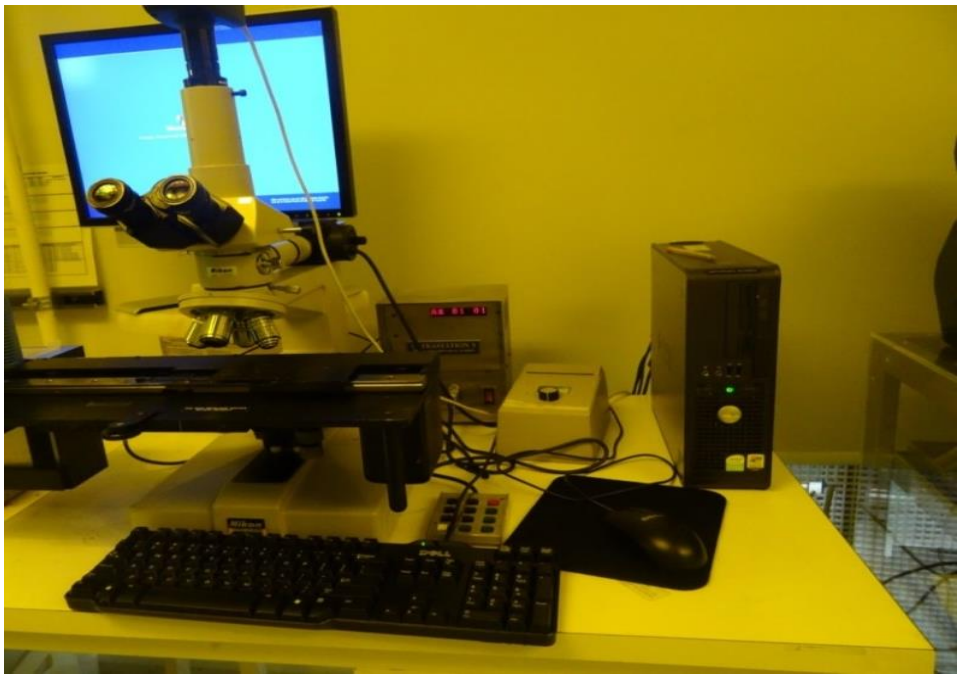

Figure 3.14. Front view of Nikon optical microscope in HIDEC.

3.2 Experimental procedures

In this section, the procedures used in all the experiments will be described starting from cleaning the samples until the fabrication of the whole device.

3.2.1 Cleaning the samples

The cleaning of silicon samples was done in the HIDEC clean room.

3.2.1.1 Silicon substrate cleaning

Two types of solutions were used for cleaning the silicon samples. The first solution was the piranha solution. Piranha solution is used to remove organic material off of the silicon samples. The volume ratio of the two components that were used in the piranha solution was (1:1 of $H_2 SO_4$: H_2O_2). For cleaning the silicon samples with piranha solution, a glass beaker was used due to the high temperature that resulted from the interaction between the H_2SO_4 and H_2O_2. After the silicon samples were placed in the sample holder, they were immersed in the mixed solution for 10 min. After the cleaning was finished, the samples were taken out of the glass beaker and rinsed with deionized water (DI) and dried with a nitrogen gun. The next step of cleaning was removing the oxide layer from the silicon samples by using diluted hydrofluoric acid (1:10 HF: H_2O). The samples were dipped in this solution for two min and then taken out and dried with a nitrogen gun. After the cleaning was done for all the samples, they were kept inside an evacuated container in order to prevent any oxidation before loading the samples into the deposition systems.

3.2.1.2 Glass sample cleaning

The cleaning of glass samples was done using an ultrasonic cleaner. The beaker was first filled with acetone and then the glass samples were immersed inside it. Then, the beaker that

had samples was immersed inside the ultrasonic cleaner for 5 min. After that the samples were dried. The same steps that were used with the acetone were repeated with methanol.

3.2.2 Experimental procedures

As was mentioned previously in Chapter 1, the goal of this study was fabricating SiNWs/a-Si composite based solar cell using glass as a substrate. The steps that were followed in fabricating the SiNWs/a-Si composite based solar cell in this research are shown in Figure 3.15. The first step was the fabrication of the p+ polySi substrate by means of AlIC of a-Si on glass and ITO/glass substrates. The second step was the fabrication of SiNWs on the p+ polySi substrate in the PECVD by using Al and Au nanodots as catalysts. The third step was depositing the n- type a-Si:H layer on the top of the SiNWs. The final step was depositing the Al contact layer on the top of the a-Si layer. Al makes a good Ohmic contact with n-type a-Si:H layer due to the similarity in the Fermi level between these two layers.

3.2.2.1 Fabrication of poly-Si thin film

The fabrication of p+ polySi thin film on glass substrates was done in four steps. The first step was depositing a-Si thin film on glass substrates. Second was the formation of an oxide layer on the surface of a-Si layer. Third was the deposition of Al film on the oxide/a-Si/glass substrate. Finally, the Al layer was annealed at 500 ˚C and then the Al layer was etched.

3.2.2.1.1 Deposition of amorphous silicon (a-Si) on glass substrates

After the glass substrates were cleaned with acetone and methanol, they were transferred into the MPZ2 system, and the MPZ2 chamber was pumped down to maximum vacuum pressure of $2x10^{-8}$ Torr.

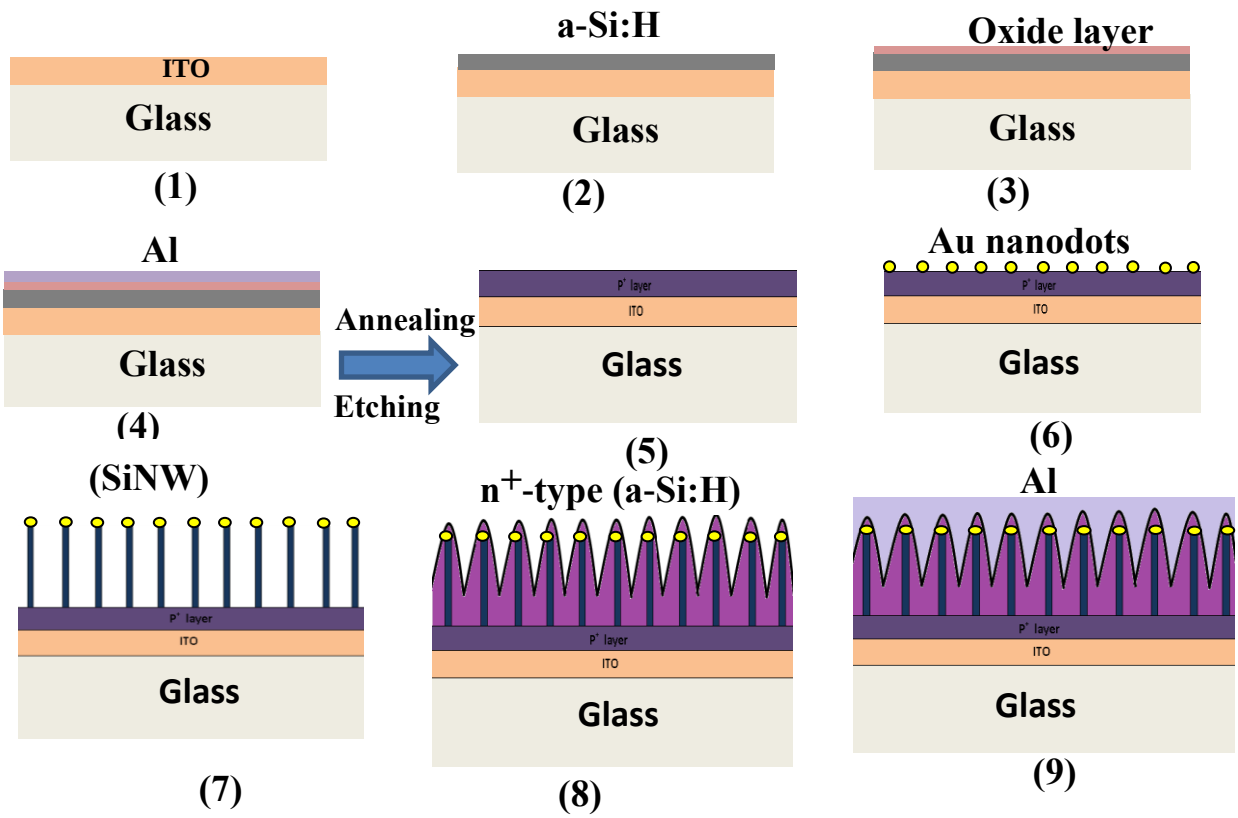

Figure 3.15. Schematic diagram of the fabrication steps for the SiNWs/a-Si composite solar cell using glass as a substrate.

Then, the substrate temperature was set to 250 ˚C. When the substrate temperature reached the 250 ˚C, silane gas with a flow rate of 20 sccm was introduced to the chamber. After that, a power of 3 watts was applied to the electrode placed under the substrate holder. The glowing of the electrode with a purple color meant the plasma was formed. The plasma decomposed the SiH_4 into its main components, like Si, SiH, SiH_2, SiH_3, to deposit onto the glass to form the a-Si:H film. The total chamber pressure during the deposition was about 500 mTorr with a deposition time of 60 min. The deposition rate of a-Si:H in the PECVD system was 10 nm/min. Therefore, the thickness of the a-Si:H film was 0.6 micron. After the a-Si was deposited on the glass substrates, they were left inside the chamber to cool down to room

temperature. In order to form an oxide layer on a-Si/ glass substrate, the samples were left exposed to air for ten days inside the lab.

3.2.2.1.2 Deposition of Al layer in the EBE system

After the a-Si:H layer on glass substrates were oxidized, they were transferred to the EBE system for Al deposition. After the substrates were placed in the substrate holder in the EBE system, the system left to pump down to its high vacuum of $2.8x10^{-8}$ Torr. During the pumping time, the parameters of the desired process were set by using the deposition controller. The deposition parameters include the film thickness, deposition rate, maximum power, ramping and soaking time. When the system reached its high vacuum and parameters was set, a power of 7.8KV was applied to filament that was placed underneath the crucible. When the emission current turned on and the start button was pressed, electron beam was emitted from the filament toward the Al source in the crucible by the effect of magnetic field in order to melt the Al source. When the Al melted, it started to evaporate toward the substrate. After the deposition of Al film reached the desired thickness (140 nm), the shutter moved quickly toward the crucible to prevent any more deposition on the substrates. The Al film deposition was done at room temperature with a deposition rate of 5 Å/sec.

3.2.2.1.3 Annealing Process

After the deposition of Al layer on the oxide/a-Si:H on glass substrates was finished some of Al/oxide/a-Si/glass substrates was treated with annealing using hydrogen gas and the other was treated with annealing process without the hydrogen gas. The annealing with H_2 was done in the annealing chamber which is part of the MVS. After the sample was placed in the chamber, the pressure was set to 1 Torr. When the substrate temperature reached the desired temperature, a

current of 14 mA was applied to the tungsten filament that was placed above the substrate holder. Table 3.1 shows the parameters that were used during the annealing with H_2 and without H_2.

For the annealing process without H_2, the samples were transferred into the EBE system. After the system pumped down to its high vacuum of $2.8x10^{-8}$ mbar, the halogen lamp was heated up to 500˚C for annealing. It usually took around 40 min to reach this temperature. After the substrate temperature reached 500 ˚C, it was annealed for 30 min. After the annealing was finished, the substrates were left inside the chamber to cool to room temperature. After the sample cooled, Raman spectroscopy, Hall effect measurement, and optical microscopy tools were used for samples that were annealed with H_2 and without it.

Table 3.1. Parameters used during the annealing process with hydrogen and without hydrogen.

H_2 flow Rate (sccm)	**Temperature (˚C)**	**Time (min)**	**Chamber Pressure (Torr)**	**Current (mA)**
20	200	2	1	14
20	200	30	1	14
20	250	10	1	14
20	300	10	1	14
20	300	15	1	14
20	300	30	1	14
20	500	30	1	14

3.2.2.1.4 Aluminum etching

In order to get the final structure of the p+ polySi thin film, the Al layer was etched off of the Al/oxide/a-Si/AZO/ glass substrates.

The solution that was used for etching the Al layer was aluminum etchant type D solution. The aluminum etchant solution was first poured into the glass beaker, and then the glass beaker was heated to 40 ˚C. In order to raise the solution temperature faster, a magnetic stirrer was used to stir the solution so that the solution temperature was distributed homogenously. When the solution temperature reached 40 ˚C, the substrate holder that had the substrates was immersed in the solution for 12 sec. Then, the substrate holder was taken out of the etchant solution and washed with DI water and dried with a nitrogen gun. Raman spectroscopy, Hall effect measurement, and optical microscopy characterizations were done for the samples after etching the Al layer.

3.2.2.1.5 Deposition of AZO on glass substrate

The AZO contact film was prepared using the sputtering system (MPZ4). (1 inch x1 inch) Corning (1737) glass substrates were cleaned by the acetone and methanol as was mentioned in the cleaning sections of this chapter. The glass substrate was then transferred to MPZ4 for deposition process. After MPZ4 was pumped down to $4x10^{-8}$ Torr, Ar gas with a flow rate of 20 sccm was introduced to the chamber and a power of 150 watts was applied to the AZO target to form the plasma around the target. After the positive Ar ions (Ar^{+}) were created by the plasma, they were attracted to the negative AZO target. When Ar^{+} struck the AZO target, AZO atoms were ejected out of the target substrate toward the glass substrate to form the AZO thin film. The deposition process was done at room temperature (25 ˚C) with a deposition time and chamber

pressure of 30 min and 15 mTorr, respectively. After the deposition process was finished, the power supply and Ar mass flow controller were turned off. The obtained AZO film was then transferred to the MPZ2 system in order to deposit a-Si on top of it.

After the AZO thin film was formed on the glass substrate, a-Si:H layer was deposited on AZO/glass, and then it was oxidized. After the oxide layer formed on the top of a-Si:H layer, an Al layer of 140 nm thick was deposited on it. Then, the Al layer was annealed for 30 min at 500 ˚C. After the sample cooled to room temperature, it was etched with Al etchant solution to remove the Al layer. Unfortunately, after the Al etching process was finished, the fabricated film on the AZO/glass substrates peeled off due to poor adhesion between the AZO and glass substrate. Therefore, indium tin oxide coated Corning glass (ITO/glass) (25x25 inches) with sheet resistivity of 5-15 Ω/square was used as an alternative substrate to AZO/glass substrate in order to complete the rest of the fabrication steps of p+ polySi thin film. The final structure of poly-Si thin film on ITO/glass substrate was characterized by Raman spectroscopy, optical microscopy, SEM, and Hall effect measurement.

3.2.2.2 Growth of SiNWs

After the fabrication of p+ polySi thin film of a-Si by the means of AlIC method, the second step of the fabrication the solar cell device is the growth of SiNWs on the p+ polySi thin film to form the p-type area of the solar cell.

As a pre-step for the fabrication of SiNWs on the p+ polySi thin film, single crystalline silicon (c-Si) substrate was used first for the growth of SiNWs using Al nanodots as catalysts in the HWCVD and PECVD systems. There was difficulty in fabricating the SiNWs using Al nanodots as catalyst on c-Si substrate in both of these systems due to some limitations in these

two systems, therefore, Au nanodots were used as an alternative catalyst for the growth of SiNWs on c-Si substrate.

More details about the fabrication of SiNWs on c-Si substrate using Al nanodots as catalysts will be mentioned in the next sections.

3.2.2.2.1 Growth of SiNWs on the c-Si substrates using Al nanodots as catalysts

(1inch x1 inch) of p-type (c-Si) substrates were used for the growth of SiNWs using Al nanodots as catalysts. After the silicon substrates were cleaned, they were placed in the substrate holder and transferred into the EBE system for depositing a thin film of Al on the top of silicon substrates.

3.2.2.2.2 Formation of Al nanodots

After transferring silicon substrates into the EBE system, the deposition of Al film was started after the EBE system reached its high vacuum of 2.8×10^{-8} mbar. The high vacuum was required when depositing Al films due to the high sensitivity of Al to oxygen and subsequent formation of an aluminum oxide layer that prevents any SiNW growth on the Al film. After setting the required parameters such as process number, deposition rate, thickness, and maximum power by using deposition controller, a power of 7.8 KV was applied to the filament to emit an electron beam toward the crucible by the effect of magnetic field. When the Al source was melted by the electron beam, it started to evaporate toward the substrate. The thickness of the obtained Al film was 10 nm with a deposition rate of 5 Å/sec at room temperature. After the deposition of Al film was finished, the temperature of the halogen lamb was raised up to the 600 ˚C to heat the Al/c-Si substrate. When the substrate's temperature reached the 600 ˚C, the annealing process of the Al film started for 30 min. During the annealing, the Al-Si alloy was

broken down into small islands which formed the Al nanodots. After the Al nanodots were formed, the substrates were left in the EBE system until they cooled to room temperature. After that, they were transferred into the hot wire chemical vapor deposition system (HWCVD) for the SiNW growth process.

3.2.2.2.3 Growth of SiNWs in the (HWCVD) using Al as a catalyst

After the Al nanodots film was fabricated in the EBE system, it was transferred into the HWCVD system. After the sample was placed in the HWCVD system, the system was pumped down to its highest vacuum pressure which was around the $4x10^{-4}$ Torr. After the HWCVD system chamber pumped down, the substrate was heated to temperatures of 580-600 ˚C. When the substrate reached the desired temperature, a diluted silane gas with H_2 or Ar gases was introduced to the chamber. After the chamber pressure was set up to the desired pressure, current of 13-14 mA and voltage of 15-16 mV were applied to the filament to heat it up. After the filament glowed, the deposition process started with a limited time. During the deposition process, the silane gas cracked into its main components, including the silicon atoms, to deposit on the c-Si substrate and diffuse into Al nanodots to form the SiNWs. Table 3.2 shows the parameters that were used during the fabrication of SiNWs using Al nanodots as a catalyst in the HWCVD system.

After the growth of SiNWs process was finished, the current, voltage, Ar, H_2, SiH_4 switches, and substrate controller were turned off. Then, the system was purged out by using the Ar or N_2 gases. When the substrate reached room temperature, it was taken out of the system for characterization by the SEM.

Table 3.2. Parameters used during the fabrication of SiNWs using Al nanodots as a catalyst in the HWCVD system.

Sample code	SiH_4 flow rate (sccm)	H_2 flow rate (sccm)	Time (min)	Substrate temperature (˚C)	Filament temperature (˚C)	Chamber pressure (Torr)
R_1	10	60	5	600	2100	1.5
R_2	10	60	10	600	2100	1.5
R_3	5	95	30	600	2100	1.5
R_4	5	95	30	600	2100	1.5
R_5	5	95	20	580	2100	2
R_6	5	95	20	580	2100	0.3
R_7	5	95	20	580	2100	0.2
R_8	5	10	5	580	2100	1.5
R_9	5	10	10	580	2100	1.5
R_{10}	5	10	20	580	2100	1.5
R_{11}	5	10	40	580	2100	1.5
R_{12}	5	10	80	580	2100	1.5

3.2.2.2.4 Growth of SiNWs in the PECVD System using Al nanodots as catalysts

PECVD system was also used for the SiNW growth. As was mentioned previously, MPZ2 or PECVD system was located within the MVS, so the samples were transferred from EBE system into the MPZ2 system without exposing them to the air which causes the formation of the oxide layer on the Al nanodots film. After the Al nanodots films were formed on the c-Si substrates in the EBE system, they were transferred into the PECVD (MPZ2) for the SiNW growth process. After the pressure in the MPZ2 reached its high vacuum pressure of $4x10^{-8}$ torr, the substrate temperature was raised to its highest temperature around 360 ˚C. When the substrate temperature reached the 360 ˚C, the SiH_4 gas with the desired flow rate was introduced to the chamber. After that, a power of 2 watts was applied to the electrode that was placed under the substrate so that the plasma would be formed. Table 3.3 shows the parameters that were used during the growth of SiNWs on c-Si substrates by using Al nanodots as a catalyst. After the plasma was formed, the SiH_4 decomposed into its main components, including Si atoms, to deposit on the Al nanodots film and diffuse into the Al nanodots to form the SiNWs. After the growth of SiNWs on the c-Si substrate, the samples were taken out of MPZ2 and cooled to room temperature for characterization in the SEM.

3.2.2.2.5 The growth of SiNWs using Au nanodots as catalysts

The SEM results for the SiNWs that were grown by using Al nanodots as catalyst in the PECVD did not met the desired goal. Therefore, Au nanodots film was used as an alternative catalyst to the Al nanodots catalyst. After the c-Si substrates were cleaned with piranha solution and HF dip that were mentioned previously, they were transferred into the EBE system for depositing Au film on c-Si substrates. After the EBE system reached the high vacuum pressure of $2.8x10^{-8}$ mbar, a power of 7.8 KV was applied to the filament to emit electron beam toward

the crucible by the effect of magnetic field. When the Au source was melted by the electron beam, it started to evaporate toward the substrate. The thickness of obtained Au film was 10 nm with a deposition rate of 1 Å/sec at room temperature. Then, the Au/C-Si substrates were transferred into the PECVD (MPZ2) for SiNWs growth. Table 3.4 shows the parameters that were used in the growth of SiNWs on signal crystalline silicon at different substrates temperatures and time. As shown in the Table 3.4., the growth of SiNWs on samples R_{19}, $R_{20,}$ $R2_{1,}$ R_{22} was done at different substrate temperatures with constant SiH_4 flow rate, chamber pressure, time, and power. For the other three samples ($R_{23,}$ $R_{24,}$ R_{25}), the growth process was done at different time with constant SiH_4 flow rate, chamber pressure, substrate temperature, and power. After the growth of SiNWs on these samples was finished, they were taken out of MPZ2 system for the SEM characterization.

Table 3.3. Parameters for the SiNW growth in PECVD system using Al nanodots as catalysts.

Sample code	SiH_4 flow rate(sccm)	H2 flow rate(sccm)	Chamber pressure(torr)	Power (W)	Sub.Temp (˚C)	Time (min)
R_{13}	10	10	0.75	2	360	30
R_{14}	10	90	0.75	2	360	60
R_{15}	10	10	0.75	2	360	60
R_{16}	10	_____	0.75	2	360	60
R_{17}	5	50	0.75	2	360	60
R_{18}	5	50	0.75	2	360	30

Table 3.4. Parameters used in the growth of SiNWs on signal crystalline silicon at different substrate temperatures and times.

Run number	Substrate type	SiH_4 flow rate (sccm)	Chamber pressure (Torr)	Sub.temp (˚C)	Time (min)	Power watts
R_{19}	C-Si	20	1	200	15	2
R_{20}	C-Si	20	1	250	15	2
R_{21}	C-Si	20	1	310	15	2
R_{22}	C-Si	20	1	346	15	2
R_{23}	C-Si	20	1	310	5	2
R_{24}	C-Si	20	1	310	15	2
R_{25}	C-Si	20	1	310	30	2

3.2.2.2.6 Growth of SiNWs on the a-Si/ITO/glass substrate

The growth of SiNWs was also done on the a-Si:H/ITO/glass substrate. After the deposition of a-Si on the ITO/glass substrate, the samples were transferred to the MPZ2 system for SiNWs growth process. The procedures that were followed during the SiNW growth on a-Si:H/ITO/glass substrates were similar to that used with the SiNW growth on c-Si substrates except that the parameters were different. The parameters used in growth of SiNWs on the a-Si:H/ITO/glass substrate are given in Table 3.5.

3.2.2.2.7 Growth of SiNW on the polycrystalline silicon/a-Si/ITO/glass substrate

After finishing the characterization of the p+ polySi samples, they were transferred to the EBE system in order to deposit a 10 nm of Au film on the p+ polySi samples. After the deposition of Au film was finished in the EBE system, the samples were transferred directly to

the PECVD for the SiNW growth. The parameters used for SiNW growth are in Table 3.5. The procedures that were followed during the SiNW growth on the p+ polySi substrates are similar to those used with the SiNW growth on c-Si substrates.

Table 3.5. Parameters used during SiNW growth in the PECVD using a-Si/ITO/glass and p+ polySi/ITO/glass as substrate

Run number	Substrate type	SiH_4 flow rate (Sccm)	Chamber pressure (Torr)	Sub.temp (˚C)	Time (min)	Power (watt/cm^2)
R_{26}	a-Si	20	1	310	5	2
R_{27}	a-Si	20	1	310	15	2
R_{28}	a-Si	20	1	310	30	2
R_{29}	P^+-polySi	20	1	310	15	2
R_{30}	P^+-polySi	20	1	310	30	2

Chapter 4: Results and Discussions

This chapter includes the results and discussions of this study. The two most important steps in the fabrication of SiNWs/a-Si:H composite solar cell using glass as a substrate were the fabrication of heavily doped polycrystalline silicon thin film (p+ polySi) on ITO/glass substrate by means of AlIC of a-Si and the growth of SiNWs using Al and Au as catalysts on different substrates, including the p+ polySi . The results in this chapter will be divided into two parts. The first part of this chapter is devoted to analysis of the results of p+ poly Si thin film. In the second part, the analysis of the growth of SiNWs on different substrates will be discussed.

4.1 Characterization of p+ polySi thin film

The p+ polySi thin films that were fabricated on glass and AZO/glass, and ITO/glass by means of AlIC method have been characterized by different characterization tools: Raman spectroscopy, optical microscopy, SEM, and Hall effect measurement.

4.1.1 Raman Spectra Characterization

After the Al layer was deposited on the oxide layer on a-Si/glass substrate, it was annealed at different temperature with and without H_2 (see Table 3.1) . Figure 4.1 shows Raman spectra for poly-Si thin film after annealing at different temperatures. Annealing at temperatures of 200 ˚C and 250 ˚C with the presence of H_2 gas did not show any peak. When annealing temperature was increased to 300 ˚C with the presence of H_2 gas, the intensity peak increased. However, annealing the sample for 30 min at a temperature of 300 ˚C without the presence of H_2 gas, the intensity peak increased to around 5000 a.u. The intensity peak increased to 7000 a.u when annealing temperature was increased to 500 ˚C without the presence of H_2 gas.

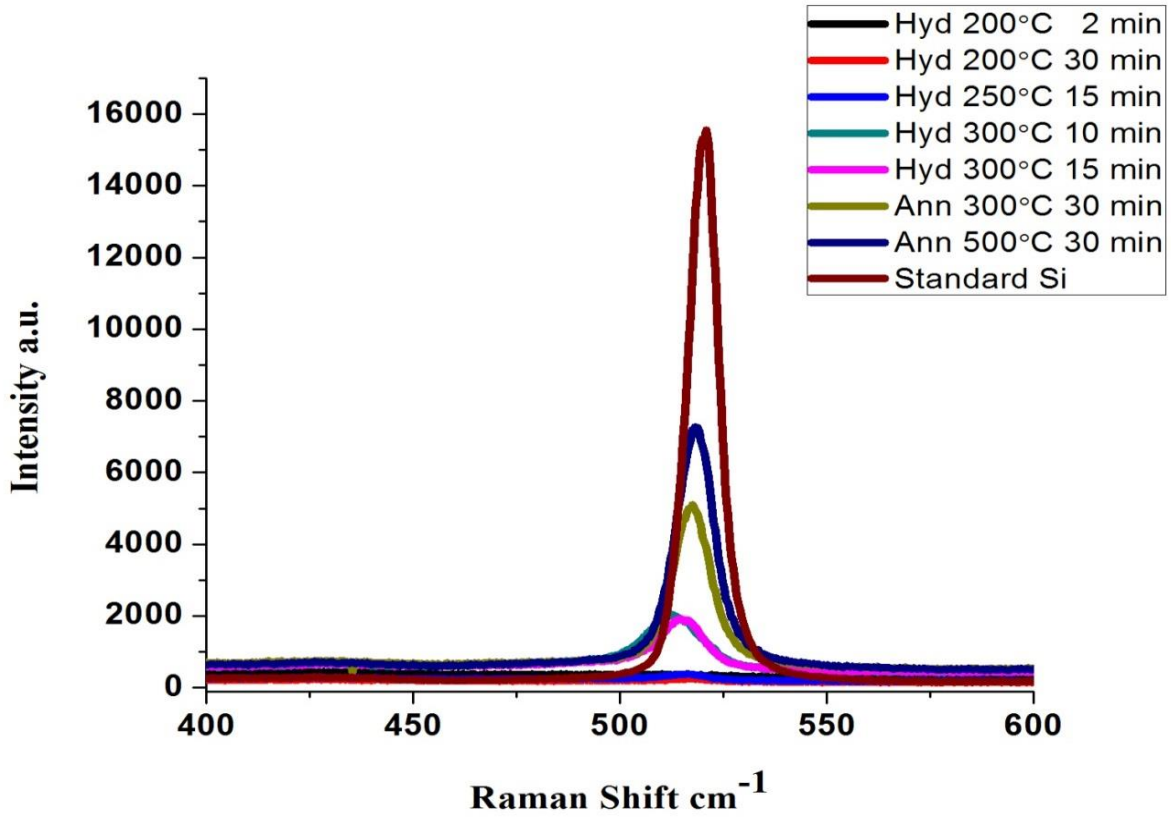

Figure 4.1. Raman spectra for poly-Si thin film on glass substrate after annealing with hydrogen and without hydrogen.

The increase in the intensity peaks as the annealing temperature was increased was because of the increasing amount of thin film material that crystallized at such temperatures. The shifts in peak locations for samples that were annealed at different temperatures was due to the compressive strain in the poly-Si thin film, and the compressive strain existed due to the defects in the thin film. The shift in the peak locations becomes closer to the peak location of standard c-Si as the annealing temperatures were increased. For example, at annealing temperature of 300 ˚C, the shift in the peak location was 517 cm^{-1}. While at annealing temperature of 500 ˚C, the peak location shifted to 518 cm^{-1} which is close to standard c-Si peak of 520 cm^{-1}.

Raman spectra were taken for the thin film on bare glass before etching the Al layer and after etching the Al layer (see Figure 4.2).

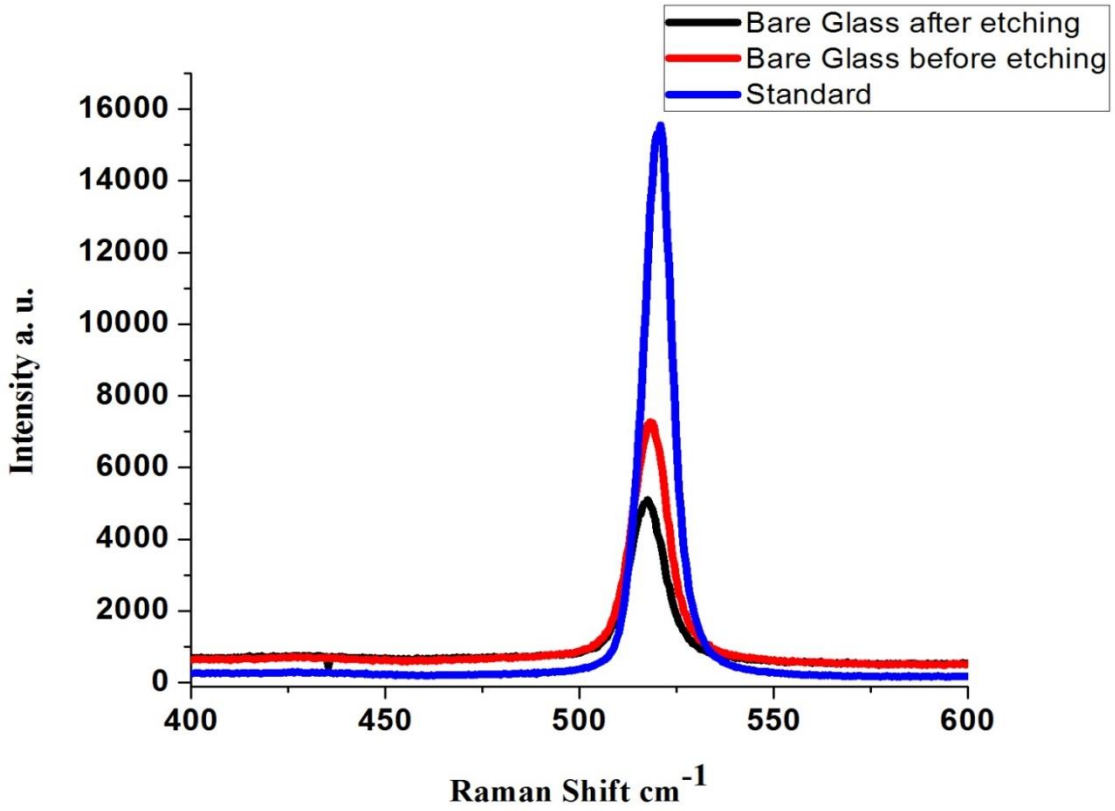

Figure 4.2. Raman spectra for the poly-Si thin film on bare glass substrate before and after etching.

Figure 4.2 shows that the intensity peak of thin film increased after etching the Al layer away from the sample surface. The reason behind increasing the intensity of the peak was that after etching the Al layer away from the surface, holes were formed on the surface of the sample, and then the laser light passed through these holes to the poly-Si underneath the surface and reflected from those areas. Before etching the Al layer, the laser light hit the surface of the Al layer and reflected up to be collected by the detector. The full-width-half-maximum (FWHM) for

these two peaks was 11.6 cm^{-1} which meant the crystallinity of the poly-Si thin film did not change before and after etching the Al layer.

4.1.2 Optical micrographs and SEM results of poly-Si thin film on glass substrate

An optical micrograph was taken for the poly-Si thin film on glass substrate in order to see the morphology of the sample surface before and after etching the Al layer away from the sample (see Figure 4.3). The optical micrograph (b) shows grains with more than 5 µm size were formed on the sample surface after etching the Al layer.

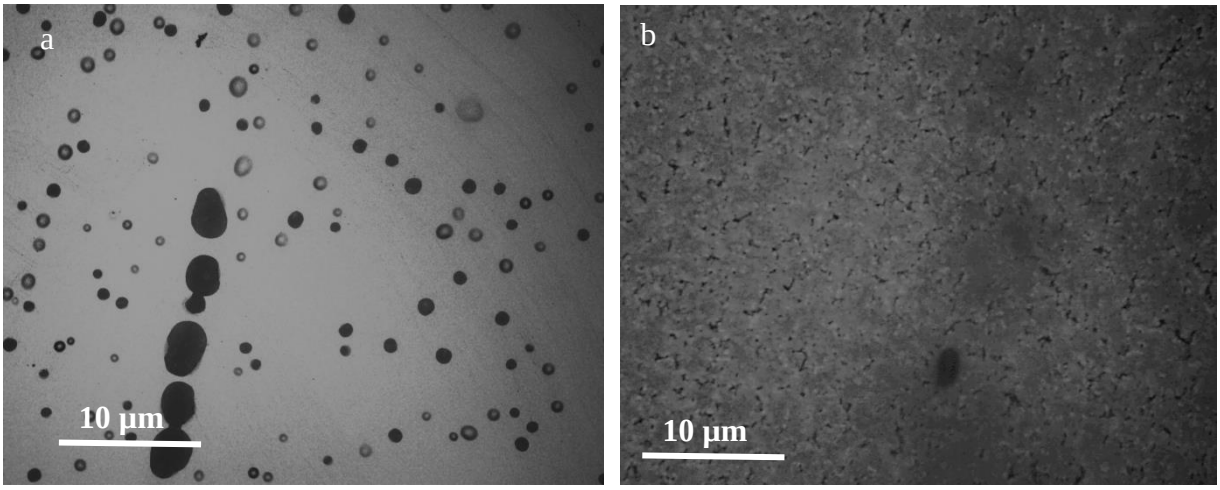

Figure 4.3. Optical micrograph for the glass samples: a. before and, b. after removing, the Al layer.

SEM image was taken for the sample after removing the Al layer away from the sample (see Figure 4.4). From the SEM images shows the size of the formed grains was more than 5 µm

4.1.3 Hall effect measurement Results for poly-Si on glass substrate

In order to study the electrical properties for the poly-Si thin film on glass substrate, Hall effect measurement was used for this purpose. Table 4.1 shows the electrical properties for poly-Si /glass substrate.

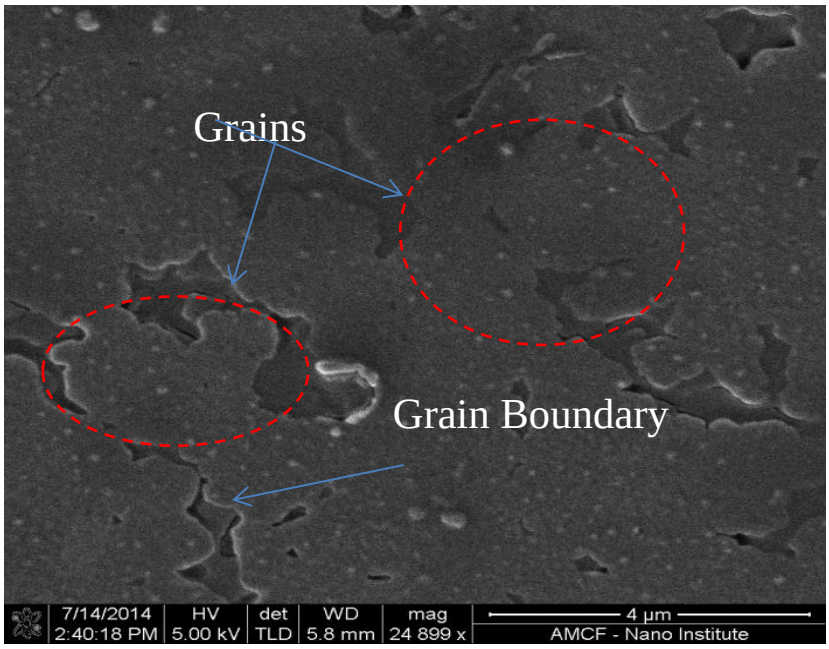

Figure 4.4. SEM image for thin film on bare glass substrate shows the formation of grains on the surface of bare glass substrate.

Table 4.1. Electrical properties for poly-Si /glass substrate.

Samples	Resistivity (ρ)(Ω/cm)	Hall Coeffcient (R_H) (cm^3/C)	Mobility(μ_m) ($cm^2/(V.s)$	Carrer concentration (cm^{-3})	Dopant type
Poly-Si/glass substrate	2.4×10^{-1}	2.72	11.3	0.2×10^{18}	p-type

From Table 4.1, it can be seen that the poly-Si film was a heavily doped p-type thin film. After successfully fabricating the heavily doped poly-Si (p+ polySi) on glass substrate, the same procedures that were used with glass substrate to produce p+ polySi thin film were applied on AZO/glass substrate.

4.1.3 Raman spectra results for the poly-Si thin film on AZO/glass substrate

After depositing the a-Si:H layer and then Al layer on the top of AZO/glass substrate, the sample was annealed at 500 ˚C for 30 min (see Figure 4.5)

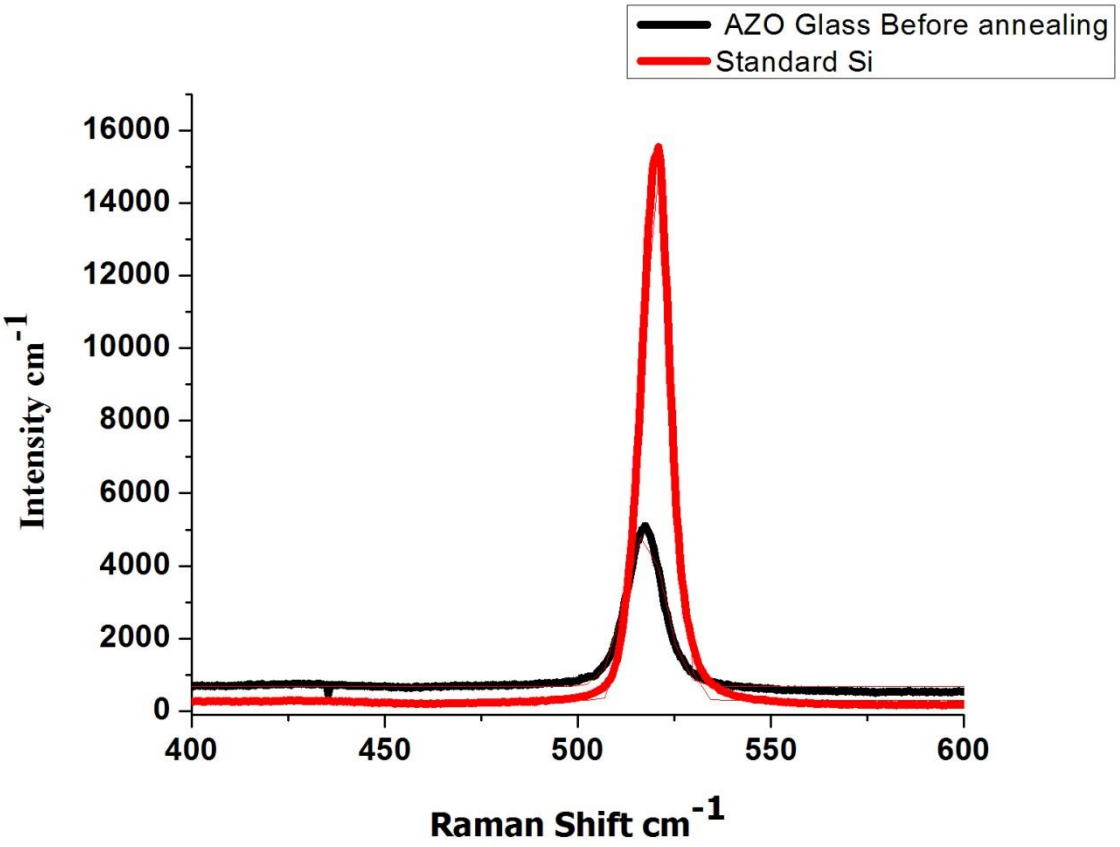

Figure 4.5. Raman spectra for poly-Si thin film on AZO/glass after annealing.

The Raman spectra show having a good peak of crystalline silicon with FWHM of 11.6 cm^{-1}, which is similar to FWHM for thin film on bare glass substrate (11.6 cm^{-1}). After etching the Al layer away from the thin film on AZO/glass sample, the thin film was peeled off the sample due to the poor adhesion between AZO film and glass substrate. Therefore, a Raman spectrum was not taken of the sample after etching the Al layer. As an alternative substrate, ITO/glass substrate was used for the fabrication of p+ polySi thin film. The fabrication of p+

polySi thin film on ITO/glass substrate was similar to that done on bare glass substrate. Raman spectra were taken for the Al/oxide/a-Si/ITO/glass substrate before and after etching the Al layer (see Figure 4.6).

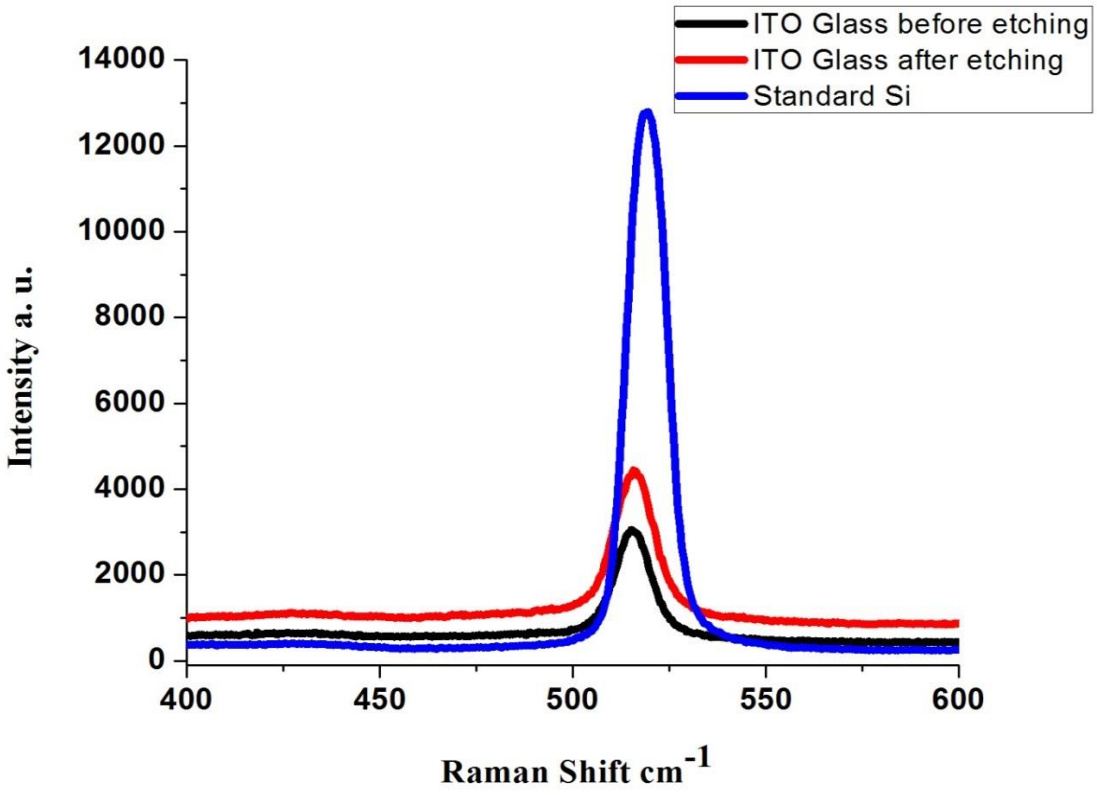

Figure 4.6. Raman spectra for poly-Si film on ITO/glass substrate before and after etching.

The intensity peak for poly-Si thin film on ITO/glass substrate as shown in Figure 4.6 increased after etching the Al layer away from the sample. The FWHM of poly-Si thin film before and after removing the Al layer away were around 13.7 cm^{-1} and 11.9 cm^{-1}, respectively, and that means crystallinity of the thin film increased after etching the Al layer away from the sample.

4.1.4 Optical micrographs and SEM results for poly-Si thin film on ITO/glass substrate

More investigations were done for the poly-Si thin film on ITO/glass substrate using optical microscopy and SEM tools. Figure 4.7 shows the optical micrographs for the poly-Si thin film before and after etching the Al layer away from the ITO/glass substrate.

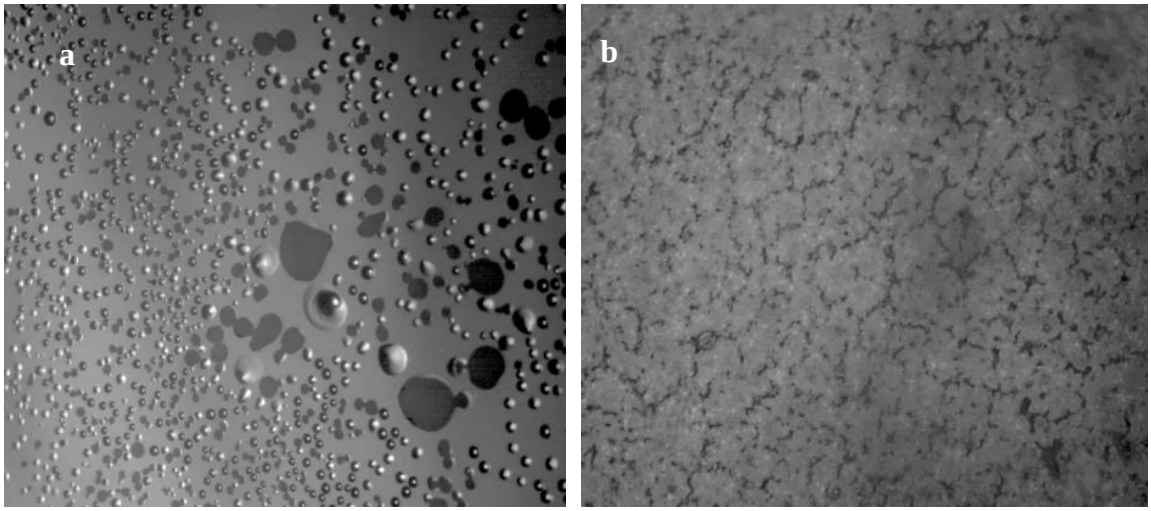

Figure 4.7. Optical micrographs for ploy-Si thin film a. before etching the Al layer b. after etching the Al layer away from the thin film.

Figure 4.7 shows the change in the surface structure of thin film on ITO/glass substrate before and after etching the Al layer. The reduction in the free energy of Si during the transformation from a-Si to crystalline silicon is the main reason behind AlIC method. When a-Si becomes in contact with the Al layer, electronic screening happens which weakens the Si bonds and then facilitates the diffusion between Al and a-Si. After the a-Si atoms dissolves in the Al layer, Al starts to diffuse quickly in a-Si due to its high mobility toward the growing Si grains and leads to the formation of a continuous poly-Si film [37]. After etching the Al away from the sample, large grains showed up on the surface of ITO/glass substrate (see Figure 4.7 b).

SEM images were also taken for the poly-Si thin film on ITO/glass substrate after etching the Al layer away. The SEM images shows the formation of crystalline grains with size of more than 5 µm on the ITO/glass substrate. Figure 4.8 shows SEM images for poly-Si thin film on ITO/glass substrate after etching the Al layer at different magnifications.

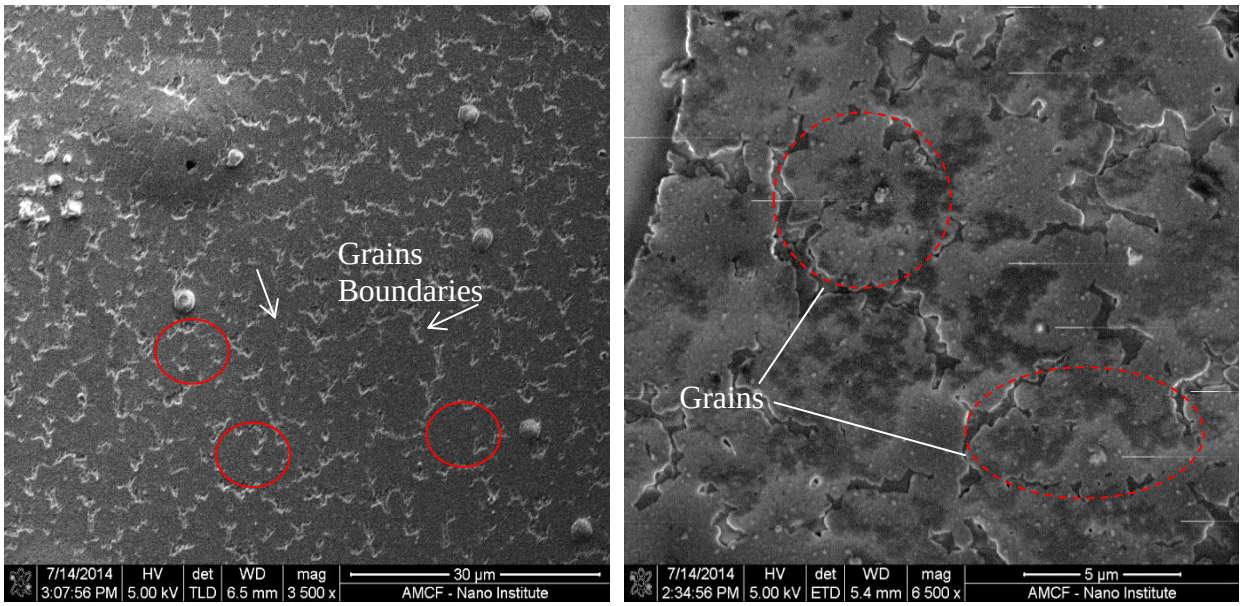

Figure 4.8. SEM images for poly-Si thin film on ITO/glass substrate after etching the Al layer at different magnifications.

4.1.5 Hall effect measurment results for poly-Si thin film on ITO/glass substrate

After the poly-Si thin film on ITO/glass substrate was characterized by Raman spectroscope, optical microscope, and SEM, subsequently; van der Pauw and Hall effect measurements on the samples were taken to determine the thin film electrical properties, including resisitivity, mobility, carrier concentartion, and Hall coeffecient. Table 4.2 shows the electrical properties of the poly-Si thin film on ITO/glass and glass substrate.

Table 4.2. Electrical properties of poly-Si thin film on ITO/glass substrate

Samples	Resistivity (ρ)(Ω/cm)	Hall Coeffcient (R_H) (cm^3/C)	Mobility(μ_m) ($cm^2/(V.s)$	Carrer concentration (cm^{-3})	Dopant type
Poly-Si/ITO/glass substrate	$5.7x10^{-3}$	$-8.1x10^{-2}$	14.2	$1.1x10^{21}$	n-type

From the result of Hall effect measurment for the poly-Si/ITO/glass substrate, the Hall coeffecient was a negative value.The reason behind the negative value is the ITO contact. ITO is a n+ type material that makes a good tunneling junction with p+. Therefore, the current tunneled through the poly-Si thin film to the ITO to measure the electrical properties of ITO contact due to its low resistivity of 5-15Ω/□ compared to the sheet resistance of poly-Si thin (see Figure 4.9). However, Hall effect measurement for thin film on bare glass substrate showed a postive Hall coeffcient. Therefore, the thin film that was fabricated on ITO/glass substrate was heavily doped p-type poly-Si.

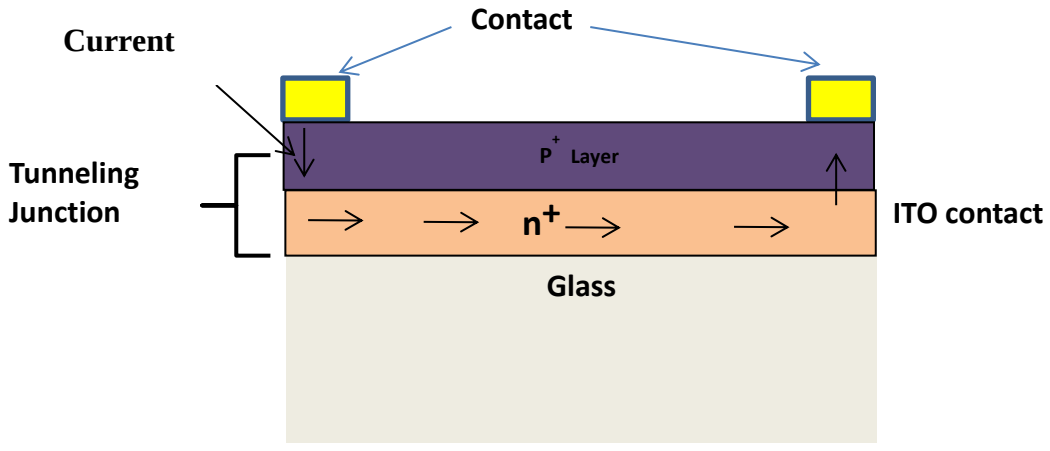

Figure 4.9. Schematic diagram of tunneling current through the ITO contact.

In conclusion, from the Raman spectra, optical micrographs, SEM images, and Hall Effect measurement, the thin films that were fabricated on ITO/glass and bare glass substrates were p+ poly-Si. Also, the thin film was a continuous film that could be used as a substrate for SiNW growth later.

4.2 SiNWs fabrication results

The second part of the fabrication of the SiNWs/a-Si composite based solar cell solar in this research is the growth of SiNWs using Al and Au as catalysts. SEM and TEM system was used for the characterization purpose of the SiNWs on different substrates.

4.2.1 SEM results for the Al nanodots

After annealing the Al film at 600 ˚C for 30 min in the EBE, the Al film on c-Si substrate started to break down into small islands. Figure 4.10 shows the Al film on the c-Si before annealing and after annealing. It is obvious from the SEM image on the right side that the Al film started to break down and accumulate as nanodots without a specific shape. It seems that there is a big cluster of "nanodots" of about 1000 nm but then the next sizes are 100 nm and below. The size of 1000 nm of Al "nanodot" is needed to be avoided. The reason behind the variation in the nanodot sizes might be because of contamination still inside the EBE at a vacuum pressure of $2x10^{-8}$ mbar.

An EDX mapping was taken for one of the Al nanodots to see what type of metal the nanodot consisted of. The result of EDX mapping showed that the nanodot consisted of pure Al metal only. Figure 4.11 shows the SEM image for one of these nanodots with EDX mapping on the right side.

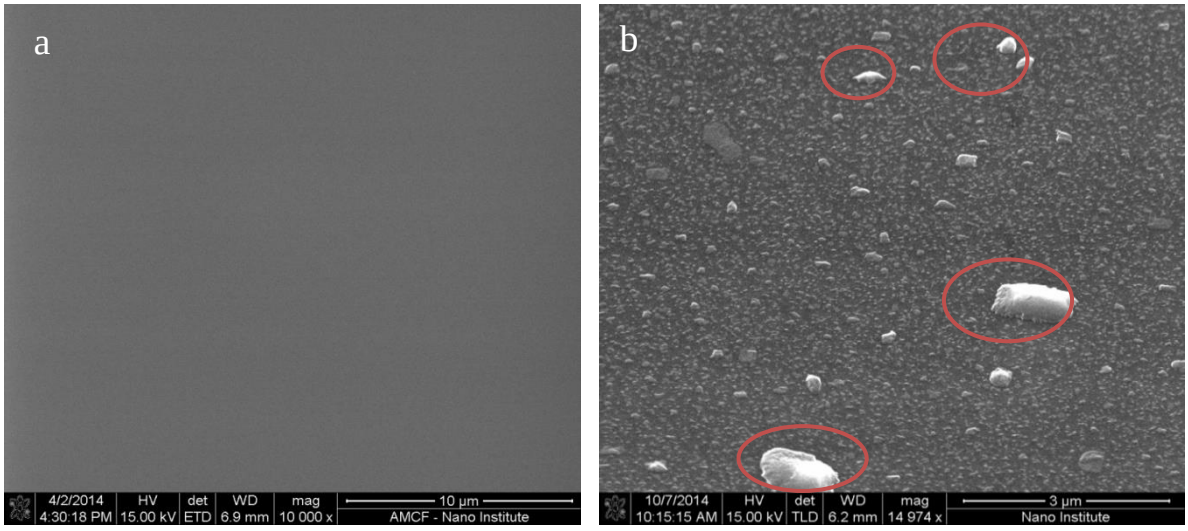

Figure 4.10. SEM images for the Al/C-Si substrate: a. before annealing; and, b. after annealing.

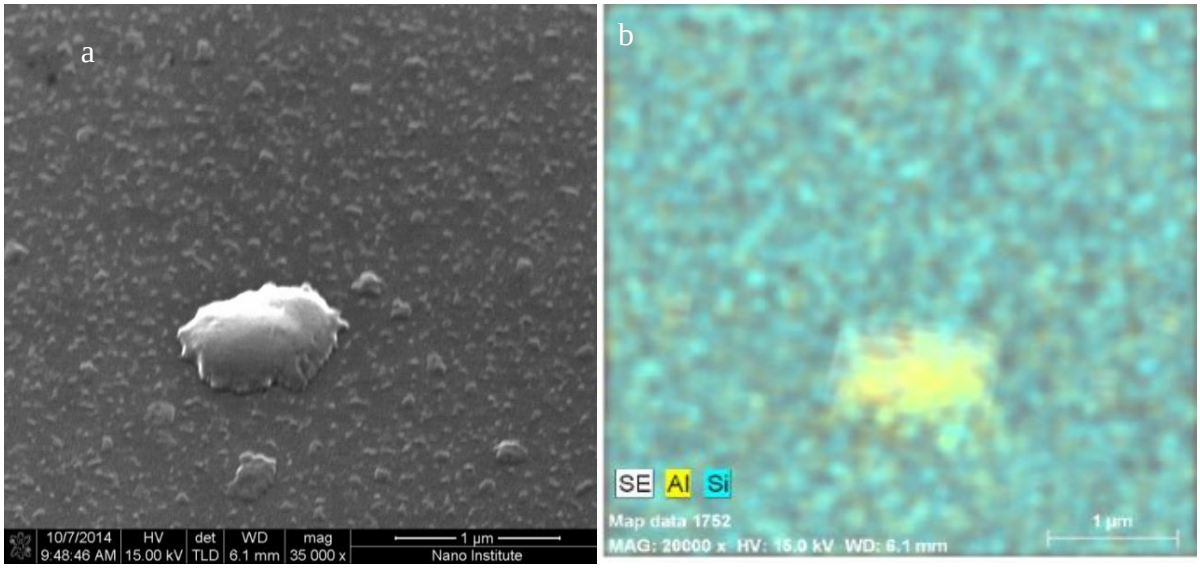

Figure 4.11. (a) SEM image (b) EDX mapping for Al nanodot.

4.2.2 SEM result for the SiNWs growth using Al nanodots in the HWCVD system

After the formation of Al nanodots on c-Si substrate, it was transferred to the HWCVD system for SiNW growth. The parameters used for each sample were mentioned in Table 3.2.

Four samples were picked out of the twelve samples to discuss to the similarity in the results. Figure 4.12 shows the SEM images for samples (R_1, R_2, R_3, R_4).

Sample R_1 and R_2 were done under same conditions (dilution ratio (H_2:SiH_4, 6:1), substrate temperature = 600˚C, filament temperature = 2100 ˚C) except that the deposition time was 5 and 15 min, respectively. It is clear from the SEM images in Figure 4.12, there was not any SiNW growth on the surface of these two samples. The dilution ratio (H_2:SiH_4) for samples R_3 and R_4 was increased to 9.5:0.5 with the other parameters the same as applied for samples R_1 and R_2. From the SEM images for samples R_3 and R_4 in Figure 4.12, there was no change in the surface morphology from previous samples R_1 and R_2. In all these depositions a rather thick film was produced.

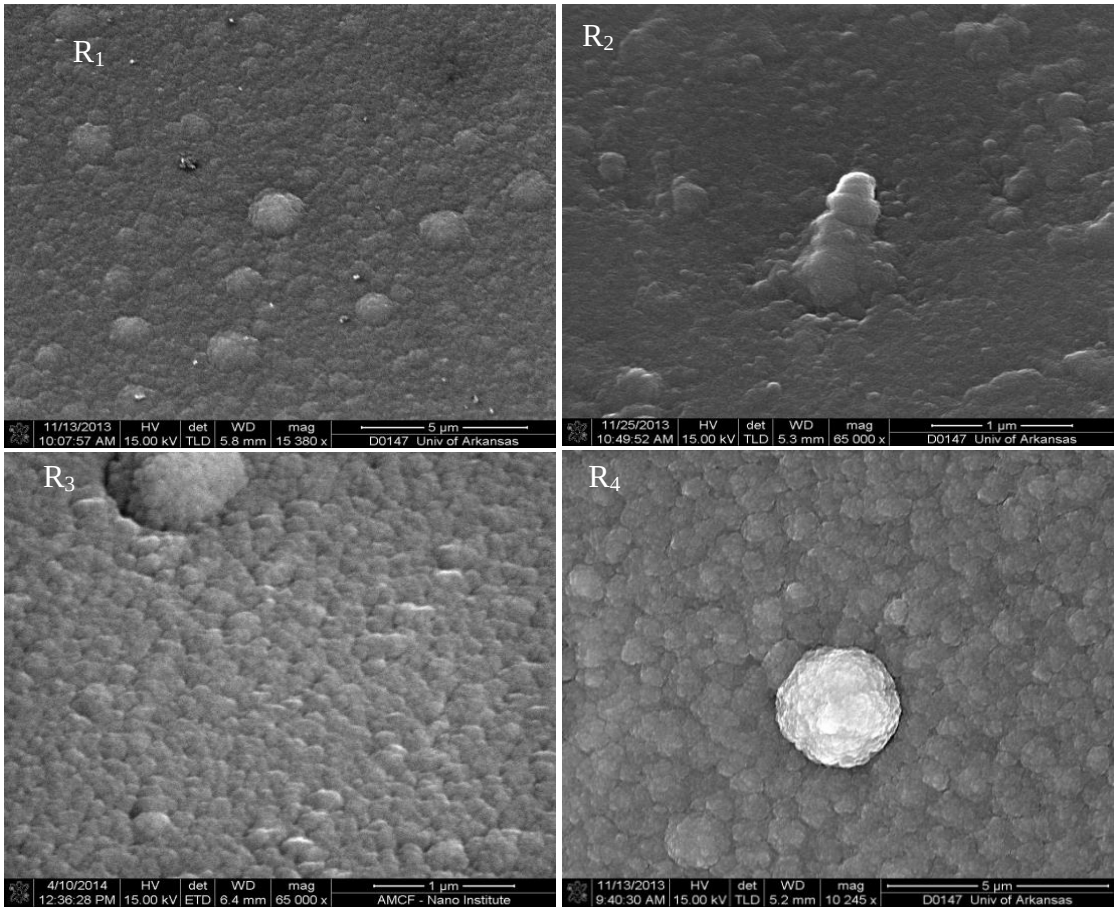

Figure 4.12. SEM images for microstructure and surface morphology of deposited films.

The other eight samples were done under different parameters either by changing in the deposition time, substrate temperature, dilution ratio, chamber pressure, and filament temperature, however, the results were similar to those from samples R_1, R_2, R_3, R_4.The reason for not being successful in growing any SiNW on c-Si in the HWCVD system may have been that exposing the Al nanodots samples to air during transfer from the EBE system to the HWCVD system led to an oxide layer formation. Moreover, the HWCVD system is not an ultra-high vacuum or high vacuum system. The vacuum inside the HWCVD chamber was around to $4x10^{-4}$ torr which means there were still significant oxygen molecules or water vapor inside the chamber. So the possibility of formation the oxide layer on the Al nanodots was high and could have prevented any SiNW growth. Another reason may be that the deposition rate was too high which could have buried the SiNWs in their earlier phase of growth.

4.2.3 Growth of SiNWs using Al nanodts in the PECVD system

After not being successful in of fabricating SiNWs in the HWCVD system, the PECVD system was used as an alternative system for the SiNWs growth. The PECVD system was located within MVS system. Al nanodots/c-Si samples were transferred from the EBE system to MPZ2 (PECVD) for the SiNWs growth without exposing them to air. Table 3.3 shows the parameters that were used during the SiNWs growth on c-Si substrate in the PECVD system.

Sample R_{13} was done with H_2:SiH_4 dilution ratio of 1:1, substrate temperature of 360 ˚C and deposition time of 15 min. Figure 4.13, the SEM image for SiNWs of sample R_{13}, shows that SiNWs started to grow in different directions and shapes. The most prevalent structure for these SiNWs was the worm-like structure (see the red circles on SiNWs in Figure 4.13). Samples (R_{13} and R_{15}) were fabricated under the same conditions (substrate temperature = 360 ˚C, power = 2

W, H_2:SiH_4 dilution ratio, 1:1) except that the deposition time was different at 15 and 60 min, respectively (see Figure 4.14).

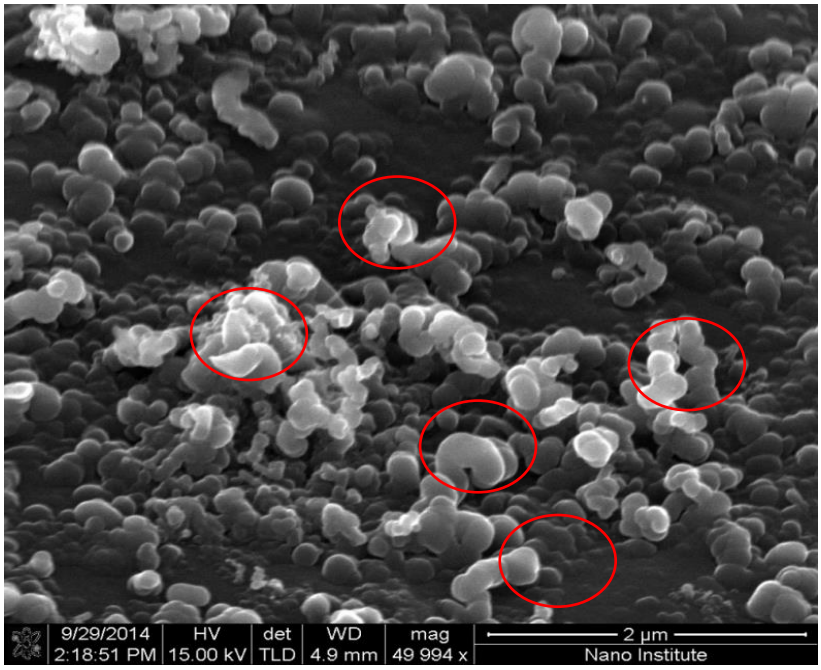

Figure 4.13. SEM image for sample R_{13}.

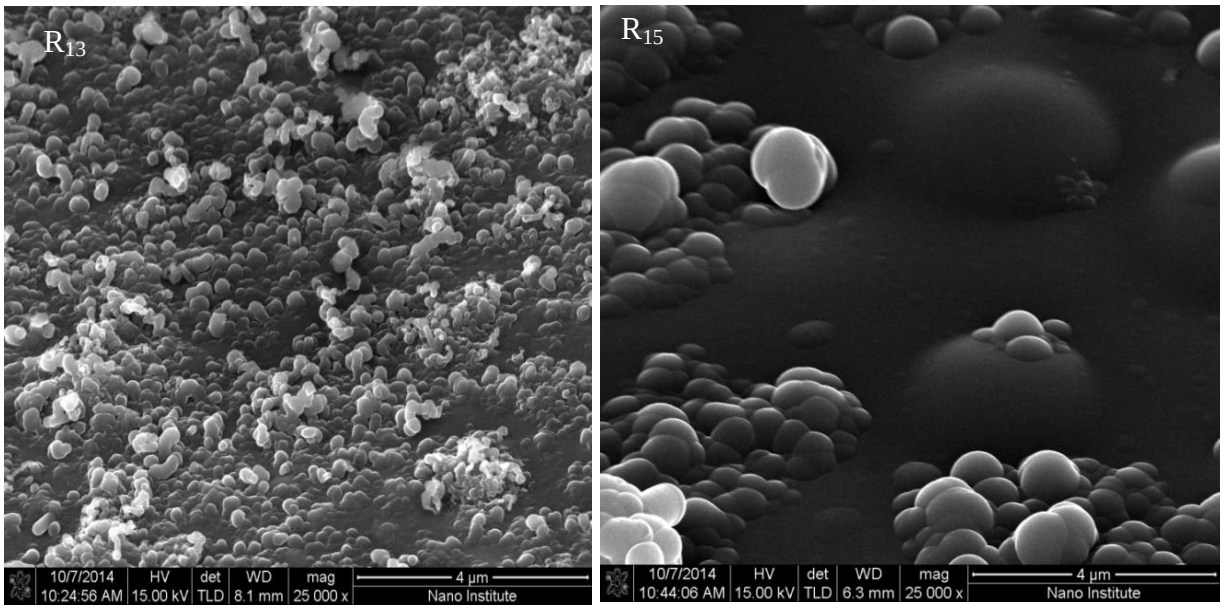

Figure 4.14. SEM images for samples R_{13} and R_{15}.

SEM images in Figure 4.14 show the difference in the SiNW density. The density of the SiNWs started to decrease with increasing deposition time. Metal assisted solid phase crystallization with Al at these temperatures was a slow phenomenon and amorphous silicon could overwhelm the former and eventually bury the SiNWs that started to form in the earlier phase.

Comparing between SiNW growth on samples R_{14} and R_{15} that were fabricated at the same conditions (substrate temperature = 360 ˚C, deposition time = 1 h, power = 2 W) except the H_2:SiH_4 dilution ratios were different. In sample $R_{14,}$ the H_2/SiH_4 dilution ratio was 9, while in sample R_{15} it was 1. The density of SiNWs was more in sample R_{14} than that in sample $R_{15,}$ so the density of SiNWs decreases with decreasing the dilution ratio. Figure 4.15 shows the effect of increasing the dilution ratio (H_2/SiH_4) on the SiNW growth.

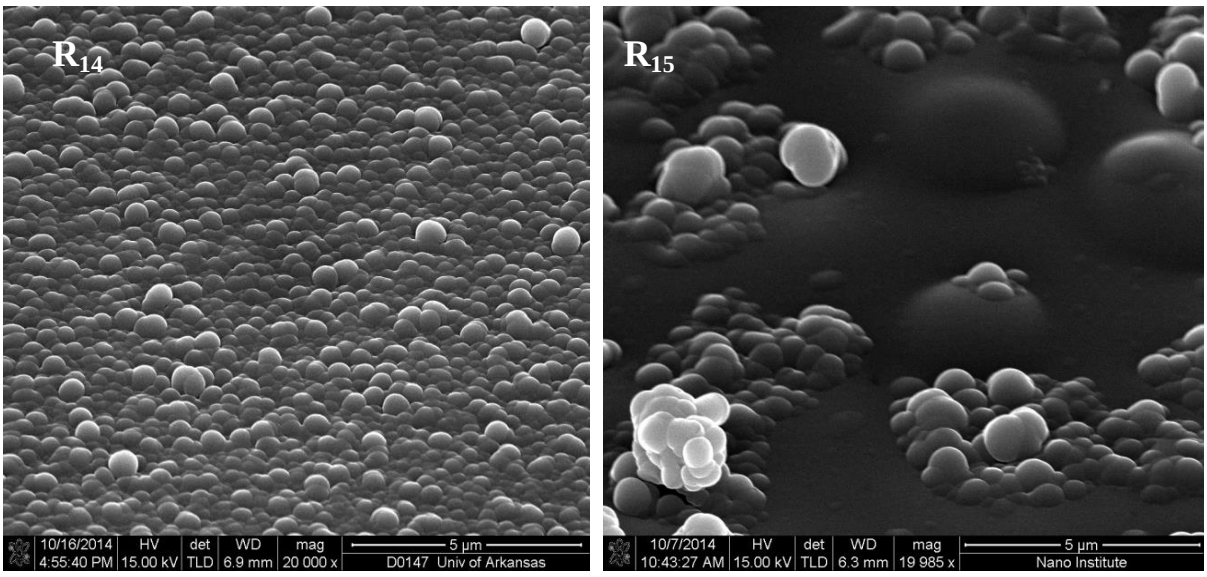

Figure 4.15. SEM images for sample R_{14} and R_{15}.

In sample R_{16}, the growth of SiNWs was done without diluting the SiH_4 gas with H_2; the deposition time and substrate temperature were 1 h and 360 ˚C, respectively. Figure 4.16 shows

the SiNW growth on sample R_{16} with different magnifications. In the right side of Figure 4.16, it can be seen that the growth of SiNW was in specific areas rather on the whole sample surface. In the left side of the SEM images in Figure 4.16, it can be seen that SiNWs started to grow vertically rather worm-like-structures (see the red circles on Figure 4.16).

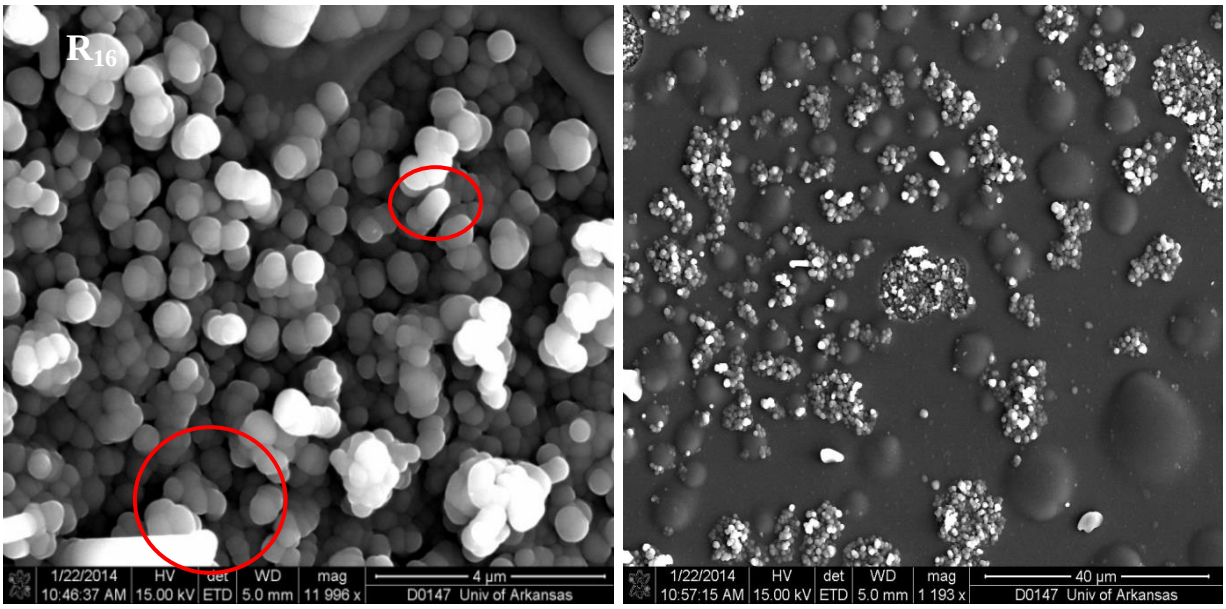

Figure 4.16. SEM images for samples R_{16} with different magnification.

Samples R_{17} and R_{18} were done at the same parameters (H_2/SiH_4 dilution ratio 10%, substrate temperature = 360 ˚C) except the deposition time was different (30 min and 60 min, respectively). The density of SiNW growth in sample R_{17} was more than that on sample R_{18}, and the reason seems to be because of the fast amorphous Si deposition on the already grown SiNWs with increasing the deposition time. The SEM image for sample R_{17} in Figure 4.17 shows some of the SiNWs started to grow vertically on the substrate (see red circle on Figure 4.17).

There were some limitations in PECVD that prevented the growth of SiNWs on c-Si substrate using Al as a catalyst.

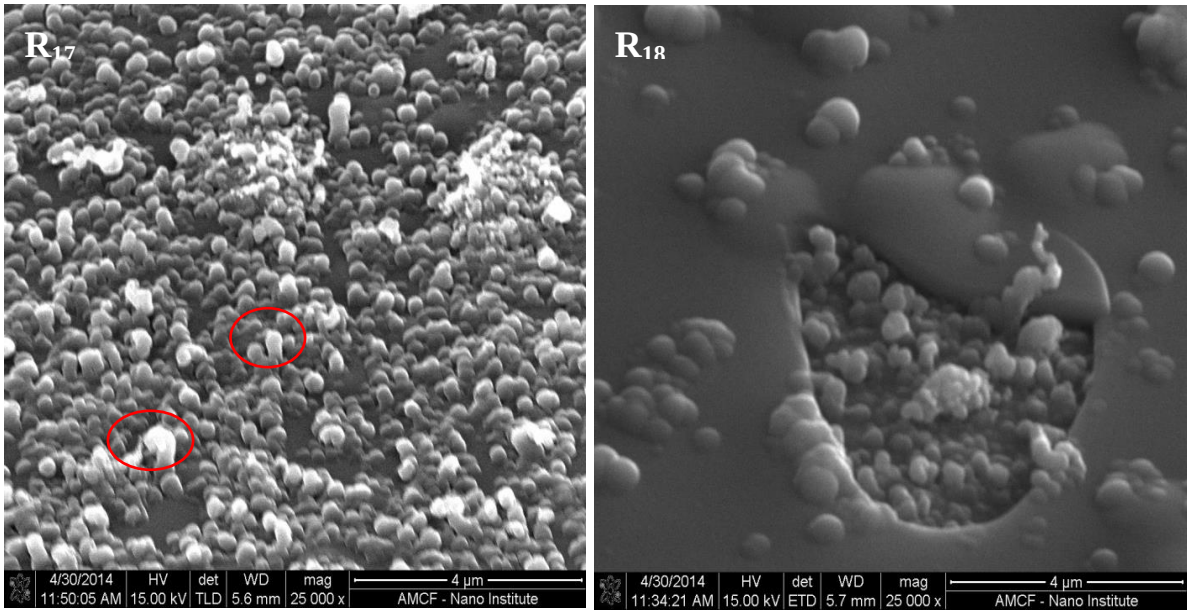

Figure 4.17. SEM images for samples R_{17} and R_{18}

The first limitation of PECVD was the low substrate temperature. The highest temperature that substrate can reach was 360 ˚C which is lower than the eutectic temperature of Al-Si alloy (577 ˚C). The lowest growth temperature of SiNWs using Al as catalyst reported by Moutanabbir et al. [28] was around 410 ˚ C (70% of the eutectic temperature of Al-Si). The growth temperature used in this study was 360 ˚C (62% of Al-Si eutectic temperature) and was beyond the minimum growth temperature [28] .

The other limitation was that the vacuum pressure of the system used in this research was around 2.8×10^{-8} Torr. However, ultrahigh vacuum systems (10^{-10} Torr) are reported to be needed during the SiNW growth using Al as a catalyst [26].

4.2.4 SEM results for SiNWs on C-Si substrate using Au nanodots as catalyst in the PECVD

As was mentioned in Chapter 3, the growth of SiNWs on c-Si substrate using Au nanodots as a catalyst was done at different growth temperatures and times to see the effect of these two parameters on the SiNW diameter, length, and density. The effect of temperature on the growth of the SiNWs will be discussed first followed by the effect of time. Table 3.4 shows the parameters used during the SiNW growth on c-Si substrate using Au as a catalyst. Figure 4.18 shows the SEM images for SiNWs were grown on c-Si substrate using Au as a catalyst at different substrate temperatures 200-346 ˚C.

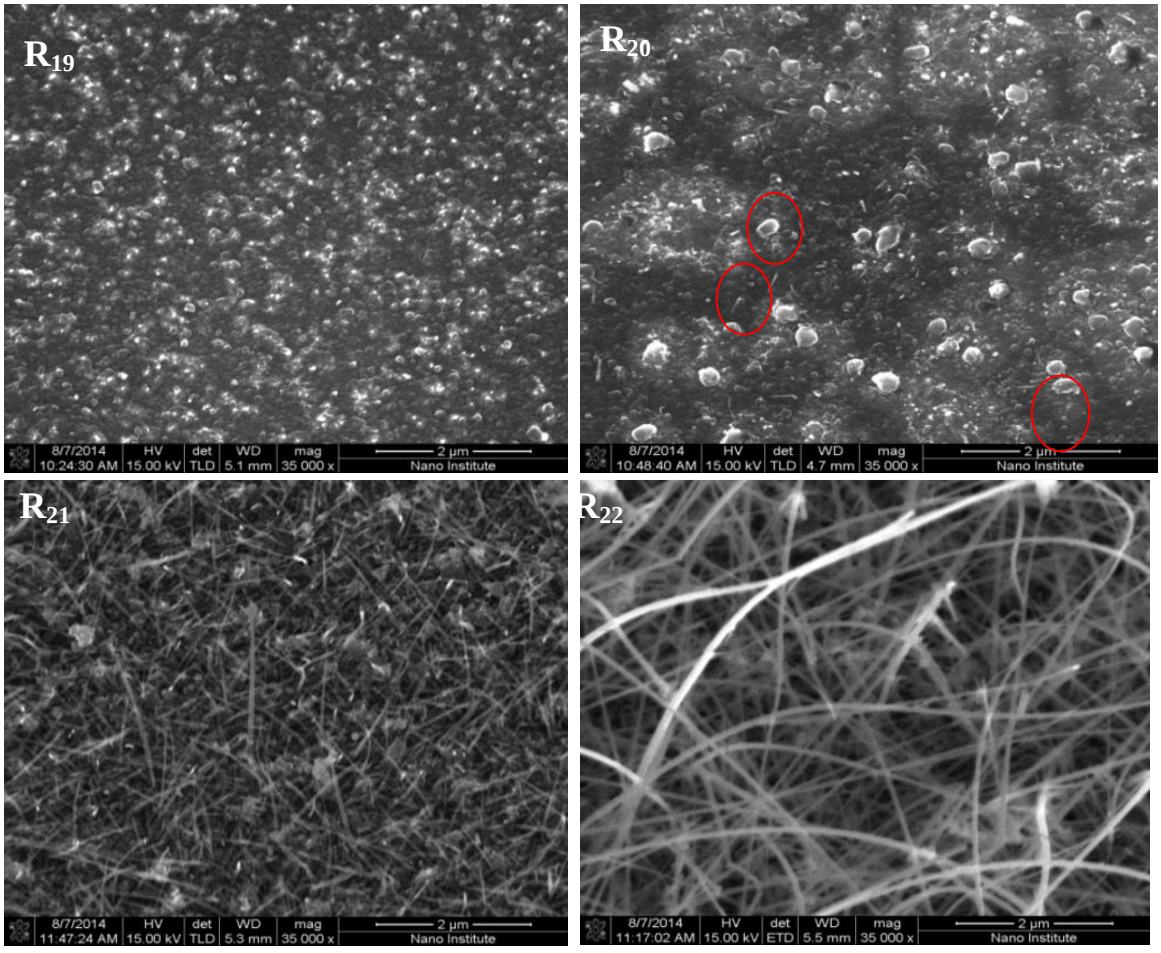

Figure 4.18. SEM images for SiNWs grown on samples R_{19}, R_{20}, R_{21}, R_{22} at different temperatures.

In sample $R_{19,}$ the growth temperature was 200 ˚C. As is clear from the SEM images for this sample, there were no wires found on the surface of the sample. This means that SiNWs never grew at a temperature of 200 ˚C which is much lower than the eutectic temperature of Au-Si (363 ˚C). When the growth temperature was increased to 250 ˚C, a few SiNWs with 0.3-0.5 µm length and 30 nm diameter were observed on the surface of sample R_{20}. They were distributed separately on the surface of the sample (see the red circle in SEM image for sample R_{20}).

By increasing the growth temperature to 310 ˚C, the length, diameter and density of the obtained SiNWs increased as shown in the SEM image of sample R_{21} in Figure 4.18. The length and diameter of the obtained SiNWs were 1-1.8 µm and 35-39 nm, respectively. The growth temperature of these SiNWs was below the eutectic temperature of Au-Si, therefore; these SiNWs were not grown by the VLS mechanism which needs a growth temperature above or at the eutectic temperature (363 ˚C) of Au-Si. Instead, they were grown by the VSS mechanism due to the low growth temperature. When the growth temperature was raised to 346 ˚C, the length of the obtained SiNW was around 14 µm with diameter of 76 nm. It is obvious from the SEM image of sample R_{22} that these SiNWs started to bend in different directions as the temperature increased to 346 ˚C.

After the comparing between the SEM images for the four samples (R_{19}, R_{20}, R_{21}, R_{22}), it was found that the growth of SiNWs at 310 ˚C was reasonable compared to the other samples due to the length, diameter, and density of the SiNWs obtained at 310 ˚C.

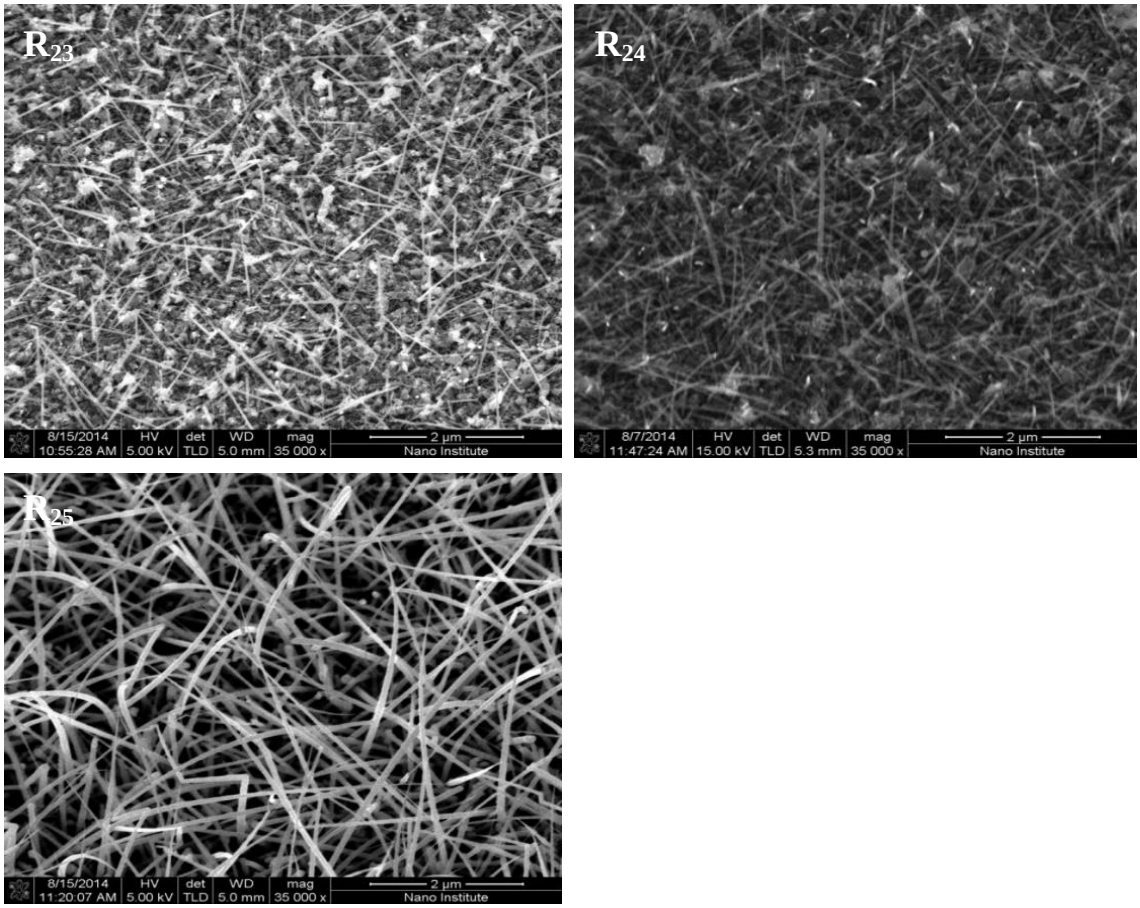

Figure 4.19. SEM images for SiNWs were grown on c-Si substrate in the PECVD system at different deposition time.

After finishing the growth of SiNWs at different temperatures, the growth of SiNWs was done at different times with constant growth temperature of 310 ˚C to see if there was any effect of time on the SiNW growth. Figure 4.19 shows the SEM images for SiNWs on samples R_{23}, R_{24}, R_{25} at different times 5, 15, and 30 min, respectively.

At 5 min of deposition time (sample R_{23}), the length and diameter of these SiNWs were around 0.8 µm and 30 nm, respectively. As the deposition time was increased to the 15 min, the density, length and diameter of SiNWs increased. The length and diameter increased to 1.8 µm and 39 nm, and the density of SiNWs was more than that with 5 min deposition time

With further increase in the deposition time to 30 min, the length and diameter of SiNWs also increased to reach 4 μm in length and 85 nm in diameter while increasing the SiNW density to double what it was with 15 min deposition time. The diameter, length and density of SiNWs increased as the growth temperatures and times were increased.

The schematic diagram in Figure 4.20 shows the increase in the diameter and length of SiNWs with increasing deposition time.

4.2.5 TEM Result for SiNW grow on c-Si substrate

TEM images were taken of SiNWs that were grown at a deposition time of 30 min and growth temperature of 310 ˚C. The TEM image in Figure 4.21 shows an a-Si:H layer coated the shell of SiNWs. While, the core of the SiNW was c-Si with two growth directions <111> and <100>.

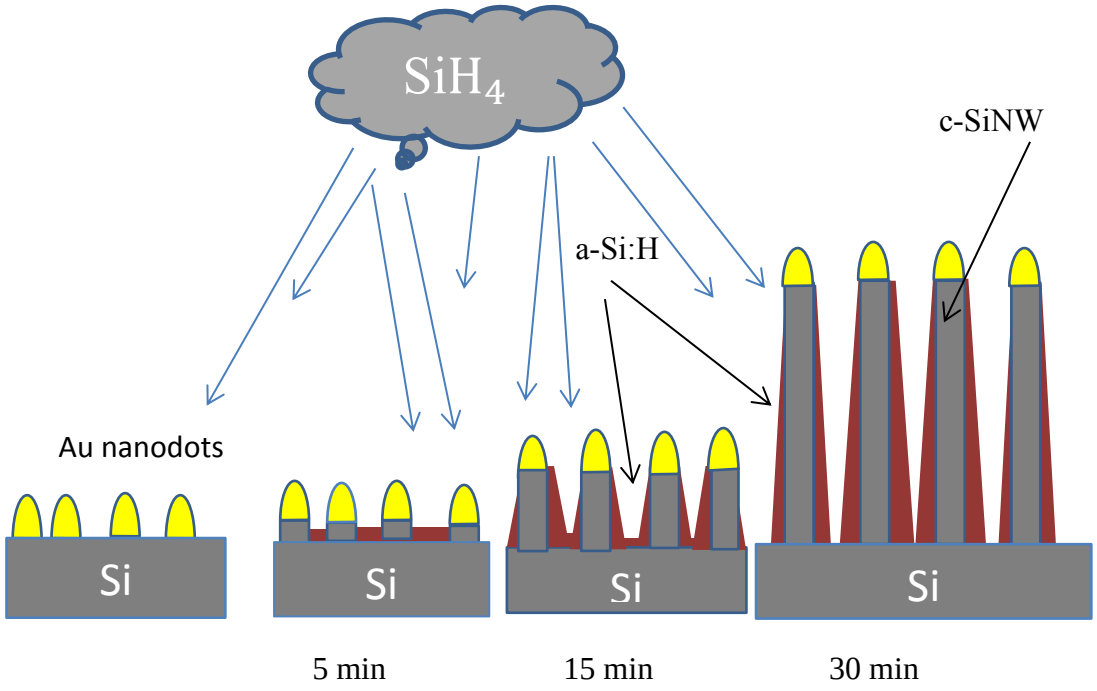

Figure 4.20. Schematic diagram of SiNW diameter and length increase as the deposition time is increased.

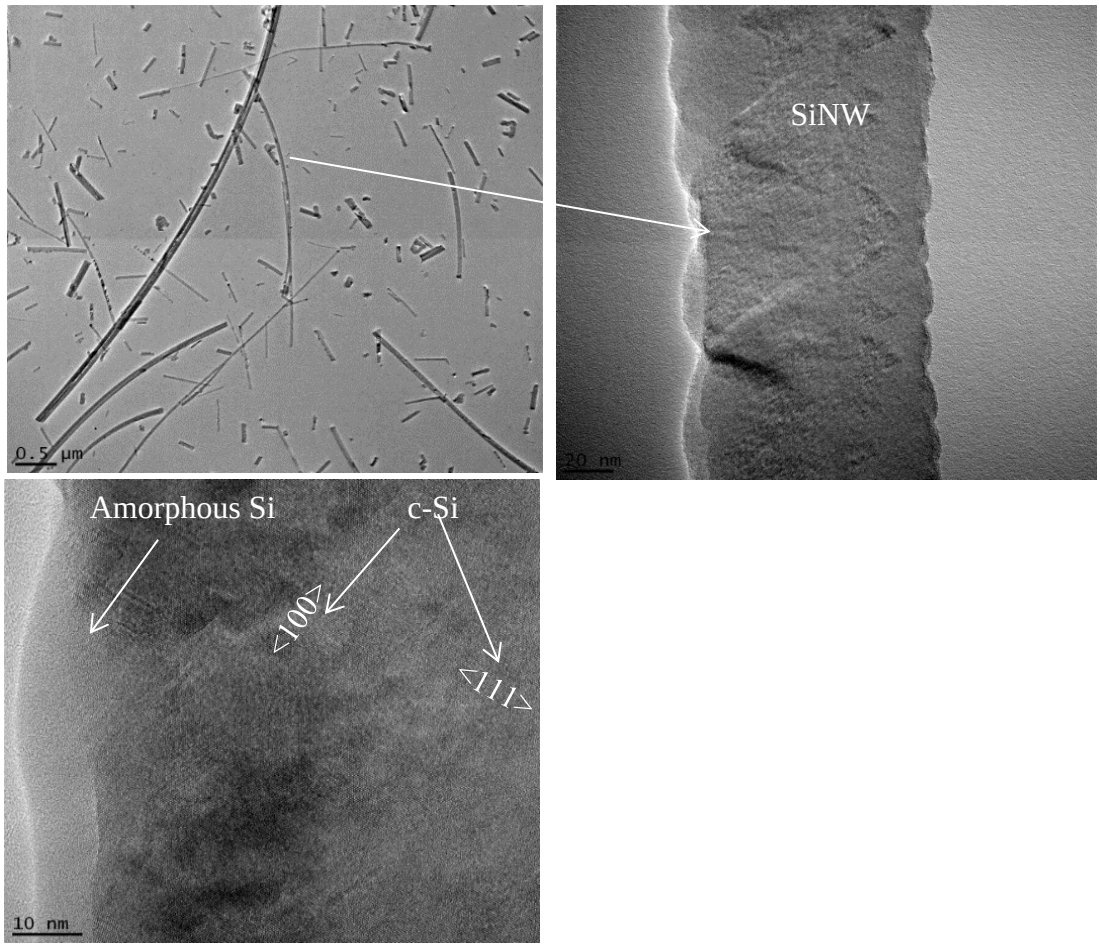

Figure 4.21. TEM images for SiNWs fabricated on c-Si substrate at temperature of 310 ˚C for 30 min.

4.2.6 SEM results for SiNWs grown on a-Si/ITO/glass substrate

Growth of SiNWs on a-Si/ ITO/glass substrate was done as a pre-step for growth of SiNWs on p^+ polySi/ ITO/glass substrate. Figure 4.22 shows the SEM images of SiNWs grown on a-Si/ITO/glass substrate at different deposition times. SEM images for the SiNWs that were fabricated at different deposition time showed different length, diameter, and density. At 5 min deposition time, the length of the obtained SiNWs was around 0.5-0.8 µm and diameter of 30-50 nm. At 15 min deposition time, the length and diameter of the obtained SiNWs increased to reach 75 nm in diameter and 2-3 µm in length.

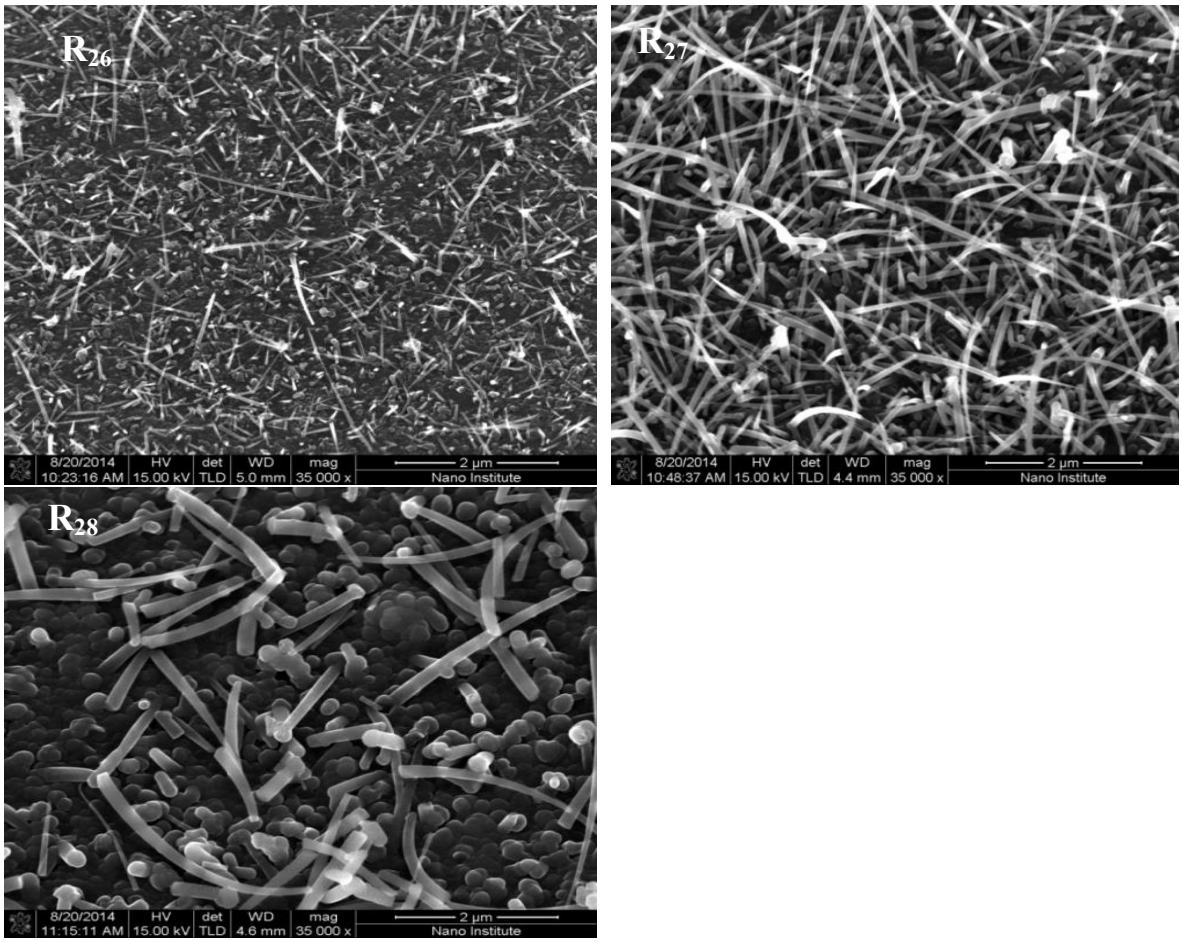

Figure 4.22. SEM images for SiNWs grown on a-Si/ITO/glass substrate on different deposition times.

The density of the SiNWs also increased to double what it was at 5 min deposition time. At 30 min deposition time, the SiNWs length increased to reach 4 µm with a diameter of 179 nm. From the SEM image for sample R_{29}, the density of the SiNWs started to reduce due to increase of a-Si:H deposition with increasing deposition time which buried the earlier grown SiNWs.

4.2.7 SEM result for the SiNWs growth on p+ polySi/ITO/glass substrate

After success of growing SiNWs on the a-Si/ITO/glass substrate, p+ polySi/ITO/glass substrate was used for SiNW growth. The growth of the SiNWs was done at constant growth

temperature of 310 ˚C with different deposition times (see Table 3.5). Figure 4.23 shows the SEM images for the SiNWs grown at deposition times of 15 min and 30 min.

SEM images show the difference in the SiNWs density, diameter, and length with increasing the deposition time, so as the time was increased to 30 min, the SiNWs started to grow in different directions with different lengths and diameters. The average length for the SiNWs that were grown at 30 min deposition time was from 2-4 µm with diameter of 60-100 nm.

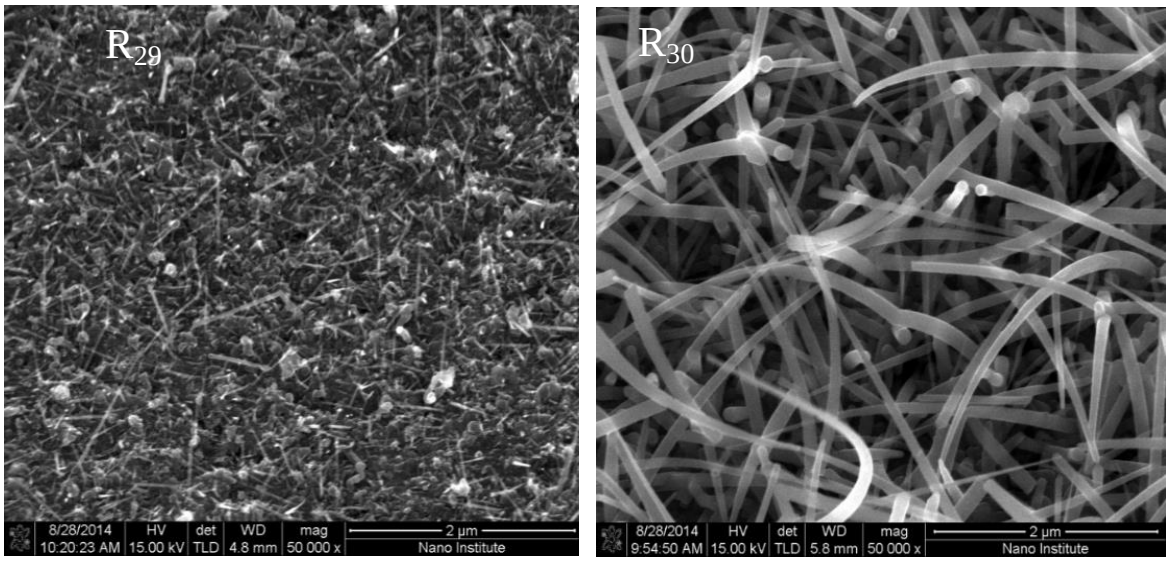

Figure 4.23. SEM images for SiNWs grown on p+ ploySi/ITO/glass substrate at different deposition time.

4.2.8 TEM results for SiNW grown on c-Si substrate

In order to know the morphology and structure of the SiNW, TEM images were taken of the SiNWs that grown on the p+ poly Si/ITO/glass substrate with a deposition time of 30 min. The structure of the SiNW that was analyzed by the TEM was c-Si in the core of the SiNW with amorphous silicon on the shell of the SiNW (see Figure 4.24).

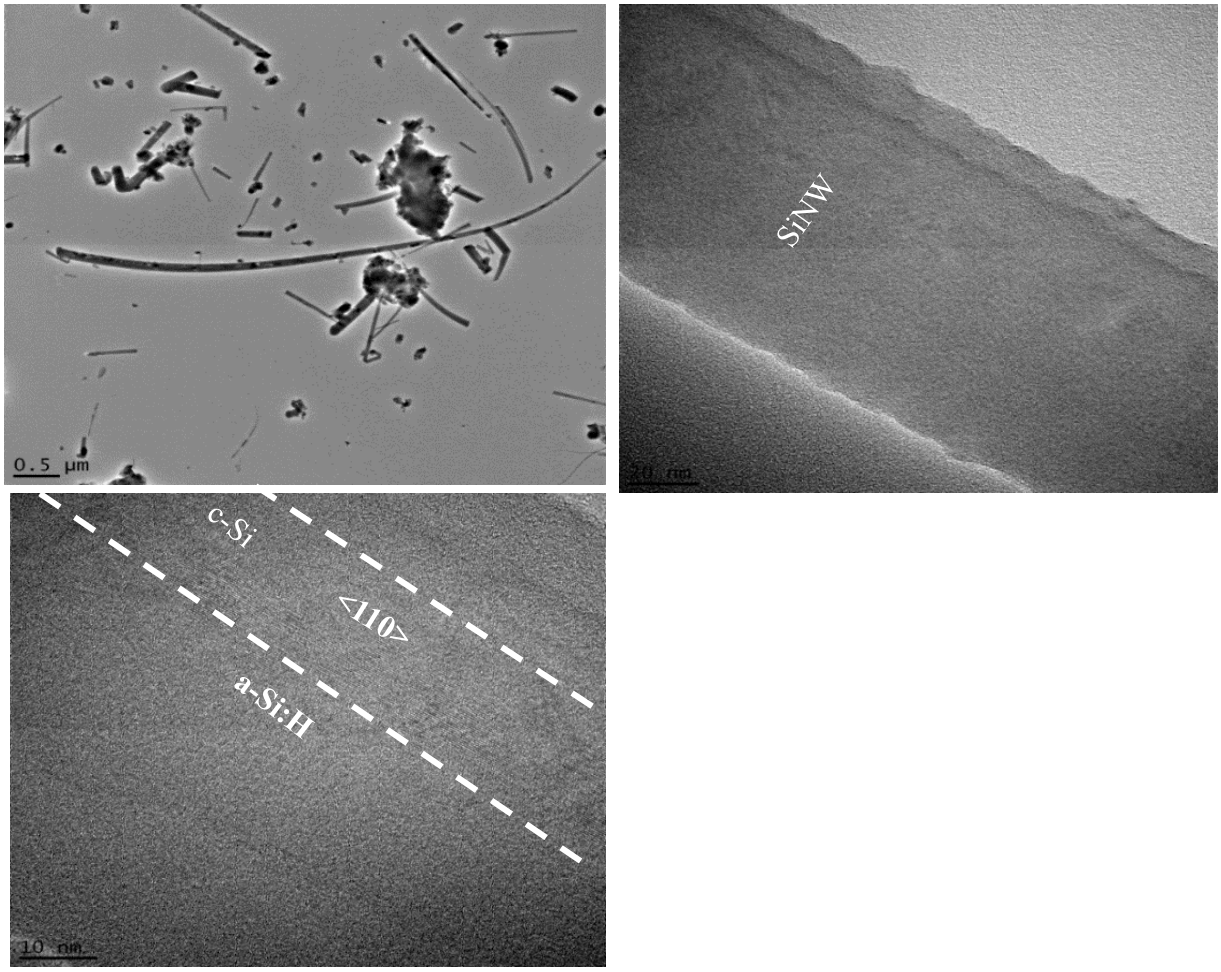

Figure 4.24. TEM image for SiNW that was fabricated on p+ poly Si/ITO/glass substrate with different magnification.

The c-Si part was around 25 nm of the total diameter of the SiNW (60 nm). The direction of the c-Si growth was in the <110>. The c-Si area was surrounded with a thick layer of a-Si:H on both sides.

The TEM image was also taken for the same SiNW in Figure 4.25 but in the dark field. The image showed the brightness area in the core of the SiNW, and that confirmed the

crystallinity of this part of SiNW. Having the a-Si layer surrounding the core of SiNW gave the advantage in enhancing the light absorption for the short wave length < 550 nm [38].

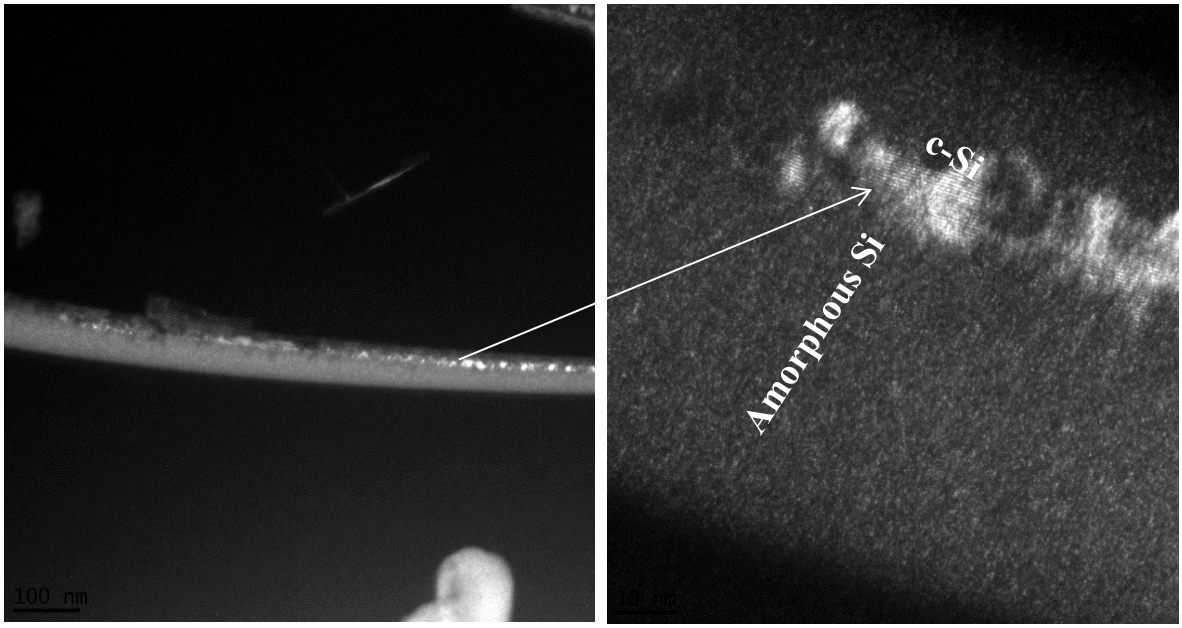

Figure 4.25. TEM image for SiNW grown at 310 ˚C for 30 min in the dark field.

From the TEM images, it may be concluded that the SiNW fabricated on p+ poly Si combines the c-Si structure in the core of the SiNW and a-Si:H on the shell of it. The formation of a-Si:H on the shell of SiNWs was considered a good result because having amorphous Si layer on the shell of the core of the SiNW will enhance light absorption.

Chapter 5: Conclusion and Future Work

Heavily doped p-type poly-Si thin film was fabricated successfully on glass and ITO/glass substrates using the aluminum induced crystallization method of amorphous Si with grain size of more than 5 μm. P-type SiNWs were grown successfully on c-Si, a-Si:H/glass, and p+poly Si/ITO/glass substrates using Au as a catalyst. The morphology SiNWs that were grown on c-Si and p+ poly Si/ITO/glass substrates were studied by TEM system, and the results showed an amorphous Si (a-Si:H) layer on the shell of the SiNW and c-Si in the core of the SiNW. The formation of a-Si:H layer on the shell of the SiNWs can be considered a good result because it enhances the light absorption by the SiNW.

Future work will include completing the fabrication of the SiNW/a-Si composite solar cell by using heavily doped n-type Si on the top of the SiNW, and then depositing an Al contact and testing the device. The growth of SiNW can be optimized into vertical direction by changing in some parameters. The growth of SiNWs on c-Si substrate using Al nanodots can be optimized by increasing the substrate temperature to 500 ˚C using different heating plate that heats the samples in the PECVD system. The growth of SiNWs using Al nanodots as a catalyst can be done on glass and a-Si/glass substrate.

References

[1] S. A. Kalogirou, "Solar Thermal Collectors and Applications," *Progress in Energy and Combustion Science ,* vol. 30, p. 231–295, 2004.

[2] http://www.altenergy.org/renewables/renewables.html, [Accessed 15 June 2014].

[3] http://www.science.nasa.gov/science-news/science-at-nasa/2002/solarcells/, [Accessed 23 september 2014].

[4] S. R. Wenham, M. A. Green, M. E. Watt and R. Corkish, Applied Photovoltaics, second ed., Earthscan, 2007, pp. 1-99.

[5] S. W. Glunz and R. P. Biro, Comperhensive Renewable Energy, 2012, pp. 1-62.

[6] A. I. Hochbau and P. Yang, "Semiconductor Nanowires for Energy Conversion," *Chemical Reviews,* vol. 110, no. 1, p. 527–546 , 2010.

[7] Y. Chu , "Review and Comparison of Different Solar Energy Technologies," Augest 2011.

[8] H. J. Choi , Semiconductor Nanostructure Optoelectronic Devices, Perocessing, Characterization and Applications, G. C. Yi, Ed., 2012.

[9] M. L. B. Y. C. a. M. D. M. Erik C. Garnett, "Nanowire Solar Cells," *Annual Review of Materials Research,* vol. 41, p. 269–95, 2011.

[10] R. E. Schropp and M. Zeman, "Technology of Solar Cells," in Amorphous and Microcrystalline Silicon Solar cells, 1998, pp. 71-72".

[11] C. Kendrick, C. Bomberger, N. Dawley and J. Georgiev, "Silicon Nanowire Growth on Poly-Silicon-on-Quartz".

[12] D. V. Gesteln, I. Gordon and J. Poortmans, "Aluminum-Induced Crystallization for Thin-Film Polycrystalline Silicon Solar cells: Achievements and perspective," *Solar energy materials & solar cells,* vol. 119, pp. 261-270, 2013.

[13] O. Nast and A. J. Hartmann, "Influence of Interface and Al Structure on Layer Exchange during Aluminum-Induced Crystallization of Amorphous Silicon," *Applied Physics,* vol. 88, no. 2, pp. 716-727, 2000.

[14] C. Jaeger, M. Bator, S. Matich and M. Stutzmann , "Two-step Crystallization during the Reverse Aluminum-Induced Layer Exchange Process," *Applied Physics,* vol. 108, p. 513,

2010.

[15] L. Filipponi and D. Sutherland, "Nanoyou teachers training kit-Model 1 chapter 7," January 2010.

[16] V. Schmidt, J. V. Wittermann, S. Senz and U. Gosele, "Silicon Nanowires: a Reveiw on Aspect of their growth and their Electrical Properties," *advanced material,* vol. 21, pp. 2681-2702,
2009.

[17] H. J. Fan, P. Werner and M. Zacharias, "Semiconductor Nanowires:from Self-Organization to Patterned Growth," *small,* no. 6, pp. 700-714, 2006.

[18] R. Curly, C. M. Thomas and M. Phipps, "http://www.ece.umd.edu/class/enee416/GroupActivities/LPCVD-PECVD.pdf," [Online]. [Accessed 23 Augest 2014].

[19] S. Mingwang, M. D. Dorthy and L. T. Shuit, "silicon Nanowires-synthesis, Properties, and Applications," *Euopean Journal of Inorganic Chemistry,* pp. 4264-4278, 2010.

[20] V. Schmidt, J. V. Wittemann and U. Gosels, "Growth, Thyrmodynamics, and Electrical Properties of Silicon Nanowires," *Chemical Reviews,* vol. 110, no. 1, pp. 361-388, 2010.

[21] R. S. Wagner and W. C. Ellis, "Vapor-Liquid-Solid Mechanism of Single Crystal Growth," *Applied Physics Letters,* vol. 4, no. 5, pp. 89-90, 1964.

[22] W. Y. Yee, M. Yahaya, M. M. Salleh, Mieee and Burhanuddin, "Synthesis of Silicon Nanowires," *ICSE,* pp. 379-382, 2004.

[23] S. Hofmann, C. Ducati, R. J. Neill, A. C. Ferrari, J. Geng, R. E. Borkowski and J. Robertson, "Gold Catalyzed g Growth of Silicon Nanowires by Plasma Enhanced Chemical Vapor Deposition," *Applied Physiscs,* vol. 94, no. 9, pp. 6005-6011, 2003.

[24] H. Hamidinezhad, Y. Wahab, Z. Othaman and A. Ismail, "Synthesis and Analysis of Silicon Nanowire below Si-Au Eutectic Temperatures using very High Frequency Plasma Enhanced Chemical Vapor Deposition," *Applied Surface Science ,* vol. 257, pp. 9188-9192, 2011.

[25] Y. Ke, X. Weng, J. M. Redwing, C. M. Eichfeld, T. R. Swisher, S. E. Mohney and Y. Habib, "Fabrication and Electrical Properties of Si Nanowires Synthesized by Al Catalyzed Vapor-Liqiud-Solid Growth," *Nano Letters,* vol. 9, no. 12, pp. 4494-4499, 2009.

[26] D. Kohen, C. Cayron, E. D. Vito, V. Tileli, P. Faucherand, C. Morin, A. Brioude and S. Perraud, "Aluminum Catalyzed Growth of Silicon Nanowires:Al Atom Location and the Influence of Silicon Precursor Pressure on the Morphology," *Crystal Growth,* vol. 341,

pp. 12-18, 2012.

[27] Wang, Y. Wang, V. Schmidt, S. Senz and U. Gosele, "Epitaxal Growth of Silicon Nanowires using an Aluminium Catalyst," *nature nanotechnology,* vol. 1, pp. 186-189, 2006.

[28] O. Moutanabbir, S. Senz, R. Scholz, M. Alexe, Y. Kim, E. Pippel, Y. Wang, C. Wiethoff, T. Nabbeefeld, F. Heringdrof and M. Hoegen, "Fabrication and Electrical Properties of Si Nanowires synthsized by Al Catalyzed Vapor-Liquid-Solid Growth, " *Nano Letters,* vol. 9, no. 12, pp. 4494-4499, 2009.

[29] H. Abu-Safe, Physics Department, University of Arkansas, "Calibration chart of PECVD system," Private Communication, 2014.

[30] http://www.heraeus-targets.com/en/technology/_sputteringbasics/sputtering.aspx, [Accessed 14 June 2014].

[31] B. Voutou and E. C. Stefanaki, "Electron Microscopy: the basics," 2008.

[32] http://www.micron.ucr.edu/public/manuals/Sem-intro, [Accessed 23 July 2014].

[33] http://www.nist.gov/pml/div683/hall.cfm," [Accessed 8 August 2014].

[34] S.A. Al Ghetmiri, Nano Science and Engineering Institute, University of Arkansas, "Raman spectroscope setup," private communication, 2014.

[35] http://www.princeton.edu/~achaney/tmve/wiki100k/docs/Optical_microscope.html, [Accessed 13 June 2014].

[36] http://www.google.com/url?sa=t&rct=j&q=&esrc=s&source=web&cd=10&ved=0CFUQFjAJ&url=http%3A%2F%2Fbiofiz.semmelweis.hu%2Frun%2Fdl.php%3Fid%3D1183&ei=GwJPVMyeCNieyATgs4CQDA&usg=AFQjCNEpf4WUsaGEP88wchIVBsycF991JQ," . [Accessed 12 May 2014].

[37] A. M. Mahamad and G. K. Mamidipudi, "Metal Induced Crystallization," Hyderabad, p.461-480, 2011.

[38] M. Adachi, M. P. Anantram and K. S. Karim, "Optical Properties of Crystalline-Amorphous Core-Shell Silicon Nanowires," Nano Letters, vol. 10, p. 4093–4098, 2010.

Appendix A: Description of Research for Popular Publication

When Photons Can Be Trapped, Good Things Can Happen

By: Asmaa Sadoon

Reducing the cost of solar cells has been a hot topic in Dr. Hameed Naseem's lab, a professor at the University of Arkansas, for several years. Asmaa Sadoon, one of his graduate students who is studying her master's degree in Microelectronics Photonics Graduate Program was selected by him to conduct this research. She claims that trapping photons can have a positive impact in the solar cells industry.

Is "trapping photons" good or bad for the solar cell performance? Does it help the device or does it act as a defect that leads to lower efficiency. Even though trapped particles can hurt some devices, trapped photons can enhance the efficiency of solar cells, which is a desired outcome.

Currently, the dominant kind of solar cells in the market are crystalline silicon (c-Si) solar cells due to the high efficiency that other technologies have yet to achieve. The idea that is behind c-Si solar cells high performance is the large thickness of the absorber layer (over 100 micrometers) which allows 90% of the incident light to be absorbed. This means more Si will be consumed and that will lead to a high manufacturing cost.

Consider this: If fewer materials with were used yet the high efficiency of c-Si solar cells was maintained, then we would have lower cost solar cells, which is a critical issue that has been researched for decades.

Going from gold to wires to inexpensive solar cells!

Gold works as a catalyst to grow Si nanowires (SiNWs). The definition of nanowires is based on the ratio between the tiny thicknesses or diameters that can be even one nanometer and

the length of the wire that can be 10s of micrometers. These SiNWs can help to keep the light trapped in between by the scattering and reflection phenomena. When photons are trapped, this means more absorption of the sunlight photons that gives higher efficiency. In this situation, we can get high efficiency with smaller thickness than c-Si solar cells, which means lower cost.

The key of this research is using an inexpensive substrate such as glass. Since glass is amorphous silicon, it requires further preparation steps to be ready as a seed layer for the nanowire growth. Therefore, aluminum induced crystallization (AlIC) technique was applied for crystallization purposes.

When seed layers are ready, they will be heavily-doped polycrystalline silicon (p+ polySi) films on indium tin oxide (ITO) coated glass substrates. This is a novel idea will lead to fabrication of the p+-i-n+ solar cell. The growth of nanowires by using gold as a catalyst resulted in SiNWs with a shell of a-Si that improves the light absorption for short wave lengths < 550 nm. If you got all of these advantages of SiNWs, you could not have asked for more. Nanowires will change the nanotechnology perspectives and change the world to a better place as well.

Appendix B: Executive Summary of Newly Created Intellectual Property

The following list of new intellectual property items were created in the course of this research project

1. The fabrication of heavily doped poly-Si film on ITO/glass substrate
2. The fabrication of SiNWs on heavily doped poly-Si /ITO/glass using Au as a catalyst at low temperature.

Appendix C: Potential Patent and Commercialization Aspects of listed Intellectual Property Items

There are no potential patent and commercialization aspects of the two listed intellectual property items.

C.1 Patentability of Intellectual Property (Could Each Item be Patented)

There is no patentability of intellectual property in this research.

C.2 Commercialization Prospects (Should Each Item Be Patented)

There is no commercialization prospect in this research.

C.3 Possible Prior Disclosure of IP

There is no possible prior disclosure of IP in this research.

Appendix D: Broader Impact of Research

D.1 Applicability of Research Methods to Other Problems

During the fabrication steps for solar cell device of this research, we found that SiNWs and poly-Si substrate that have fabricated as major steps in this device have potential to be used in various applications. SiNWs can be used in the fabrication sensors, transistors, lithium batteries, diodes, and photovoltaic devices. For poly crystalline silicon thin film also can be used as a seed layer for epitaxial growth. Moreover, poly silicon can be used in fabrication of sensors transistor, display, and photovoltaic devices including the solar cells.

D.2 Impact of Research Results on U.S. and Global Society

The results of this research have the potential to make a positive impact on the U.S and global society. The main goal of this research was fabricating a solar cell device with low cost and high efficiency. Therefore, power could be provided at low cost, which would boost the economy of the U.S., and then of the whole world. Moreover, materials, equipment, and fabrication methods that were used in fabrication the solar cell device in this research were non-toxic. The fabrication methods were based on chemical vapor deposition and physical vapor deposition processes that are considered a safe and cost effective method. The solar cell device, in general, is a renewable energy resource based on converting the energy of sunlight to electricity. Today, more research has been conducted to improve the performance of solar cell which will be the most used resource for power in the future.

D.3 Impact of Research Results on the Environment

The results of this research have friendly impact on the environment due to the main principle that solar cells are based on in general. Solar cell devices are one form of renewable energy sources based on converting the natural phenomenon to beneficial sources. The substrates that were used in fabricating the poly-Si thin film and SiNWs, glass and Si, were non-toxic material. Also, metals, Al and Au, were used in fabricating SiNWs are also non-toxic material. So, the materials and fabrication methods that were used to fabricate SiNW/a-Si composite solar cell were non-toxic, and also there is no emission of carbon dioxide to the air like that associated with use of fossil fuel sources.

Appendix E: Microsoft Project for MS MicroEP Degree Plan

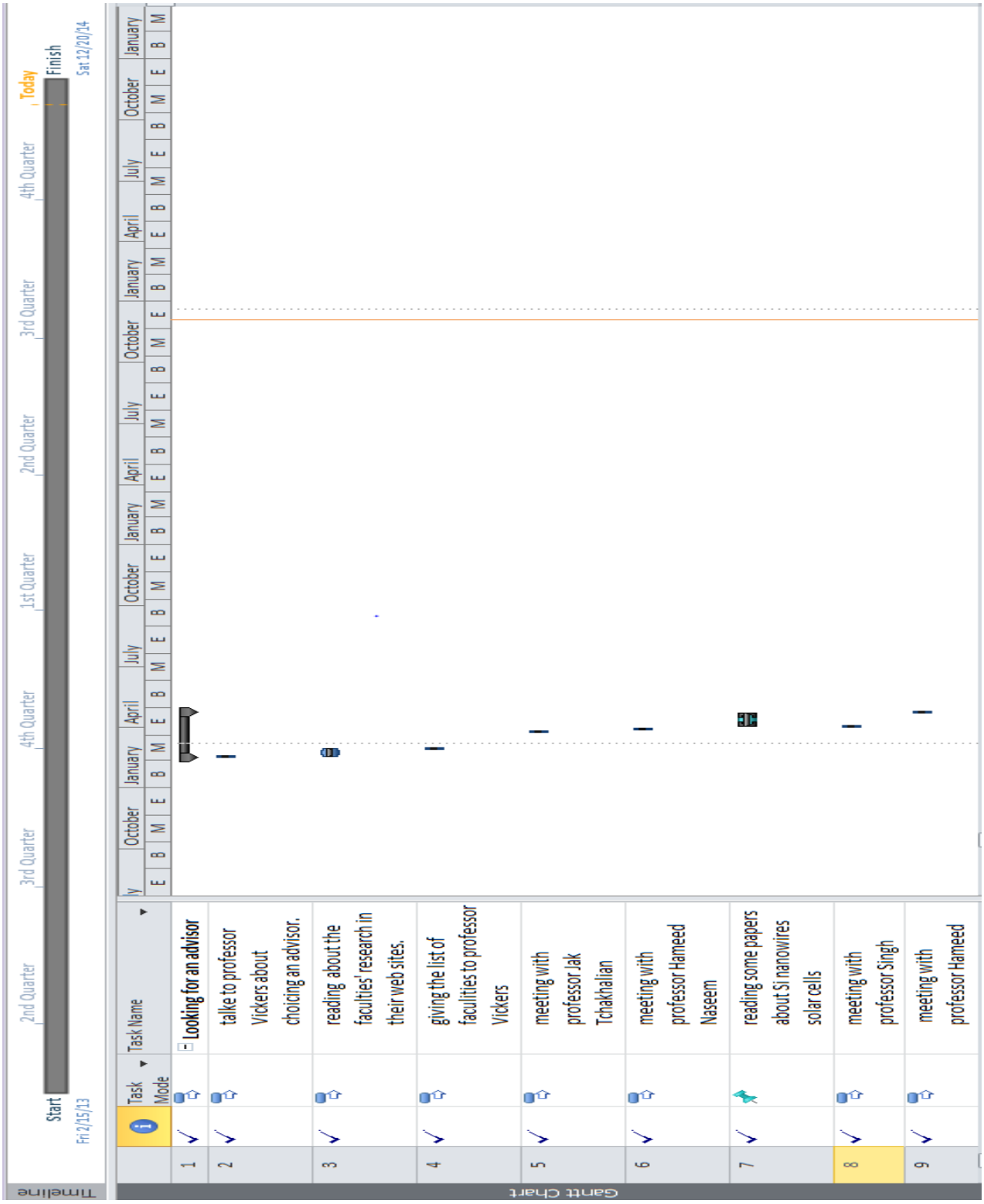

Timeline

Start: Fri 2/15/13

2nd Quarter | 3rd Quarter | 4th Quarter | 1st Quarter | 2nd Quarter | 3rd Quarter | 4th Quarter

Today

Finish: Sat 12/20/14

Gantt Chart

	Task Mode	Task Name
10		meeting with Professor Hameed Naseem and choosing him as an advisor
11		**Equipment training section**
12		attending in ENRC to absorve e-beam installation
13		attending in ENRC to absorve e-beam installation
14		training in the lab for hot wires CVD experiment
15		training in the e-beam evaporation system
16		training about Aluminum sputtering
17		reading some papers about my research
18		**Al nanodots expermints**

Timeline
Start
Fri 2/15/13
2nd Quarter
3rd Quarter
4th Quarter
1st Quarter
2nd Quarter
3rd Quarter
4th Quarter
Today
Finish
Sat 12/20/14
Gantt Chart
Task Mode
Task Name
sample 1-40
SiNWs experiment
SiNWs experments using c-Si as a substrate and using Al as a catalyst
SiNWs experiment using c-Si as a substrate and Au as a catalyst
SiNWs experments using glass as a substrate and using Au as a catalyst
poly-Si fabrication experiments
The rest steps to creat the solar cell device
I-V charactrization
writing my thesis
chapter one:introduction
chapter2: literature
October
January
April
July
October
January
April
July
October
January
April
July
October
January

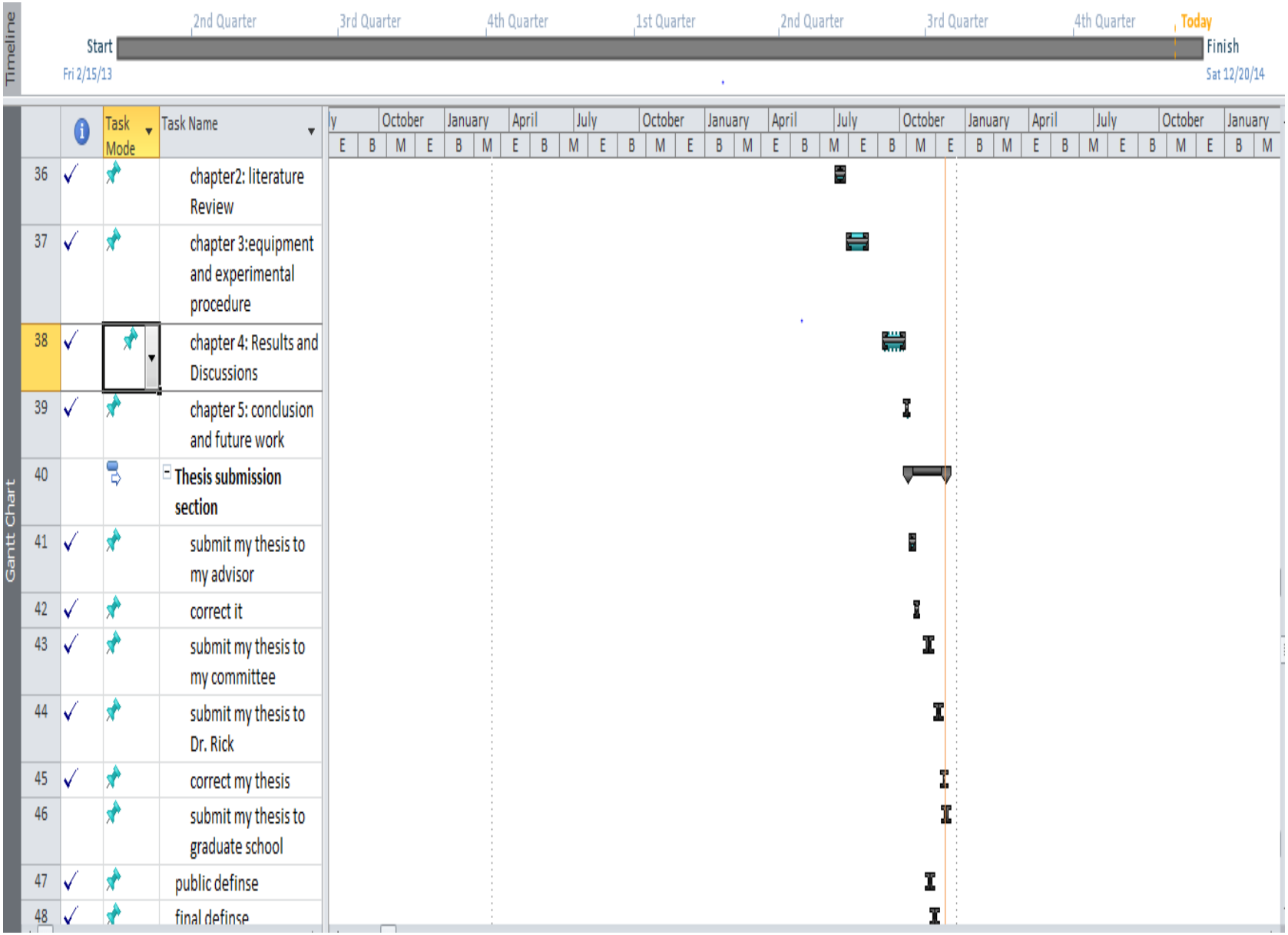
Timeline
2nd Quarter
3rd Quarter
4th Quarter
1st Quarter
2nd Quarter
3rd Quarter
4th Quarter
Today
Start
Fri 2/15/13
Finish
Sat 12/20/14
Gantt Chart
Task Mode
Task Name
36 chapter2: literature Review
37 chapter 3:equipment and experimental procedure
38 chapter 4: Results and Discussions
39 chapter 5: conclusion and future work
40 Thesis submission section
41 submit my thesis to my advisor
42 correct it
43 submit my thesis to my committee
44 submit my thesis to Dr. Rick
45 correct my thesis
46 submit my thesis to graduate school
47 public defense
48 final defense
October
January
April
July
October
January
April
July
October
January
April
July
October
January

Timeline
Start
Fri 2/15/13
2nd Quarter
3rd Quarter
4th Quarter
1st Quarter
2nd Quarter
3rd Quarter
4th Quarter
Today
Finish
Sat 12/20/14
Gantt Chart
Task Mode
Task Name
47 public definse
48 final definse
49 expected gratuded date
October
January
April
July
October
January
April
July
October
January

Appendix F: Identification of All Software Used in Research and Thesis Generation

Computer #1:

Model Number: x86-64Full_14Sep2

Serial Number: Dell 1707FP

Location: ENRC

Owner: Department of Electrical Engineering

Software #1:

Name: Microsoft Office 2007

Purchased by: UA Department of Electrical Engineering

Computer #2:

Model Number: MACBook Pro 9,2

Serial Number: C1ML8ETTDTY3

Location: 900 N.Leverett.Ave#303

Owner: Asmaa Sadoon

Software #1:

Name: Microsoft Office 2007

Purchased by: UA Department of Electrical Engineering